STUDY OF THE REACTIVITY OF 5-HYDROXYMETHYLFURFURAL WITH HYDROGEN IN THE PRESENCE OF SUPPORTED TRANSITION METAL CATALYSTS IN AQUEOUS MEDIUM

DIANA PAOLA DUARTE DUARTE

UNIVERSIDAD INDUSTRIAL DE SANTANDER
FACULTAD DE INGENIERÍAS FÍSICO-QUÍMICAS
ESCUELA DE INGENIERIA QUÍMICA
DOCTORADO EN INGENIERÍA QUÍMICA
BUCARAMANGA
2016

STUDY OF THE REACTIVITY OF 5-HYDROXYMETHYLFURFURAL WITH HYDROGEN IN THE PRESENCE OF SUPPORTED TRANSITION METAL CATALYSTS IN AQUEOUS MEDIUM

DIANA PAOLA DUARTE DUARTE

Dissertation presented in partial fulfillment of the requirements for the degree of Doctor of Philosophy in Chemical Engineering

ADVISOR
RAMIRO MARTÍNEZ REY
Chemical Engineering, Ph.D.

CO-ADVISOR
LUIS JAVIER HOYOS MARÍN
Chemical Engineering, Ph.D.

UNIVERSIDAD INDUSTRIAL DE SANTANDER
FACULTAD DE INGENIERÍAS FÍSICO-QUÍMICAS
ESCUELA DE INGENIERÍA QUÍMICA
DOCTORADO EN INGENIERIA QUIMICA
BUCARAMANGA
2016

Dedicated to:

My best friend, my love and my husband, Ludwing thanks for making my dreams come true

My parents who have passed down the value of hard work and helped me throughout my life

My sister Jenny

All my family

ACKNOWLEDGEMENTS

I thank my advisors Dr. Hoyos and Prof. Dr. Martínez for sharing their knowledge and assisting me throughout my PhD studies.

I thank the following for help in technical support: MSc. Maribel Castañeda in developing the chromatographic method, Ph.D. Jorge Armando Orrego in IR analysis, Prof. Dr. Victor Baldovino in XPS analysis, Prof. Dr. Enrique Mejía in HPLC analysis and Prof. Dr. José Henao in XRD analysis.

I would also like to thank a number of contractors, people of the Colombian Petroleum Institute who were somehow involved in the development of my research. In particular, I thank Javier M., Jose Luis J., Pedro F., Sayde, Sergio, Erika, Paula, Alix and Fernando.

I am grateful to my friends Kelly, Jennifer, Diego A., Luis Carlos, Jose Luis A., Miguel, Priscilla, Daniel, Nicholas and Vicki for their words of encouragement.

I thank Prof. Dr. Daniel Resasco for the internship opportunity at the Oklahoma University.

I thank the Colombian Petroleum Institute of Ecopetrol S.A for their financial support and to Colciencias for awarding me a PhD fellowship (Doctoral scholarships Francisco José de Caldas, Convocatoria No. 494 – 2009).

TABLE OF CONTENTS

LIST OF TABLES

Page

LIST OF FIGURES

Page

LIST OF SCHEMES

Page

LIST OF ANNEXES

Page

ABBREVIATIONS

APD	Average Pore Diameter
ASTM	American Society for Testing and Materials
ATR	Attenuated Total Reflectance
BE	Binding Energy
BET	Brunauer, Emmett and Teller
BHF	2,5-bis(hydroxymethyl)furan
BHTHF	2,5-bis(hydroxymethyl)-tetrahydrofuran
C12	n-dodecane
DFF	2,5-diformylfuran
DMF	2,5-dimethylfuran
DMTHF	2,5-dimethyltetrahydrofuran, cis & trans
DOE	U.S. Department of Energy
ECN	Effective Carbon Number
FAL	Furfural
FID	Flame Ionization Detector
FOL	2-furfuryl alcohol
FDCA	2,5-furandicarboxylic acid
GC	Gas Chromatography
HD	2,5-hexanedione
HHD	1-hydroxy-2,5-hexanedione

HDO	Hydrodeoxygenation
HMF	5-hydroxymethylfurfural
HPLC	High Performance Liquid Chromatography
HYD	Hydrogenation
ICP	Inductively Coupled Plasma
IR	Infrared
m-C5one	3-methyl-cyclopentanone
MF	2-methylfuran
MFAL:	5-methylfurfural
MFOL	5-methylfurfuryl alcohol
MS	Mass Spectroscopy
MTHFOL	5-methyltetrahydrofuran-2-methanol (cis & trans)
OES	Optical Emission Spectroscopy
RRF	Relative Response Factor
TCD	Thermal Conductivity Detector
THFOL	2-tetrahydrofurfuryl alcohol
TPD	Temperature-Programmed Desorption
TPR	Temperature-Programmed Reduction
TPV	Total Pore Volume
XPS	X-ray Photoelectron Spectroscopy
XRF	X-ray Fluorescence spectroscopy
WHSV	Weight Hourly Space Velocity

RESUMEN

TÍTULO:
ESTUDIO DE LA REACTIVIDAD DEL 5-HIDROXIMETILFURFURAL CON HIDRÓGENO EN PRESENCIA DE CATALIZADORES SOPORTADOS DE METALES DE TRANSICIÓN EN MEDIO ACUOSO[*]

AUTOR:

Diana Paola Duarte Duarte[**]

PALABRAS CLAVE:

5-hidroximetilfurfural, hidrodesoxigenación, descarbonilación, metales de transición, alúmina, sílice

DESCRIPCIÓN:

Nuevas políticas para la protección del medio ambiente y la sostenibilidad económica han llevado al desarrollo e implementación de tecnologías para la producción de combustibles y químicos a partir de recursos renovables. Una ruta para la producción de biocombustibles y químicos es a través del 5-hidroximetilfurfural (HMF) derivado a partir de la conversión catalítica de biomasa. La hidrodesoxigenación es un proceso idóneo para convertir HMF en productos de valor agregado. En este trabajo, la hidrodesoxigenación del HMF se estudió en la presencia de catalizadores soportados en sílice y en alúmina en medio acuoso. El efecto de metales tales como Ni, Pd, Cu y Ru se evaluó en la conversión del HMF. La actividad catalítica fue evaluada en un reactor de flujo descendente en vista de una posible aplicación a un proceso de biorefinería a gran escala. Una variedad de compuestos valiosos fue obtenida dependiendo de la naturaleza del metal depositado en el soporte. Los catalizadores de Ni, Pd y Ru soportados favorecieron principalmente la reacción de descarbonilación del grupo carbonilo del HMF, mientras que reacciones de hidrogenólisis y ciclización fueron observadas sobre los catalizadores de Cu soportados. Además, los catalizadores de Pd soportados fueron bastante selectivos a hidrogenar el anillo furano, especialmente a altas temperaturas. Los catalizadores basados en alúmina promovieron las reacciones de hidrogenólisis, hidrogenación del anillo y apertura del anillo del HMF comparado a los catalizadores basados en sílice. Además, catalizadores de Ni-Cu soportados en alúmina fueron también estudiados con el fin de mejorar los rendimientos hacia productos de hidrogenólisis. El catalizador CuNi/A-CoImp exhibió el mejor rendimiento para la hidrogenólisis del HMF a 155 °C y 0.41 MPa.

[*] Tesis doctoral

[**] Facultad de Ingenierías Físico-Químicas. Escuela de Ingeniería Química. Directores: Dr. Ramiro Martínez Rey y Dr. Luis Javier Hoyos

ABSTRACT

TITLE:
STUDY OF THE REACTIVITY OF 5-HYDROXYMETHYLFURFURAL WITH HYDROGEN IN THE PRESENCE OF SUPPORTED TRANSITION METAL CATALYSTS IN AQUEOUS MEDIUM*

AUTHOR:

Diana Paola Duarte Duarte**

KEYWORDS:

5-hydroxymethylfurfural, hydrodeoxygenation, decarbonylation, transition metals, alumina, silica

DESCRIPTION:

New policies for environmental protection and economic sustainability have led to the development and implementation of technologies for production of fuels and chemicals from renewable resources. One route for producing biofuels and chemicals is through 5-hydroxymethylfurfural (HMF) derived from catalytic conversion of biomass. Hydrodeoxygenation of HMF is a suitable process to convert it into added-value products. In this work, hydrodeoxygenation of HMF was studied in the presence of silica- and alumina-supported catalysts in aqueous medium. The effect of metals such as Ni, Pd, Cu and Ru was evaluated in the conversion of HMF. The catalytic activity was evaluated in a downflow reactor in view of a possible application to a large scale biorefinery process. A variety of valuable compounds was obtained depending on the nature of the metal deposited on the support. The Ni-, Pd- and Ru-supported catalysts favored mainly the decarbonylation reaction of the HMF carbonyl group, whereas hydrogenolysis and cyclization reactions were observed on the Cu-supported catalysts. In addition, the Pd-supported catalysts were quite selective to hydrogenate the furan ring, especially at high temperatures. Alumina-based catalysts promoted the hydrogenolysis, ring-hydrogenation and ring-opening reactions on HMF as compared to the silica-based catalysts. Furthermore, alumina-supported Ni-Cu catalysts were also studied with the aim of improving the yield toward hydrogenolysis products. CuNi/A-CoImp catalyst exhibited the best performance for hydrogenolysis of HMF at 155 °C and 0.41 MPa.

* Doctoral thesis

** Facultad de Ingenierías Físico-Químicas. Escuela de Ingeniería Química. Advisors: Ramiro Martínez Rey, Ph.D. and Luis Javier Hoyos, Ph.D.

INTRODUCTION

Concerns about fossil fuel depletion, environmental pollution and global warming have led to the development and implementation of technologies for generation of sustainable energy and production of fuels and chemicals from renewable resources. New technologies are emerging to produce biofuels and chemicals from biomass through catalytic processes. One of the options considered for conversion or upgrading of biomass into more valuable products is the catalytic hydrodeoxygenation of 5-hydroxymethylfurfural (HMF) derived from biomass.

HMF is a versatile compound because it contains an aldehyde aromatic and an alcohol, and can be transformed into high value-added products for the industry. In the last two decades, numerous studies were performed at laboratory scale showing the technical feasibility of the hydrodeoxygenation of HMF. However, most of these works were developed using carbon-supported and bulk alloy catalysts evaluated in batch reactor systems.

These previous studies provide valuable information about the catalyst activity for the hydrodeoxygenation/hydrogenation of HMF. Nevertheless, the evaluation of the reaction in a continuous flow reactor would allow a better understanding of the industrial-scale process within the concept of a biorefinery. Most of the reported reactions are evaluated usingrelatively expensive solvents in the reaction medium, which would be a drawback for their environmental management in an industrial application. In addition, the catalysts studied in the literature are typically noble metal catalysts supported on carbon, which are prone to deactivation by carbonaceous material deposition and have a low attrition resistance.

Therefore, the exploration of a serie of transition metal catalysts was carried out to understand the catalytic properties of these metals in the hydrodeoxygenation of

HMF. This information is relevant for having insight into how to develop a catalyst with improved stability and selectivity for the hydrodeoxygenation. The hydrodeoxygenation/hydrogenation of HMF is studied in the presence of Ni, Pd, Cu and Ru catalysts based on supports widely used in industrial-scale applications like silica and γ-alumina. The reactions were performed in a continuous flow reactor and in an aqueous medium since the process to obtain HMF is carried out in water.

In *Chapter 2* it is detailed the synthesis of the different supported catalysts, as well as their characterization. The catalysts were prepared by a wet impregnation method. A detailed description of the reactor equipment, catalyst characterization equipment and analysis conditions are also given. *Chapter 3* presents a study of the silica-supported catalysts based on Ni, Pd, Cu and Ru metals in the hydrodeoxygenation of HMF in aqueous medium. In this chapter, the effect of the supported active metal on the catalyst activity and selectivity of the reactionis elucidated. A general hydrodeoxygenation reactions pathway of HMF is presented from the obtained results.

The influence of the alumina-supported catalysts on the reaction is investigated in *Chapter 4*.The influence of the addition of a small amount of copper to the alumina-supported Ni catalyst is studied in the *Chapter 5*.It is also shown the influence of the impregnation sequence on the properties of the catalyst and its catalytic performance.

A discussion of how the nature of both metals and supports influences the reaction is exposed in *Chapter 6* from the outcome of the activity and selectivity. Finally, *Chapter 7* concludes the main findings of this research.

1. STATE OF THE ART

1.1 BIOMASS AS A RENEWABLE SOURCE OF CARBON

New policies for environmental protection and economic sustainability have led to the research of renewable sources of fuels and chemicals. Biomass could be used as an alternative resource to fossil oil because it is abundant, sustainable and renewable. Biomass is typically composed of three major organic fractions on a dry-weight basis: 35-50% cellulose, 20-35% hemicellulose and 12-20% lignin [1]. Cellulose is a crystalline structure that comprises long chains of glucose sugars. Hemicellulose is an amorphous chain of a mixture of sugars, usually including arabinose, galactose, glucose, mannose and xylose. Lignin is not a sugar-based structure but is a complex organic polymer based on a phenol-propene backbone [1]. Biomass also contains smaller amounts of triglycerides, alkaloids, pigments, resins, sterols, terpenes, terpenoids and waxes [2].

Several routes to produce fuels from biomass are under intensive research and development efforts. Lignocellulosic ethanol, biomass pyrolysis and gasification are among the technologies of interest. However as their development progresses important challenges are appearing. Energy and water management in lignocelullosic ethanol, bio-oil upgrading in biomass pyrolysis, tar treatment and economies of scale in gasification remain as significant scientific and technological issues to solve.

In recent years, a growing interest in other routes to produce chemicals and biofuels from catalytic conversion of biomass is being considered. Hydrolysis of cellulose to fermentable sugars for bioethanol and acid-catalyzed etherification of glycerol are some examples of catalytic conversion process of biomass into value-added products. Biomass-derived platform molecules contain high amounts of

oxygenated compounds and their conversion to chemicals or fuels require generally reactions involving oxygen removal. Different deoxygenation reactions including dehydration, hydrogenolysis, hydrogenation, decarbonylation and decarboxylation have been reported to remove oxygen functionalities [3]. Hydrogenation (HYD) of biomass-derived platform molecules offers a more promising alternative to carboxylolysis, in terms of higher yields and higher quality of the liquid products [4]. Hydrogen can serve as the deoxygenating agent or it can enter the complex scheme of biomass depolymerization reactions improving the effective H/C ratio. The key challenge of hydrodeoxygenation process is the selective removal of the oxygen functionalities.

The most recent research efforts are being focused on the hydrogenolysis of glycerol, hydrogenolysis of cellulose and hydrodeoxygenation (HDO) of furan compounds. Glycerol can be hydrogenolyzed to 1,3-propanediol, 1,2-propanediol, 1-propanol, 2-propanol and propane potential more valuable products for the production of polyester fibers, fuel gas and other important chemicals.

Cellulose is converted to more valuable sugar alcohols, glycerol, propylene or ethylene glycol through two reaction steps: acid hydrolysis to yield glucose and further hydrogenation/hydrogenolysis reactions to polyols. Biomass-derived furan compounds are obtained from dehydration of pentoses and hexoses. Furfural and 5-hydroxymethylfurfural are mentioned in the top 10 list of an updated evaluation of the U.S. Department of Energy (DOE) of biobased chemicals with high potential for the production of chemicals and fuels [5].

Biomass-derived furan compounds have generated considerable interest around the world because they have an enormous scope of application. In the last years, numerous researches are being developed on the synthesis and applications of HMF and its derivatives. Furan derivatives are considered a potential alternative source of carbon for the transport, polymer and chemical industries.

1.2 HYDRODEOXYGENATION OF 5-HYDROXYMETHYLFURFURAL

One alternative route for producing biofuels and chemicals is through 5-hydroxymethylfurfural (HMF) [6]. This chemical platform can be produced from acid-catalyzed dehydration-cyclization reactions of hexoses which are formed by hydrolysis of carbohydrates in aqueous phase [7]. Several mechanisms have been suggested in the literature for the formation of HMF, although a consensus on the actual mechanism has not been reached. The mechanism more reported is that proposed by Anet [8], in which an aldose-ketose isomerization of fructose is carried out through a 1,2-enediol species, followed by two consecutive β-dehydrations and a ring closure with a final water elimination to obtain HMF (Scheme 1).

Scheme 1. Mechanism pathway in the dehydration of hexoses to HMF proposed by Anet [8]

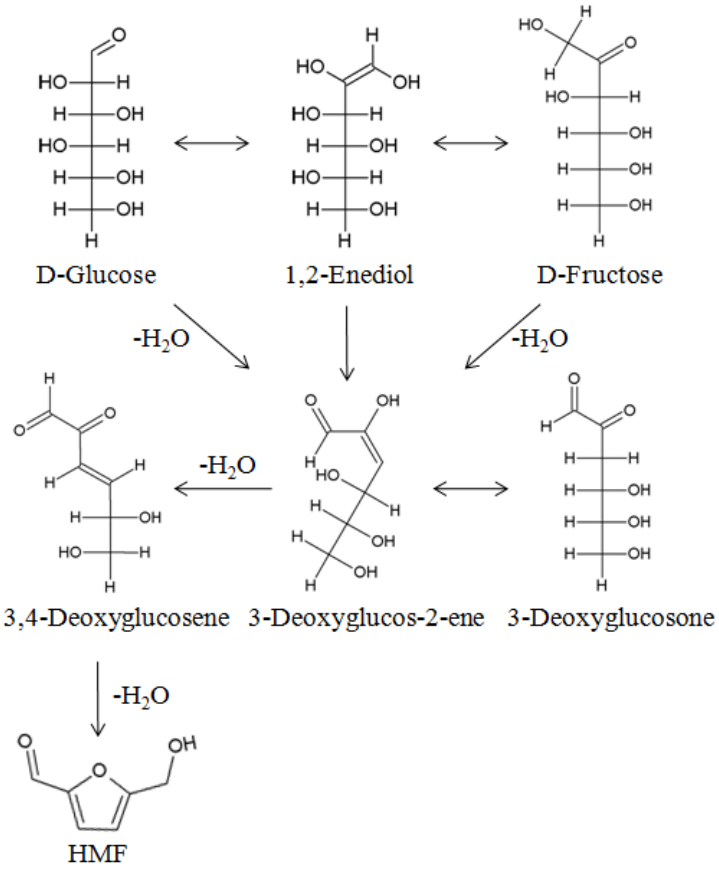

HMF has a high reactivity due to its polyfunctionality, that is, contains an aromatic alcohol, an aromatic aldehyde and a furan ring in the molecule. Reduction, oxidation, condensation and esterification reactions, among others, can be applied to convert HMF into a diversity of compounds for the biofuels, polymers, pharmaceutical and chemical industries. The reduction of HMF to 2,5-dimethylfuran (DMF) for use as a transportation fuel [9,10], the partial hydrogenation of HMF to 2,5-bis(hydroxymethyl)furan (BHF) for use as a monomer[11] and the oxidation of HMF to 2,5-furandicarboxylic acid (FDCA) for the synthesis of polyesters and pharmaceutical products [6,12], are some examples of chemical transformations of HMF to added value products. Nonetheless, this work will focus only on the hydrogenation and hydrodeoxygenation reactions of HMF using heterogeneous catalysts.

Hydrogenation of the C=O bond in HMF produces 2,5-bis(hydroxymethyl)furan (BHF). BHF can be used in the manufacture of polyurethane foams [11]. The product obtained from total hydrogenation of HMF is 2,5-bis(hydroxymethyl)-tetrahydrofuran (BHTHF), which can be used as a monomer for polyester [11]. Schiavo et al. [13] reported the hydrogenation of HMF at 140 °C and 70 bar in presence of Ni, Cu, Pt, Pd and Ru based catalysts. The HMF conversion in aqueous phase over copper chromites and carbon-supported platinum produced BHF, whereas Raney nickel and carbon-supported palladium caused the hydrogenation of the furan ring producing mainly BHTHF.

Schiavo et al. [13] also reported that the hydrogenation of HMF in acidic aqueous phase led to two other products: 1-hydroxyhexane-2,5-dione and hexane-1,2,5-triol in the presence of carbon-supported Pt and Ru catalysts, whereas the Raney Ni and $CuCr_2O_4$ catalysts were inactive. BHF, BHTHF, 1-hydroxyhexane-2,5-dione and hexane-1,2,5-triol were selectively obtained on Ru/C catalyst by varying the reaction conditions and the ruthenium content. A general scheme of the HMF

hydrogenation in aqueous phase reported by Schiavo and co-workers is shown in Scheme 2.

Scheme 2. Reduction of HMF in neutral and acid aqueous medium reported by Schiavo and co-workers [13], (in parentheses the result of product yield obtained for each catalyst)

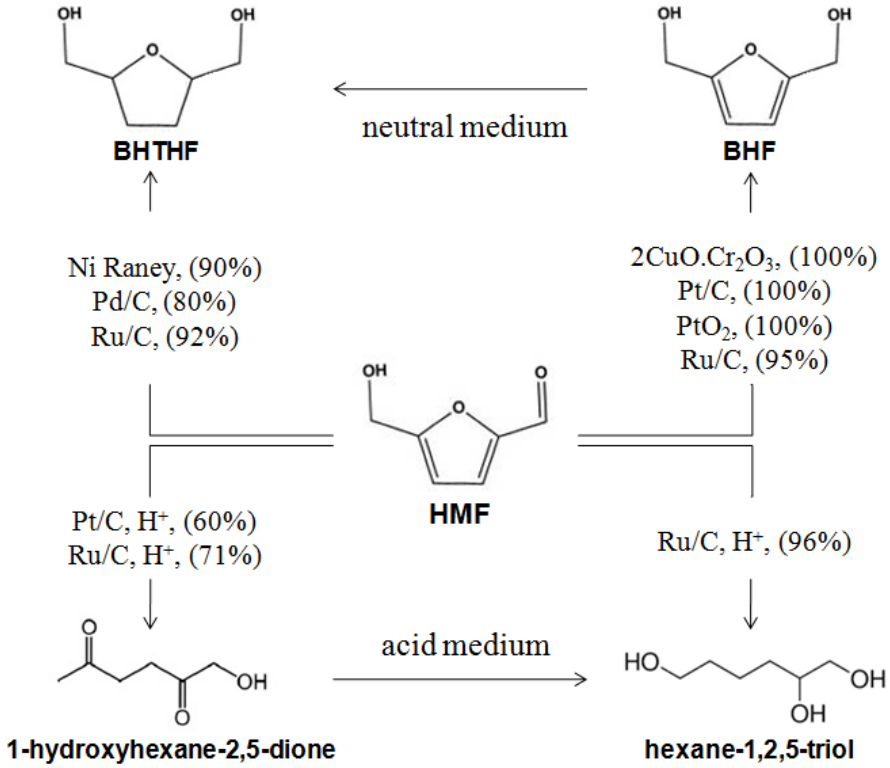

During the catalyst screening study performed by Buntara and co-workers [14] in the conversion of HMF into caprolactam (the monomer for nylon-6), a yield of BHTHF greater than 99% was achieved at 100 °C and 90 bar using Raney nickel catalyst and ethanol as a solvent. Then, BHF was hydrogenated to 1,6-hexanediol (yield of 86%) using a Rh-Re/SiO_2 catalyst in presence of Nafion SAC-13 (acid catalyst). Alamillo et al. [15] also reported the conversion of HMF to BHTHF over Ru catalysts supported on CeO_2, Mg-Zr and γ–alumina with a good yield of BHTHF between 88% and 91%.

The selective hydrogenolysis of HMF to 2,5-dimethylfuran (DMF) has received increasing attention as promising liquid transport biofuels. DMF compared to bioethanol, has a higher calorific value, higher boiling point and a higher octane number and is immiscible with water [9]. Dumesic and co-workers [9] have developed a catalytic strategy to produce DMF from fructose in a two-step process. In the first step, HMF is produced by the acid-catalyzed dehydration of fructose in a biphasic reactor using water and 1-butanol as solvents. The aqueous phase is the reactive phase containing the catalyst and the fructose, and 1-butanol is the phase that extracts the HMF product.

Subsequently in the second step, the purified organic phase (HMF and 1-butanol) is hydrogenolyzed to convert the HMF to DMF. They prepared a carbon-supported Cu:Ru catalyst for the hydrogenolysis of HMF. When the reaction was carried out in a batch reactor the DMF yield was 71%, whereas the DMF yield was 76-79% in a continuous flow reactor for 1.5 and 10 wt% HMF feeds [9]. All reactions were carried out at 100% conversion at a temperature of 220 °C, 6.8 bar initial hydrogen pressure for the batch reactor system, and a liquid feed rate of 0.2 cm^3/min of HMF/1-butanol and a weight hourly space velocity of 0.15 h^{-1} and 0.98 h^{-1} for 1.5 wt% and 10 wt% HMF feeds respectively for the continuous reactor system [9].

Luijkx et al. [16] also reported the HMF hydrogenolysis in alcoholic solvents. They observed unexpected intermediate compounds and selectivity toward DMF of up to 36% using a 10% Pd/C catalyst in 1-propanol at 60 °C under 1 atm of hydrogen in a glass batch reactor. When a 5% Pd/alumina catalyst was evaluated, selectivity to BHF of 73% was obtained and no formation of DMF was observed. However the formation of DMF increased up to 28% adding a small amount of concentrated HCl (Scheme 3).

Therefore, they concluded that the presence of a trace of acid is necessary for the hydrogenolysis of HMF to DMF [16]. Besides, the reaction in water at pH 2.5 led to

the formation of BHF and 1-hydroxyhexane-2,5-dione, with selectivities of 46% and 28% respectively. The selectivity of DMF in water under the conditions mentioned did not exceed 1% [16].

Scheme 3. Reduction of HMF in 1-propanol over 5% Pd/alumina with or without HCl added (R = C_3H_7) reported by Luijkx and co-workers [16], (product selectivities are shown in parentheses)

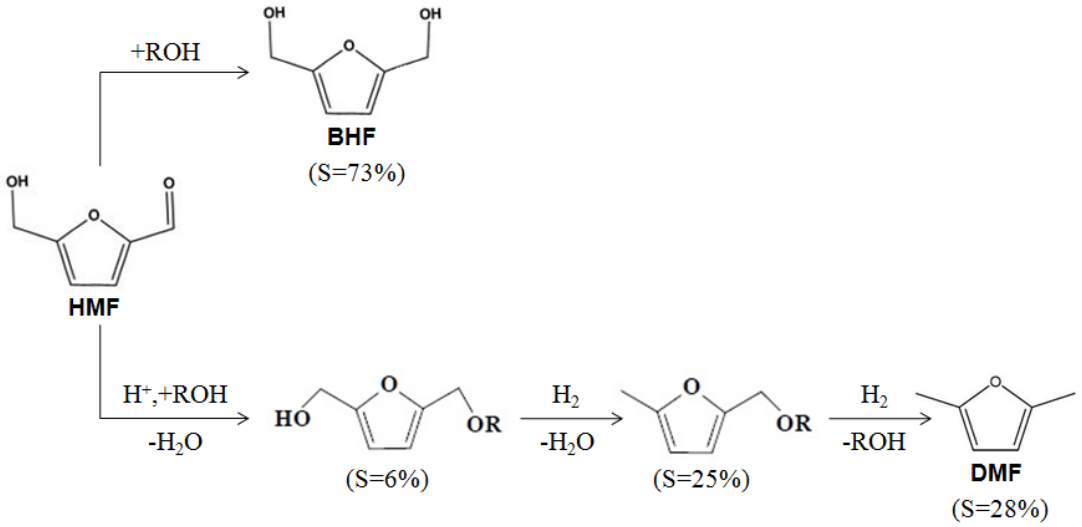

Chidambaram and Bell [17] reported the hydrogenolysis of HMF to DMF in 1-ethyl-3-methylimidazolium chloride (EMIMCl) and acetonitrile over Pd/C. The reaction was carried out in a Parr autoclave at 120 °C, 62 bar of hydrogen pressure and 12 h of reaction. The conversion of HMF was 63% and the selectivity of DMF was 28%. The selectivity of 5-methylfurfural (MFAL) was comparable to that obtained for DMF. Other products like 5-methylfurfuryl alcohol (MFOL) and 2,5-hexanedione (HD) are also observed (Scheme 4). MFAL is used as a natural flavor and fragrance enhancer and as an intermediate for the production of medicines [18].

Scheme 4. Reduction of HMF in EMIMCl and CH_3CN over Pd/C catalyst reported by Chidambaram and Bell [17], (conversion of HMF and product selectivities are shown in parentheses)

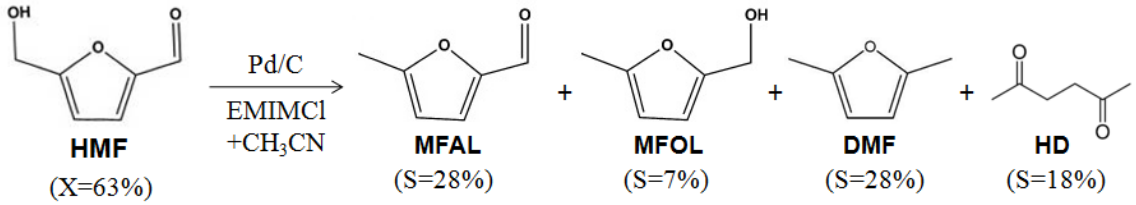

More recently, Zu et al. [19], Nishimura et al. [20], Wang et al. [21], Hu et al. [22], Huang et al. [23], Saha et al. [24] and Kong et al. [25] have reported the selective hydrogenolysis of HMF to DMF. They carried out the reaction over Ru/Co_3O_4, PdAu/C, PtCo in hollow carbon nanospheres, Ru/C, active carbon-supported nickel-tungsten carbide, PdZn/C and Raney Ni catalysts. The hydrogenolysis reaction was performed in presence of solvents like tetrahydrofuran, 1-butanol or 1,4-dioxane. Results show excellent DMF yields (> 85%) with complete conversion of HMF in the range of temperatures between 60 °C and 200 °C.

In most of the researches mentioned above, the hydrodeoxygenation (HDO) of HMF has been performed on batch reactor systems using bulk and carbon-supported catalysts in alcoholic or ionic solvent medium. However, although these contributions have promoted progress in the field, the HDO of HMF presents certain drawbacks: the high cost of the catalysts studied and the use of relatively expensive solvents in the reaction medium. Therefore, the development of a HDO process of biomass-derived furan compounds, that involves the design of new catalysts as well as the application of continuous flow reactor systems, is needed to turn the HDO process into economically feasible one for a large scale biorefinery.

2. EXPERIMENTAL TECHNIQUES

In this research, the reactivity of 5-hydroxymethylfurfural with hydrogen in the presence of supported transition metal catalysts is studied. This chapter describes the procedures for the preparation of the supported catalysts and the characterization techniques thereof. In the same way, the reaction equipment is detailed as well as the methodology used for the catalytic activity evaluation and the analysis of the reaction products.

2.1 SUPPORTS PREPARATION

Silica and gamma-alumina were the supports used for the catalysts preparation. These supports are the most widely used in the industry for their high surface area and thermal stability. The preparation of each support is briefly described as follow:

2.1.1 ***Preparation of silica support.*** The silica support was prepared from a Ludox AM-30 colloidal silica solution (30 wt% in water, Sigma-Aldrich). A volume of 55 cm3 of an aqueous solution of nitric acid (5 wt%) was added to 500 g of Ludox under continuous stirring to produce destabilization of the colloidal system. Afterward, an aqueous solution of NH4OH (20 wt%) was slowly added to neutralize the pH of the solution causing gelation. The gel was aged during 24 h. Later, the aged gel is pelletized using a syringe. The obtained solids were first dried at 105 °C during 12 h and then calcined at 500 °C during 6 h in an oven furnace using a heating ramp of 5 °C/min. Finally, the solids were crushed and sieved to obtain a support of silica in the range of 850-1400 μm.

2.1.2 ***Preparation of γ-alumina support.*** The γ-alumina support used in this study was prepared from commercial Boehmite Catapal B (Sasol) of surface area

of 220 m^2/g. A volume of 450 cm^3 of an aqueous solution of HNO_3 (1 wt%) was added to 600 g of Catapal B alumina. The mixture was kneaded to form a malleable paste and then it was extruded in a cylindrical shape of 1 mm in diameter. The formed extrudates were first dried at 105 °C during 12 h and then calcined at 500 °C during 6 h in an oven furnace using a heating ramp of 5 °C/min.

2.2 SUPPORTED MONOMETALLIC CATALYSTS PREPARATION

Monometallic catalysts were prepared using transition metals precursors of Ni, Pd, Cu and Ru supported on silica or γ-alumina. The incipient wetness impregnation was the method used to prepare the monometallic catalysts. This method consists in adding to the support a metal precursor solution corresponding to the pore volume of the support. The procedure of the catalysts preparation is detailed below.

2.2.1 ***Silica- and alumina-supported Ni catalysts.*** Silica and γ-alumina were impregnated with an aqueous precursor solution of $Ni(NO_3)_2.6H_2O$ (99 wt%, Aldrich). The precursor solution was dropped on the calcined extruded support in order to obtain catalysts with nominal content of 10 wt% Ni. The impregnated solids were rotoevaporated under vacuum (80 mbar) at 60 °C.

The impregnated samples were dried in an oven at 120 °C overnight and then calcined in a gas stream of a 70:30 mixture of air:N_2 (1200 cm^3/min) using the heating ramp presented in Scheme 5. The temperature is increased from room temperature to 150 °C at a rate of 10 °C/min and stays at 150 °C for 1 h, and then it is increased to 260 °C at a rate of 5 °C/min and holds at 260 °C for 2 h. The next ramp continues by rising the temperature up to 500 °C at a rate of 5 °C/min and holds that temperature for 8 h. It is finally cooled to room temperature.

Scheme 5. Heating ramp conditions used in the calcination step of the monometallic Ni and Cu catalysts

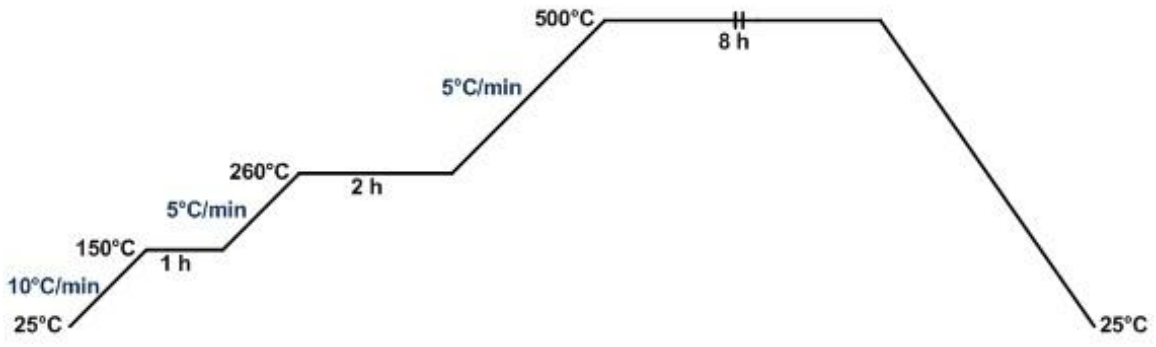

2.2.2 ***Silica- and alumina-supported Pd catalysts.*** Pd-based catalysts were prepared by incipient wetness impregnation of the extruded supports (silica and γ-alumina) using as precursor palladium acetylacetonate (99 wt%, Aldrich) dissolved in toluene (99 wt%, Merck). Each precursor solution was dropped on the calcined extruded support in order to obtain catalysts with nominal content of 1 wt% Pd. The impregnated solids were rotoevaporated under vacuum (80 mbar) at room temperature.

The impregnated samples were first dried in an oven at 120 °C overnight and then calcined at 350 °C in a gas stream of a 70:30 mixture of air:N_2 (1000 cm^3/min) during 4 hours. The temperature was increased from room temperature to 150 °C at a rate of 10 °C/min and held at 150 °C for 30 min; then temperature was increased to 350 °C at a rate of 5 °C/min and held at 350 °C for 4 h and was finally cooled to room temperature.

2.2.3 ***Silica- and alumina-supported Cu catalysts.*** Silica and γ-alumina were impregnated with an aqueous precursor solution of copper nitrate trihydrate (99.5 wt%, Aldrich). The precursor solution was dropped on the calcined extruded support in order to obtain catalysts with nominal content of 10 wt% Cu. The

impregnated solids were rotoevaporated under vacuum (85 mbar) at 60 °C. The impregnated samples were dried in an oven at 120 °C overnight and then calcined at 500 °C in a gas stream of a 70:30 mixture of air:N_2 (1200 cm^3/min) using the heating ramp similar to that employed to prepare the Ni-based catalyst.

2.2.4 ***Silica- and alumina-supported Ru catalysts.*** Ru-based catalysts were prepared by incipient wetness impregnation of the extruded supports (silica and γ-alumina) using an aqueous solution of ruthenium chloride hydrate (99.98 wt%, Aldrich). The precursor solution was dropped on the calcined extruded support in order to attain catalysts with nominal content of 1 wt% Ru. The impregnated solids were rotoevaporated under vacuum (80 mbar) at 65 °C. The impregnated samples were dried in an oven at 120 °C overnight and then calcined at 350 °C in a gas stream of a 70:30 mixture of air:N_2 (1000 cm^3/min) using the heating ramp applied to prepare the Pd-based catalyst.

A summary of the various catalysts supported on silica and alumina, prepared by the incipient wetness impregnation method, is presented in Table 1.

Table 1. Monometallic catalysts supported on silica and alumina

Series of catalysts	Metal	Name	Metal content (wt%)*
Supported on silica	Ni	Ni/silica	10
	Pd	Pd/silica	1
	Cu	Cu/silica	10
	Ru	Ru/silica	1
Supported on alumina	Ni	Ni/alumina	10
	Pd	Pd/alumina	1
	Cu	Cu/alumina	10
	Ru	Ru/alumina	1

*Nominal metal content (wt%)

2.3 SUPPORTED BIMETALLIC CATALYSTS PREPARATION

Four catalysts were prepared by changing the impregnation sequence using the incipient wetness impregnation method in all cases. Nickel nitrate hexahydrate (99 wt%, Aldrich) and copper nitrate trihydrate (99.5 wt%, Aldrich) were the precursors used. Each precursor solution was dropped on the calcined extrudate alumina support in order to obtain bimetallic catalysts with nominal contents of 8 wt% Ni and 2 wt% Cu.

Alumina support was impregnated with the first precursor (Ni or Cu), dried in an oven at 120°C overnight and then calcined in a gas stream of a 70:30 mixture of air:N_2 for 4 h at 500°C using a heating ramp of 10°C/min. Afterwards, the samples were again impregnated with the second precursor and subsequently these were again dried and calcined with the same procedure as described above. The catalysts obtained by this procedure were named as CuNi/A-Int.cal and NiCu/A-Int.cal. That is, in CuNi/A-Int.cal the nickel precursor was impregnated first on alumina, followed by drying and calcination steps, whereas in NiCu/A-Int.cal the first precursor was the copper nitrate. Other catalyst was prepared by removing the intermediate calcination step after first impregnation with the Ni precursor (CuNi/A-Int.dry). Co-impregnation method was used for the preparation of the last catalyst named as CuNi/A-CoImp.

2.4 CATALYST CHARACTERIZATION METHODS

2.4.1 ***Nitrogen adsorption/desorption isotherms.*** Surface area (SA_{BET}) was determined from the nitrogen adsorption isotherm at the boiling point of the liquid nitrogen (-196 °C). The data are modeling according to the BET method (Brunauer, Emmett and Teller [26]), which determines the amount of adsorbed gas corresponding to a monolayer of nitrogen from the isotherm experimental data as described by the next equation:

$$\frac{1}{\left[V_a\left(\frac{P_0}{P}-1\right)\right]} = \frac{C-1}{V_m C} \times \frac{P}{P_0} + \frac{1}{V_m C}$$ Equation 1

being,

P: partial vapor pressure of adsorbate gas in equilibrium with the surface at the boiling point of the liquid nitrogen, in pascals.

P_0: saturated pressure of adsorbate gas, in pascals.

V_a: volume of gas adsorbed at standard temperature and pressure (STP, 273.15 K and 1.013 x 10^5 Pa), in mL.

V_m: volume of gas adsorbed at STP conditions to produce an apparent monolayer on the surface, in mL.

C: dimensionless constant that is related to the enthalpy of adsorption of the adsorbate gas on the catalyst sample. A negative value of this constant is physically meaningless.

From Equation 1, when $V_a(\mathrm{P_0/P - 1})$ is plotted against P/P_0, a straight line should be obtained in the relative pressure range 0.05 to 0.3. The data are considered acceptable if the correlation coefficient, r, of the linear regression is not less than 0.9975. From the linear plot, the slope, S, is $(C-1)/V_mC$ and the intercept, Y_{INT}, is $1/V_mC$. The value of the slope and the intercept are used to calculate V_m and C.

From the value of V_m, the specific surface area, SA_{BET}, in m^2g^{-1}, is calculated as:

$$SA_{BET} = \frac{V_m \ \sigma \ N_A}{(22414 \ cm^3 \ STP)\left(10^{18}\frac{nm^2}{m^2}\right)(m_C)}$$ Equation 2

being,

σ: effective cross-sectional area of one adsorbate molecule (0.162 nm^2 for nitrogen)

N_A: Avogadro number ($6{,}023*10^{23}$)

m_C: mass of the catalyst (g)

Total pore volume and pore size distribution was calculated at P/Po = 0.99 using the BJH model.

This analysis was carried out using a Micromeritics ASAP 2020 instrument at Colombian Petroleum Institute (ICP). The catalysts were previously degassed at 350 °C for 12 h. The technical test procedure is supported by the ASTM D4365-95 and ASTM D3663-03. The instrument was calibrated with a silica-alumina reference material P/N. 004/16821, Lot No. A-501-56 (Multiple point specific surface area: 200.0 ± 6 m^2/g; Total pore volume was determined at Po 0.990 to 0.998).

2.4.2 ***Inductively coupled plasma – optical emission spectroscopy.*** Chemical composition of the catalysts was measured by inductively coupled plasma-optical emission spectroscopy (ICP-OES) with the aim of quantifying the content of Ni, Cu and Pd present in the samples. This technique is based upon the emission of photons from atoms and ions of a sample after being excited within a plasma. Thus the wavelength of the photons is used to identify the elements and the total number of photons is directly proportional to the concentration of the considered element in the sample [27].

Prior to the analysis, the calcined Ni and Cu-based catalysts were subjected to an acid digestion treatment with nitric acid following the ASTM 1977 method. In the case of Pd-based catalysts, the samples were subjected to a mixed treatment of acid digestion with fusion following the UOP 961 method.

The analysis was carried out in a Perkin-Elmer Optima 2100 DV, equipped with a high-resolution double monochromator with a CCD array detector and using argon as plasma gas.

2.4.3 ***X-ray fluorescence spectroscopy (XRF).*** X-ray fluorescence spectroscopy (XRF) was used for the analysis of the Ru-based catalyst samples, since ICP-OES method is not satisfactory for this element. Ru tends to form volatile oxides when the solids are digested. The determination of the ruthenium content was performed in a Bruker S8 Tiger spectrometer. For sample preparation 0.5 g of grounded catalyst were mixed with 10 g of sodium tetraborate and then fused at 1200 °C to form a solid bead.

2.4.4 ***Temperature-programmed reduction (TPR).*** The analysis of temperature-programmed reduction (TPR) allows knowing indirectly the reduction state of the species supported on catalyst. This analysis gives the reduction temperature of the species and from reference material TPR profiles it is possible to infer which species are present.

In the case of this research, the supported species are oxides that in presence of hydrogen are reduced to obtain their corresponding metal according to the next reaction:

$$MO_{X(s)} + xH_{2(g)} \rightarrow M^{0}_{(s)} + xH_2O_{(g)} \qquad \text{Equation 3}$$

Prior to the analysis, the calcined catalyst samples were pretreated at 120°C for 2 h using an Ar flow rate of 50 cm^3/min (20 psi). The reduction of the catalysts was carried out under a 10% H_2/Ar flow rate of 50 cm^3/min (20 psi), at a heating ramp of 10°C/min from room temperature to 1000°C. The hydrogen uptake was monitored by the change in the thermal conductivity detector (TCD) signal. This analysis was carried out in a Micromeritics Autochem II 2920 instrument. The equipment was

calibrating using a silver oxide reference material P/N. 004/16836/00, Lot No. A1207 (Peak temperature: 119.0 ± 15 °C; Hydrogen consumption: 93.9 ± 3 cm^3/g).

To determine the hydrogen consumption per active metal of the catalysts, a pure copper oxide reference material (P/N. 004/16828/00, Lot No. 905692-4) was used to calculate the response factor of the equipment, as it is shown below:

$$Hydrogen consumption\ per\ active\ metal = \frac{H_2}{Me^*}\left(\frac{mol}{mol}\right)$$

$$= \frac{TPR\ area\ \ of\ \ catalyst\ \ \ (m^2)}{mol\ \ of\ \ Me^*} \times \frac{1\ mol\ \ H_2\ consumption\ \ \ by\ \ CuO}{TPR\ area\ \ of\ \ CuO\ \ (m^2)} \qquad \text{Equation 4}$$

Me^*: active metal presents on the catalyst (Ni, Pd, Cu or Ru)

$TPR\ area\ of\ CuO$: 46,829 m^2

2.4.5 ***Gas chemisorption.*** The selective chemisorption of probe molecules as H_2 and CO onto the catalyst surface allows estimation of metal dispersion as well as the specific surface area and medium-size of the metal particles.

This technique consists in determining the quantity of chemisorbed gas during the formation of a monolayer of gas on the exposed metal surface. This analysis is performed saturating the sample with successive pulses of a known volume of a probe gas. From both the quantity of chemisorbed gas and the stoichiometry that represent the gas-metal adsorption mechanism, it is possible to determine the metal dispersion (*D*) as follow:

$$D = \frac{N_M}{N_T} \qquad \text{Equation 5}$$

$\mathbf{N_M}$ represents the moles of surface metal atoms over weight of catalyst, defined as:

$$N_M = \frac{V_{ads}\,\nu}{V_g\,m_C} \qquad \text{Equation 6}$$

where:

V_{ads}: volume of gas adsorbed when a monolayer is formed at STP (cm^3)

ν: stoichiometry factor of adsorption (molecules of gas per atom of exposed metal)

V_g: molar volume gas at STP (22,414 cm^3/mol)

m_C: catalyst weight (g)

STP: Standard Temperature and Pressure conditions (273.15 K and 1.013 x 10^5 Pa)

$\mathbf{N_T}$ represents the total moles of metal atoms per unit weight of catalyst, defined as:

$$N_T = \frac{W}{M} \qquad \text{Equation 7}$$

where:

W: percentage of metal in the catalyst (grams of metal/grams of catalyst)

M: atomic weight of the supported metal (grams per mol of metal)

The stoichiometry factors of gas-metal adsorption and the cross-sectional area of a metal atom of Ni, Pd, Cu and Ru are presented in Table 2, which were established from the results reported in literature for catalysts with similar composition [28-31].

Table 2. Stoichiometry factor of gas-metal adsorption

Metal	ν[a]		σ (nm^2/atom)[b]
	H_2/Me	CO/Me	

Ni	0.5	1.0	0.0649
Pd	0.5	0.67	0.0787
Cu	-	1.0	0.0711
Ru	1.0	1.0	0.0613

[a]ν: stoichiometry factor of adsorption (molecules of gas/atom of metal)
[b]σ: cross-sectional area of the metal atom

The medium diameter of the metal particles (d_m) is calculated from the dispersion data, assuming that the particles are spherical:

$$d_m = \frac{6}{\rho N_T \sigma N_A \mathrm{m_C}} \qquad \text{Equation 8}$$

being,

ρ: density of metal (g/cm^3)

N_T: total moles of metal atoms per gram of catalyst (mol/g cat)

σ: surface of metal atom (nm^2/at.)

N_A: Avogadro's number (6.023*10^{23} molecules of gas/mol gas)

$\mathrm{m_C}$: catalyst weight (g)

Metal dispersion (*D*) of the catalysts was determined with a Micromeritics Autochem II 2920. Prior to the analysis, the calcined catalyst sample was dried at 120°C using He at a flow rate of 20 cm^3/min (20 psi) for 1 h to remove the physically adsorbed water. All catalysts were reduced in a H_2 flow of 20 cm^3/min (20 psi), with a heating ramp of 10°C/min and once the reduction temperature was attained the catalyst was kept at this temperature for 2 h. The Ni and Cu-supported catalysts were reduced at 500°C and the Ru and Pd-supported catalyst were reduced at 350°C. Metal dispersion (*D*) and active metal particle size (d_m) were determined from quantification of the irreversibly chemisorbed gas molecules at 35 °C and 20 psi. The probe molecule for the monometallic Ni, Pd and Cu catalysts

was carbon monoxide and for the Ru based catalysts was hydrogen. The specific use of these probe molecules was chosen in order to minimize the effects of phenomena such as SMSI (support-metal strong interaction) and spillover, which interfere in the accurate determination of the quantity of chemisorbed gas on the metal surface. The equipment was calibrated with a Pt/alumina reference material P/N. 004/16825/00, Lot No. CH030016-7 (Metal dispersion: 31 ± 5%).

2.4.6 ***Elemental analysis of carbon.*** Elemental analysis of carbon of the spent catalysts after the activity tests was measured on a LECO CS230 carbon determinator. The analysis consists in determining the concentration of CO_2 through IR absorption cell. A sample of 0.1 g of catalyst is combusted in a stream of purified oxygen. The carbon present in the sample is oxidized primarily to CO_2 with some CO possibly being produced. The gases are then routed through a heated catalyst which converts CO to CO_2. Then CO_2 is measured in an IR cell. This procedure is repeated three times and the average carbon content is reported. The equipment is calibrated using a cast iron reference material P/N. 501-024, Lot No. 1019 (%Carbon: 3.29 ± 0.04; %Sulfur: 0.041 ± 0.002).

2.4.7 ***Attenuated total reflectance – infrared spectroscopy (ATR-IR).*** Measurements in ATR-IR spectroscopy are performed in order to elucidate the type of carbonaceous material deposited on the catalyst. Infrared spectra (IR) of the calcined and spent catalysts were measured on a Shimadzu IR- Prestidge 21 spectrometer equipped with an ATR attachment (Pike-Miracle) and a DTGS detector. Samples were grinded in a mortar before the analysis. 5 mg of the sample was pressed to obtain a self-supported wafer. Each spectrum was recorded with a resolution of 8 cm^{-1} and 32 scans from 4000 to 650 cm^{-1}. All spectra were collected every 15 s.

2.4.8 ***X-ray photoelectron spectroscopy (XPS).*** XPS measurements were performed on a SSI-X-probe (SSX-100/206) photoelectron spectrometer (Surface

Science Instruments) equipped with a monochromatic microfocused Al Kα X-ray source (1486.6 eV).

For this analysis, fresh tablets were first grounded in an agate mortar and the obtained powder was then pressed into small stainless steel troughs mounted on a multi-specimen ceramic holder. The pressure in the analysis chamber was around $1.3x10^{-6}$ Pa. The analyzed area was approximately 1.4 mm^2 (1000 µm x1700 µm) and the pass energy was 150 eV. In these conditions, the full width at half maximum (FWHM) of the Au $4f_{7/2}$ peak of a clean gold standard sample was about 1.6 eV. A flood gun set to 8 eV and a Ni grid placed 3 mm above the sample surface were used for charge stabilization.

The following spectra were recorded: general spectrum, C 1s, O 1s + V $2p_{3/2}$, Al 2p, N 1s and C 1s again to check the stability of charge compensation in function of time. The spectra were decomposed with the CasaXPS program (Casa Software Ltd., UK) with a Gaussian/Lorentzian (85/15) product function after subtraction of a Shirley baseline.

2.5 CATALYTIC EXPERIMENTS

2.5.1 ***Description of the reaction equipment.*** The evaluation of catalytic activity of the catalysts was carried out in a commercial Parr downflow reactor, whose parts are shown in Scheme 6. This reactor system contains a feed tank of 1 L. The feed is pumped to the reactor through a HPLC pump series III Lab Alliance. The flow rate can be set from 0 to 10 mL/min in increments of 0.01 mL. The maximum pressure limit of the HPLC pump is 5000 psi.

The reactor system also contains a mass flow controller for hydrogen (Brooks Instrument ModelSLA5850SZ364), whose maximum operating pressure of the gas

is 1500 psi and the maximum flow rate range in standard cubic centimeters per minute is 200 sccm.

The reactor system features a vertical downflow tubular reactor in stainless steel, inlet diameter of 1.27 cm and length of 61.5 cm. Heating is accomplished with a vertical split tube furnace with three heating zones surrounding the reactor (maximum operating temperature is 550 °C). Temperature in the reactor is monitored by a thermocouple located in the catalyst bed.

The reactor outlet is connected to a tube-and-shell heat exchanger at the bottom to cool the products of the reaction below ambient temperature (the heat exchange area is 0.018 m^2). The liquid reaction product is collected in a tank of 300 mL connected to the output of the heat exchanger. A back pressure regulator in the downstream of the reactor maintains the reactor pressure at the desired setpoint. In addition, a rupture disc is installed into the system for protection from potential damage from overpressure (maximum operating pressure of 1500 psi).

The reactor system is controlled through a Honeywell HC900 hybrid controller with data visualization software SpecView 32 Bld#847 version 2.5.

2.5.2 *Methodology of the catalytic reaction tests*

2.5.2.1 *Charge and activation of the catalyst*. The reactor was charged with 4 g of catalyst mixed with 2.5 g of 80-mesh quartz sand to prevent poor distribution of the liquid, dried zones, hot sports and external diffusional limitations. The catalyst bed was contained in the tubular reactor by means of two end-plugs of quartz wool. The Scheme 7 shows a representation of the packed-bed tubular reactor.

Scheme 6. Reaction system used for the HMF hydrodeoxygenation tests

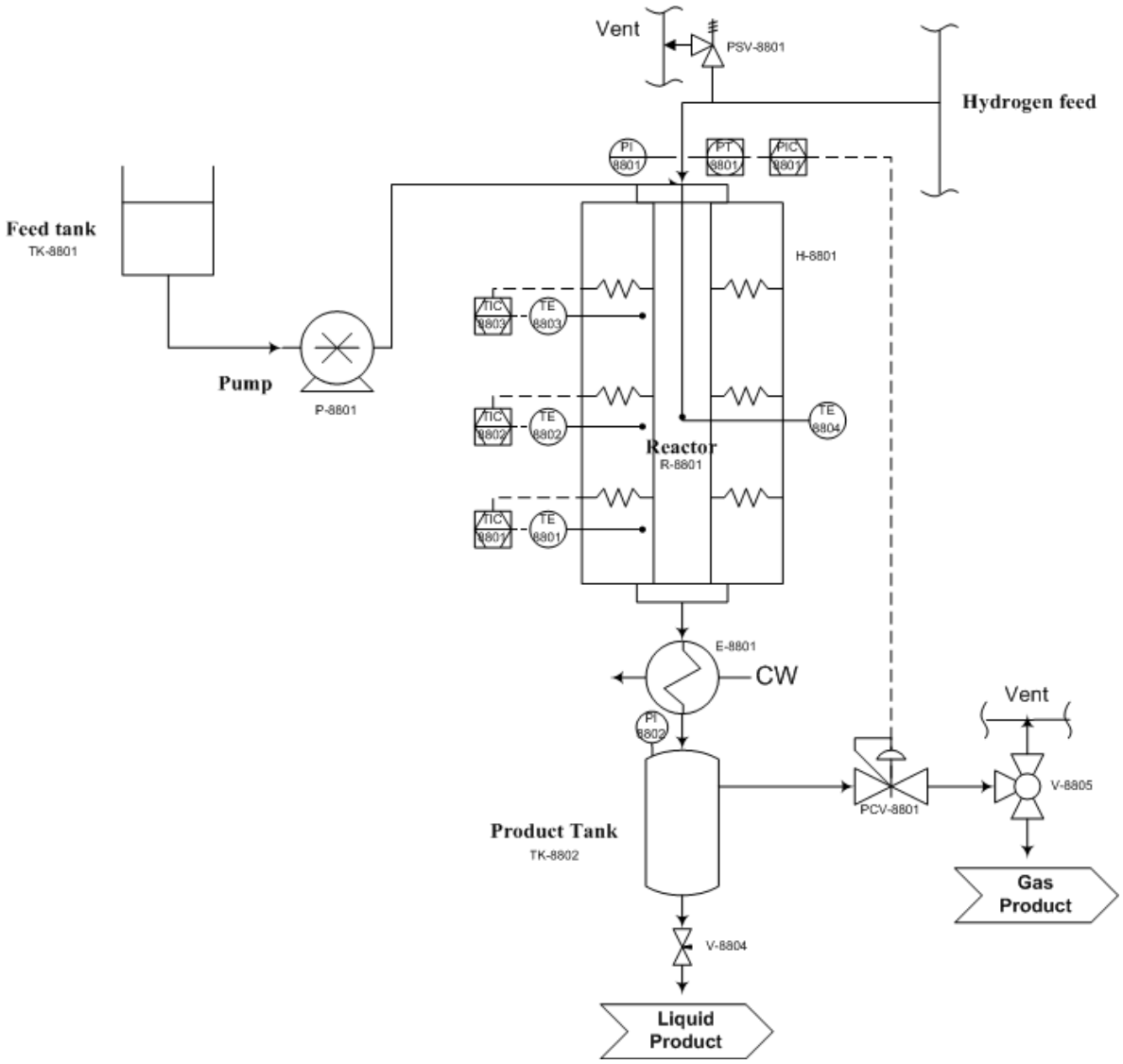

Scheme 7. The packed-bed tubular reactor for the hydrodeoxygenation of HMF

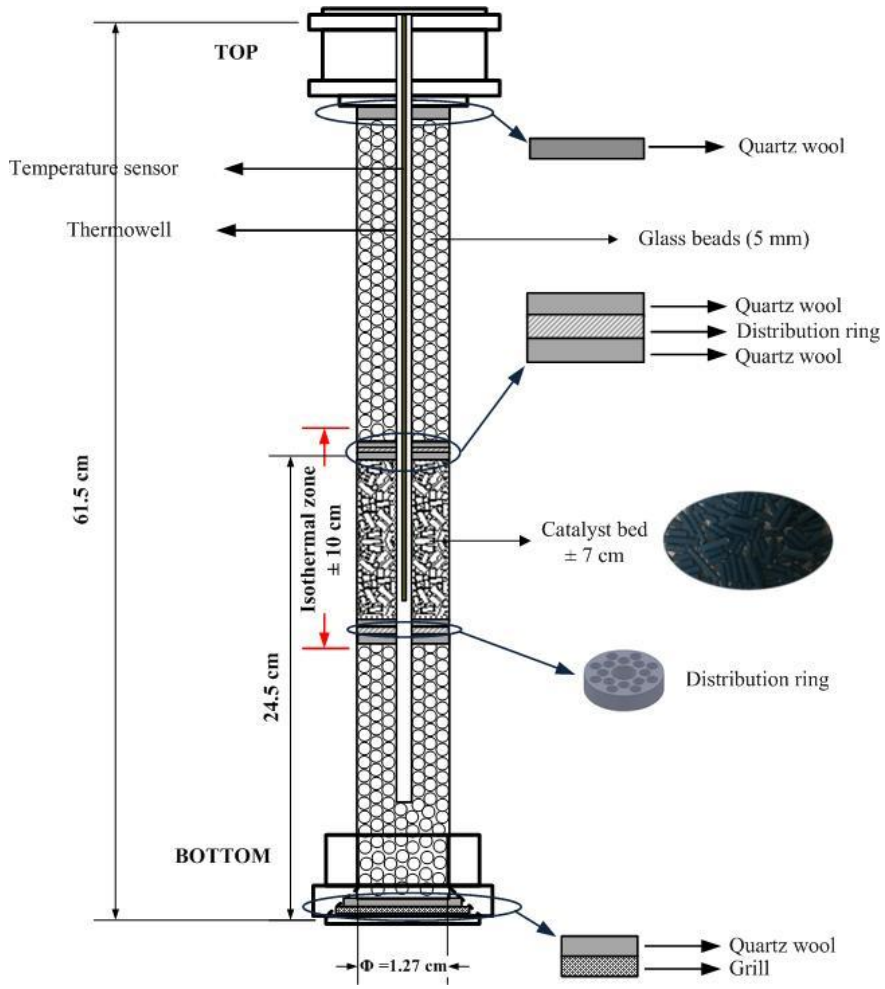

Once the catalyst was charged, a leak test was performed by pressurizing the reactor to 2 MPa with nitrogen during 2 hours. Pressure drops should not be more than 0.007 MPa per hour to proceed to the activation step. Then, the reactor was depressurized to start the drying of the catalyst at 120 °C with a N_2 flow of 100 cm^3/min for 12 h. After the drying step, the catalyst was activated with a H_2 flow of 100 cm^3/min at 500 °C for Ni and Cu-based catalysts and at 350 °C for the Pd and Ru-based catalysts during 4 h before the HMF hydrogenation tests.

2.5.2.2 *Catalytic activity tests*. In all the experiments, an aqueous solution of 5 wt% HMF is fed into the fixed-bed reactor with a liquid feed rate of 0.2 cm^3/min and a flow rate of 50 cm^3/min of H_2. Pressure in the reactor was 0.41 MPa. The effluent from the reactor was condensed at room temperature in a stainless steel separator. All of the experiments were carried out at three temperatures: 137 °C, 155 °C and 189 °C, using the same catalyst in a sequential way. Once the desired reaction temperature was achieved, 4 h was awaited before product sampling (30 min) and afterward the reaction temperature was increased to the next level. At the end of the activity test the liquid feed pump was cut off and the catalyst was maintained under a flow of hydrogen during 4 h at 189 °C. Then, the H_2 flow was shifted to N_2 flow at 189 °C during 12 h and finally temperature was decreased under N_2 flow.

2.5.3 ***Analysis of the reaction products.*** Since there is no a specific analytical method to analyze the liquid product samples, it was necessary to develop one. After several tests, it was concluded that the extraction of the aqueous samples with dichloromethane and the subsequent analysis by GC-MS and GC-FID is the best method. A sample of the aqueous product obtained in the reaction test (3 g) was extracted 3 times using 20 cm^3 of dichloromethane (99%, Merck) each time. An aliquot of the final organic sample is analyzed by GC-MS and GC-FID. The mass spectrometer was used to confirm the nature of the compound separated by the gas chromatography column and the FID to quantify the concentration of the products.

As the first step of the procedure involves extraction with dichloromethane, it was necessary to establish the partition coefficient of the different products between the aqueous and organic phases. This part was performed using high-performance liquid chromatography (HPLC). The recovery of the reaction products was determined by HPLC analysis of the aqueous sample before and after dichloromethane extraction.

The HPLC analysis was carried out in a VWR Merck-Hitachi L-2000 series LaChrom Elite system equipped with a diode array detector and an L-2400 UV detector. The reverse-phase column used was an Agilent Zorbax Eclipse XDB-C18 (150 mm x 4.6 mm ID, 5 µm particle size). The samples were eluted with 5 mM H_2SO_4 at 0.6 cm^3/min. The injection volume was 20 µL. The monitored wavelength was 282 nm. Several aqueous samples were extracted and then the average recovery of HMF was calculated to be 60%. In the HPLC analysis of the aqueous phase samples after extraction, other compounds different from HMF were not observed. So all yield calculations for other compounds different of HMF were based on products' concentration detected in the dichloromethane phase after extraction using GC-FID.

2.5.3.1 *Gas chromatography coupled with a mass spectrometer (GC-MS)*. This analysis was performed to identify the products obtained in the HMF hydrodeoxygenation reaction. The samples were injected in an Agilent 7890A gas chromatograph equipped with an Agilent 5975C mass spectrometer. The analysis conditions of the gas chromatograph are summarized in Table 3. The mass spectra of some furanic compounds are shown in Annex A.

Table 3. Analysis conditions of the gas chromatograph

Gas Chromatograph Agilent 7890A	
Column	DB-5MS (30 m x 0.25 mm x 0.25 µm)
Carrier gas	Helium
Temperature range in the column	35-300 °C
Injector temperature	250 °C

2.5.3.2 *Calibration*. The quantitative determination of extracted furanic compounds was done using both external and internal standard methods to calculate the relative response factors (RRF) of each compound. In this way, some

errors from the preparation and analysis steps of the samples can be corrected, such as deviations in the injection volume, variation in analyte concentration due to evaporation of the solvent, among others.

The methodology involves first the preparation of standard solutions of a known concentration to build a calibration curve for each compound and then the addition of an internal standard of constant concentration to each solution. The internal standard should be inert, soluble in the sample and their signal should not interfere with that of the analyte. From the calibration curve, the relative response factor (RRF) of each compound is calculated using the following equation defined by Scanlon and Willis [32]:

$$RRF_i = \frac{{}^{C_i}/_{C_s}}{{}^{A_i}/_{A_s}} \qquad \text{Equation 10}$$

being,

RRF_i: relative response factor of the analyte i
C_i, C_s: concentration of the analyte i and the internal standard, respectively
A_i, A_s: signal area of the analyte i and of the internal standard, respectively

The following compounds were acquired from Sigma-Aldrich and were used for the calibration method: 5-hydroymethylfurfural (HMF), 5-methylfurfural (MFAL), 5-methyl-2-furfuryl alcohol (MFOL), furfural (FAL), 2-furfuryl alcohol (FOL), tetrahydrofurfuryl alcohol (THFOL), 2,5-dimethylfuran (DMF), 2,5-dimethyltetrahydrofuran, cis & trans (DMTHF), 2,5-hexanedione (HD), 2,5-diformylfuran (DFF) and 2-methylfuran (MF). Dodecane (C12) was used as an internal standard. The data to calculate the RRF for each compound have a good fit line, presenting R^2 values greater than 0.998.

Other compounds were detected in very low concentrations and the relative response factors of these compounds were calculated using the effective carbon number (ECN) concept [32]. The relative response factor (RRF) of an analyte is defined as follows [32]:

$$RRF_i = \frac{ECN_s MW_i}{ECN_i MW_s} \qquad \text{Equation 11}$$

where,

ECN_S, ECN_i: are the effective carbon number of the internal standard and the analyte, respectively

MW_i, MW_S: molecular weight of the analyte and the internal standard, respectively

Jorgensen et al. [33] quantified the ECN contributions of six different types of functional groups from the analysis of 56 compounds. In the Table 4 is presented a summary of the average ECN contributions of the functional groups of interest for this work, which were reported by Jorgensen et al. [33].

Table 4. ECN contributions of some functional groups

Functional group	ECN
Ketones	-0.80
Alcohols	-0.64
Ethers	-0.78
Furans	-0.78

In Annex B is found the relative response factor of all compounds identified by GC-MS, which were calculated experimental and theoretically, as well as the retention time of each compound.

2.5.3.3 *Gas chromatography coupled with a flame ionization detector (GC-FID).* The quantification of the obtained products, previously identified by GC-MS, was performed using gas chromatography coupled with a flame ionization detector (FID). For this analysis was used an Agilent 7890A gas chromatograph using the same column and analysis conditions that were described in Table 3.

The concentration of the compounds that are present in the organic sample can be calculated from Equation 10 using the RRF of each compound determined experimentally (or theoretically in the case of compounds that were not calibrated), the peak areas of each compound and of the internal standard and the concentration of the used internal standard (which is constant for all samples). In this work, all samples (including the standards solutions) were prepared using 1 mL of solution with 1 μL of n-docecane, so the concentration of n-dodecane was 0.057 g of dodecane/g of solution.

2.5.3.4 *Data processing*. Conversion and yields of the reaction were calculated from the concentration of the compounds detected in the organic phase. It was considered complete extraction of the products in the organic phase. In the case of HMF an average recovery of 60% was considered to determine the grams of HMF in the reaction products. So all conversion and yields were calculated with the following formulas:

$$conversion(\%) = \frac{mass\ \ HMF\ \ inlet\ \ (g) - mass\ \ HMF\ \ in\ product\ \ (g)}{mass\ \ HMF\ \ inlet\ \ (g)} * 100 \quad \text{Equation 12}$$

$$yield(\%) = \frac{mass\ \ of\ \ product\ \ \ outlet\ \ (g)}{mass\ \ HMF\ \ inlet\ \ (g)} * 100 \quad \text{Equation 13}$$

3. HYDRODEOXYGENATION OF HMF OVER SILICA-SUPPORTED CATALYSTS IN AQUEOUS MEDIUM

In this chapter, the hydrodeoxygenation of 5-hydroxymethylfurfural (HMF) is studied in the presence of silica-supported catalysts in aqueous phase. The catalytic activity was evaluated in a downflow reactor in view of a possible application to a large scale biorefinery process. Silica was chosen as the catalyst support since it has been widely used in the manufacture of many industrial catalysts. The effect of metals such as Ni, Pd, Cu and Ru supported on silica were evaluated in the hydrodeoxygenation of HMF in order to compare their catalytic behavior.

3.1 CATALYSTS CHARACTERIZATION

Metal content, BET surface area, metal dispersion and active metal particle size of the silica-supported catalysts are summarized in Table 5. In general, metal content of the catalysts is similar to the theoretical expected value for each metal, although the Pd/silica and Ru/silica catalysts present a slightly lower metal content compared to the nominal ones.

The impregnation of the metals on the support causes a decrease in the catalysts surface area and this effect is more pronounced on the Ni- and Cu-supported catalysts. It might be related to the higher metal content on the support. It has been shown elsewhere that the surface area is likely to decrease as a result of the partial blocking of the support pores by the metal particles [34, 35]. Total pore volume (TPV) decreases by 16.3% and 18.6% for the silica-supported Ni and Cu catalysts respectively, whereas it does not decrease for the silica-supported Pd and Ru as compared to the silica support.

Table 5. Characterization of the monometallic Ni, Pd, Cu and Ru catalysts supported on silica

Catalyst	Metal content (wt%)	Surface area (m^2/g)	TPV[a] (cm^3/g)	D[b] (%)	d_p[c] (nm)	H_2/Me[d] (mol/mol)
silica	-	167	0.43	-	-	-
Ni/silica	10.6	136	0.36	15.3	6.6	0.96
Pd/silica	0.5	164	0.43	31.2	3.6	-
Cu/silica	10.7	131	0.35	18.0	5.8	0.99
Ru/silica	0.3	163	0.43	2.0	n.d	2.35

[a]TPV: Total pore volume (cm^3/g)
[b]D: metal dispersion (%)
[c]d_p: active metal particle size (nm)
[d]Molecular hydrogen consumption per active metal (Me: Ni, Pd, Cu, Ru) present on the catalysts

The N_2 adsorption-desorption isotherms and BJH pore size distributions of the calcined support and silica-supported monometallic catalysts are depicted in Figure 1. BJH pore size distributions were obtained from desorption branches of the isotherms. Silica support and the silica-supported catalysts show a type IV isotherm and type H2 hysteresis loops, indicating the presence of mesoporous with ink-bottle pore shape [36].

The average pore diameter is centered on 7.5 nm for both the support and the silica-supported catalysts. These results indicate that the pore structure of the silica support is unaffected by the impregnation with the metals. Sietsma et al. [37] have shown that the impregnation and calcination steps used to convert the precursor into the desired Ni metal have little effect on the pore diameter of the accessible mesoporous of SBA-15 with Ni contents between 9% and 24%.

Figure 1. Nitrogen adsorption-desorption isotherms and pore size distributions (inset) of support and silica-supported monometallic catalysts

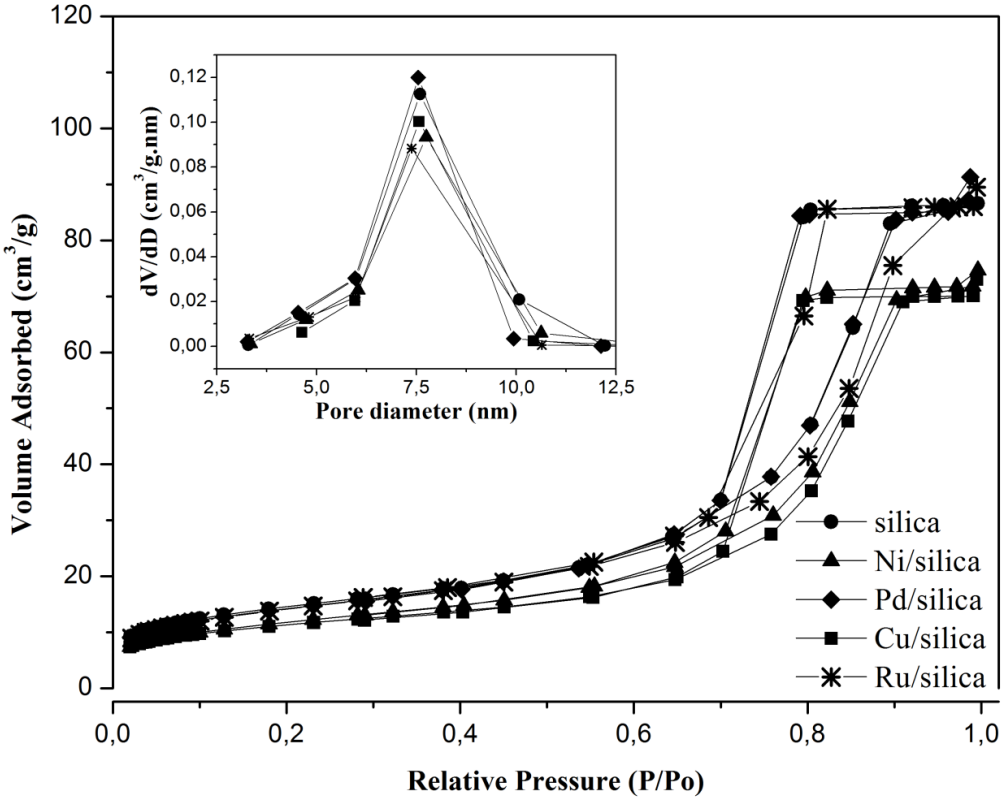

The silica-supported catalysts have a metal dispersion between 2 and 31% (Table 5). Other authors have found similar metal dispersion on Ni-, Pd- and Cu-silica catalysts [38-40]. On Ru/silica catalyst a very low value of metal dispersion is observed. Vasiliadou et al. [41] showed that the metal dispersion of the silica-supported Ru catalysts could not be determined by the H_2 chemisorption due to the low H_2 uptake at chemisorption temperatures in the range of 30-250 °C. The metal particle sizes of the silica-supported Ni, Pd and Cu catalysts are 6.6 nm, 4.2 and 5.8 nm respectively.

The TPR profiles of the calcined silica-supported catalysts are illustrated in Figure 2. The profiles of Pd, Cu and Ru-supported catalysts were magnified 30, 2 and 20 times respectively, for comparative purposes. In the case of Ni-supported catalyst a broad reduction peak is displayed, which is deconvolved into four Gaussian-type peaks for a better interpretation of the results. The two low temperature peaks have been ascribed to the reduction of NiO with a weak interaction between metal and support [42]. The reduction temperature peak centered at 463 °C could be assigned to the reduction of NiO strongly interacting with the support [42] and at 528 °C could be associated to nickel silicate species [43].

Figure 2. TPR profiles of the calcined monometallic catalysts supported on silica

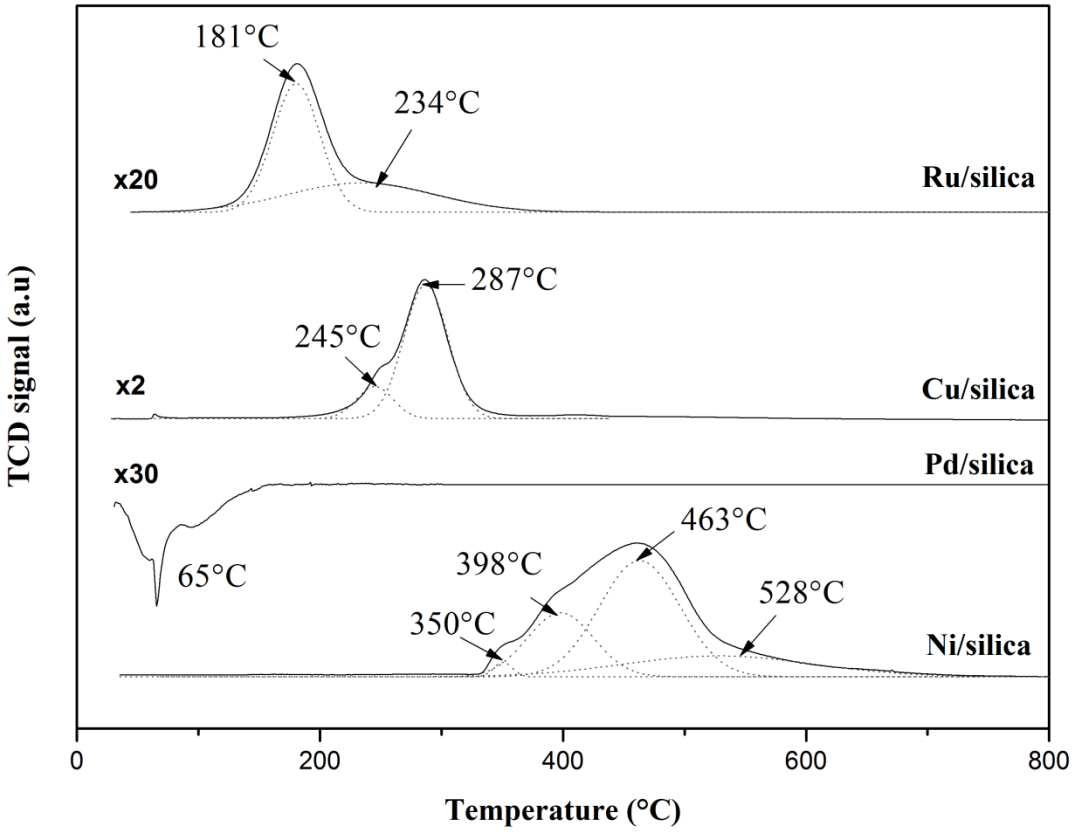

TPR profile of silica-supported Cu catalyst shows two overlapping peaks situated at 245 °C and 287 °C, which have been attributed to the reduction of highly dispersed amorphous and bulk CuO species, respectively [44].

In the case of Pd-supported catalyst, the TPR profile shows a negative peak at 65 °C assigned to the decomposition of the β-Pd hydride phase [45, 46]. PdO is not detected at the conditions of the TPR experiment since the reduction of these particles has been reported to be achieved at temperatures below 20 °C [47].

Likewise, Ru-based catalyst presents two reduction peaks situated at 181 °C and at 234 °C. The lower temperature peak has been associated to the reduction of well-dispersed RuO_x species, whereas the higher temperature peak is assigned to the reduction of RuO_2 particles [48]. Nurunnabi et al. [49] have also studied the reducibility of silica-supported Ru catalysts, finding only one reduction peak situated at 167 °C that they assigned to the reduction of RuO_2.

The total hydrogen consumption per active metal measured by TPR analysis for the silica-supported catalysts is shown in Table 5. The amount of hydrogen consumed per mole of Ni and Cu is found to be nearly equal to unity, which indicates a complete reduction of these metals [50].The reduction degree results of the silica-supported Ni and Cu catalysts are consistent with those reported elsewhere for catalysts with similar Ni and Cu content [51-53]. The hydrogen consumption of Pd/silica is not determined since no reduction peak of PdO is detected in the TPR analysis [46]. Ru/silica catalyst presents higher hydrogen consumption than the expected value.

3.2 CATALYSTS EVALUATION

Conversion and product yields obtained in the hydrodeoxygenation of 5-hydroxymethylfurfural (HMF) over the silica-supported Ni, Pd, Cu and Ru catalysts are summarized in Table 6. In the “others” column the sum of the yield of minority compounds obtained on the conversion of HMF is presented.

Some preliminary tests, developed charging the reactor with sand to evaluate the reactivity of HMF in the absence of catalyst, have shown that sand was inactive at low temperatures and a 3 wt% yield of 2,5-diformylfuran (DFF) was observed at 189 °C. The results obtained with sand are not included in Table 6.

Other tests were also performed to evaluate the activity of the bare silica support. It was found that silica support was inactive when the reaction was carried out at both low and medium reaction temperatures, but it had a conversion of HMF less than 10 wt% at 189 °C. 2,5-diformylfuran (DFF) and 5-methylfurfural (MFAL) were the products observed at this reaction temperature with yields of 5 wt% and 1 wt%, respectively. The bare silica conversion and product distribution results are not included in Table 6. DFF is likely formed from dehydrogenation of the hydroxyl group of HMF. Matsumura et al. [54] studied the dehydrogenation of ethanol to acetaldehyde over highly dehydrated silica solids. They suggested that the active site is a Si-O-Si oxygen bridge formed by dehydration of silica at high temperature, which is responsible for the dehydrogenation activity [54]. As it has been shown elsewhere MFAL is produced from hydrogenolysis of the HMF hydroxyl group [55].

HMF conversion on the silica-supported catalysts is in the range of 12-32 wt% when the reaction is evaluated at 137 °C, being the silica-supported Ni and Pd catalyst the most active. As the temperature increases to 155 °C, the conversion becomes almost complete for the Ni/silica and Pd/silica catalysts, whereas

Cu/silica and Ru/silica catalysts show very low conversions, 5 wt% and 6 wt% respectively, and some deactivation compared to the activity results at 137 °C.

Table 6. Conversion and liquid product yield obtained over Ni, Pd, Cu and Ru supported on silica as a function of temperature

Catalyst	Temp.	Conv.	Product liquid yield (wt%)					
	(°C)	(wt%)	BHF[a]	MFAL[b]	MFOL[c]	FOL[d]	THFOL[e]	Others
	137	26	-	-	-	11.9	-	0.7
Ni/silica	155	95	-	5.1	2.9	64.2	-	4.1
	189	16	-	1.9	-	3.2	0.6	1.6
	137	32	-	2.2	1.4	10.8	2.7	5.3
Pd/silica	155	96	-	5.7	2.4	49.4	14.6	7.5
	189	31	-	2.3	-	16.6	2.4	2.2
	137	15	-	-	-	-	-	3.0
Cu/silica	155	5	-	1.0	-	-	-	0.5
	189	9	-	1.0	-	-	-	2.3
	137	12	-	0.3	-	0.8	-	0.8
Ru/silica	155	6	-	1.2	-	2.0	-	2.7
	189	14	-	1.6	-	0.9	-	4.2

[a]*BHF*: 2,5-bis(hydroxymethyl)furan
[b]*MFAL*: 5-methylfurfural
[c]*MFOL*: 5-methyl-2-furfuryl alcohol
[d]*FOL*: furfuryl alcohol
[e]*THFOL*: tetrahydrofurfuryl alcohol

Unexpectedly, all silica-supported catalysts present a dramatic decrease in the conversion at 189 °C. It is likely that this drop in conversion is caused by deactivation of the catalyst. It will be shown later that the amount and type of

carbonaceous material deposited on the spent catalyst might be the cause of deactivation.

The main products obtained from the conversion of HMF over silica-supported Ni catalyst as a function of the temperature are summarized in Table 6. At all reaction temperatures furfuryl alcohol (FOL) is the major product obtained, suggesting decarbonylation of the HMF carbonyl group. In the literature it has been shown that Ni is responsible for the selective decarbonylation of aldehydes [56-61]. Isotopic labeling studies of aldehydes performed by Barteau and co-workers have suggested that decarbonylation reaction proceeds through a stable acyl species η^1(C)-acyl, as it is observed in Scheme 8(a) [62-64]. In this mechanism, the C atom of the carbonyl group interacts strongly with the metal causing the C-C scission in this acyl species to release an alkyl fragment one carbon atom shorter than the parent aldehyde and CO [62, 63]. Thus, it is probable that in the decarbonylation reaction of HMF, this acyl species leads to the formation of FOL and CO. Decarbonylation reactions have been reported to increase with temperature [56]. However a drastic decrease of the FOL yield is observed at 189 °C, probably caused by partial deactivation of the Ni/silica catalyst.

Scheme 8. Proposed oxygenated intermediates species for the conversion of HMF on transition metals supported on silica

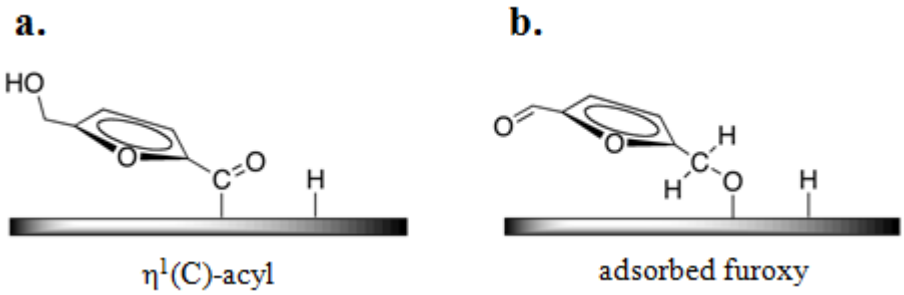

η^1(C)-acyl adsorbed furoxy

5-methylfurfural (MFAL) and 5-methyl-2-furfuryl alcohol (MFOL) are also formed on Ni/silica catalyst with low concentrations at the higher temperatures. MFAL is

probably obtained from cleavage of the C-O bond of the HMF hydroxyl group. Numerous publications about methanol decomposition on nickel surfaces have suggested that it decomposes exclusively through an initial scission of the O-H bond to produce methoxy species [64-66]. So the first step for HMF decomposition might be the hydrogen abstraction from the C-OH group leading to an adsorbed furoxy intermediate on the catalyst surface, as it is shown in Scheme 8(b) [67]. Then the C-O scission can occur to form a furfuryl intermediate, which is subsequently hydrogenated to MFAL. MFOL can be obtained from both the hydrogenation of MFAL and the hydrogenolysis of 2,5-bis(hydroxymethyl)furan (BHF).

Other compounds like DFF and 3-methyl-cyclopentanone (m-C5one) are observed on silica-supported Ni catalyst and their concentration do not exceed 4.1 wt% (reported as “others” in Table 6). Other authors have observed the appearance of cyclic compounds in the conversion of furfural over NiCu/SBA-15 at 160 °C [68] and in the conversion of HMF over supported Au catalysts at 140 °C in aqueous phase under a hydrogen atmosphere [69]. They reported that the rearrangement of the furan ring proceeds *via* selective hydrogenation of the carbonyl group to an alcohol and the following ring opening and closing reactions [68, 69].

Furfuryl alcohol (FOL) and tetrahydrofurfuryl alcohol (THFOL) are the main products observed on Pd/silica catalyst at the three temperatures studied. Pd/silica catalyst displays both a high yield of FOL and a low yield of THFOL at 155 °C. FOL and THFOL are probably produced by decarbonylation of the HMF carbonyl group and ring-hydrogenation of FOL, respectively. There are several studies that show the ability of palladium to decarbonylate aldehydes [58, 62, 70]. Moreover, some researchers have also reported that Pd tends to hydrogenate the furan ring through a strong interaction between the Pd and the furan ring [71, 72].

DFF, m-C5one, 2,5-hexanedione (HD) and1-hydroxy-2,5-hexanedione (HHD) are other compounds derived from side reactions of HMF on Pd/silica catalyst. The total yield of these compounds does not exceed 7.5 wt%. Alamillo and co-workers [15] observed the formation of conjugated diketones through ring opening reaction of BHF using bulk and supported ruthenium catalysts in a biphasic butanol-water system at 130 °C.

In the presence of the Cu/silica catalyst, 15 wt% of HMF is converted at 137 °C, but only about one-fifth of this conversion is towards HHD. The rest of HMF is probably adsorbed on the silica surface as a coke precursor. Even if the reaction temperature is increased, low conversions of HMF are obtained (less than 9 wt%) and only small amounts of MFAL and DFF are detected. This shows that the total deactivation of the catalyst would occur within a short period of time.

A similar behavior is also observed with Ru/silica catalyst, the maximum value of conversion of HMF is 14 wt% at 189°C. Only very low yields of MFAL, FOL and m-C5one and trace amounts of BHF were detected at 137 °C. As the reaction temperature increases, other compounds like DFF and HHD appear in the reaction products in very low concentrations. The above results might indicate that Ru metal is able to catalyze both the decarbonylation reaction of the HMF carbonyl group and the cleavage of the C-O bond in HMF. Panagiotopoulou et al. [73] have also reported that furfural may undergo decarbonylation to furan over Ru/C catalyst. The Ru/silica catalyst is seriously deactivated at the used reaction conditions.

All the results obtained in this chapter show that HMF in aqueous phase presents a more complex reaction network than previously reported in the literature that can be rationalized according to the chemical reactions' network depicted in Scheme 9. Unlike other studies, significant amounts of products are obtained via decarbonylation reactions simultaneously with the hydrogenation and hydrogenolysis reactions in the conversion of HMF.

Scheme 9. Hydrodeoxygenation reaction pathways of HMF over silica-supported catalysts

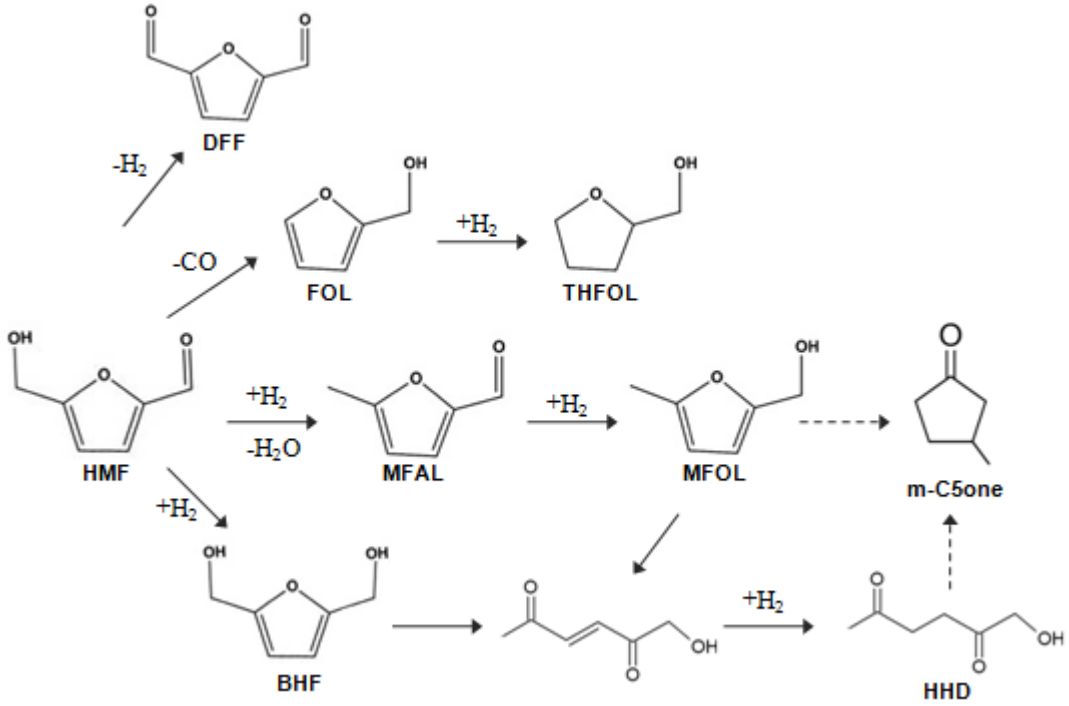

In summary, decarbonylation is the main reaction observed in the conversion of HMF on the silica-supported Ni, Pd and Ru catalysts. Ring-hydrogenated compounds are also observed on Pd/silica catalyst. Small amounts of both MFAL and MFOL are attained on the supported Ni and Pd catalysts. The appearance of small amounts of DFF, m-C5one and ring-opening compounds is also observed on the silica-supported catalysts. These ring-opening compounds can be obtained from BHF or MFOL. However, a drastic deactivation is observed on all silica-supported catalysts. In the next section, the amount and type of carbonaceous material deposited on the catalysts are studied in order to elucidate the causes of deactivation.

3.3 CARBONACEOUS MATERIAL DEPOSITION ON THE SILICA-SUPPORTED CATALYSTS

The concentration of carbonaceous material deposited on the spent Ni, Pd, Cu and Ru based catalysts is presented in Table 7. The total amount of carbonaceous material per gram of spent catalyst is determined after 13.5 h of contact between HMF and the catalysts. It is worth to mention that the temperature reaction was increased successively and the catalyst was analyzed at the end of the reaction test. The formation of a significant amount of carbon on the support/catalyst surface is observed. The silica-supported Ni, Cu and Ru catalysts have a higher amount of carbonaceous material deposits than those for silica and Pd/silica catalyst. These high values of carbonaceous deposit might be explained by coke deposition and/or adsorbed HMF/products. The high content of deposited carbonaceous material could poison the active sites on the silica-supported catalysts and could explain the drastic drop in the conversion of HMF. Atia and co-workers [74] also reported the formation of carbonaceous material on silica-supported heteropolyacid catalysts and their deactivation in the dehydration of glycerol. The presence of metal in the catalyst increases the amount of carbon deposited on the surface. This result can be explained because the active metal provides both hydrogenation and dehydrogenation sites [75]. To clarify the nature of the carbonaceous material IR studies were carried out at this point.

Table 7. Carbonaceous material concentration on spent catalysts and silica support

Support/Catalyst	silica	Ni	Pd	Cu	Ru
g carbon/g cat	0.141	0.192	0.158	0.194	0.206

Figure 3 shows the ATR-IR spectra of the fresh and spent silica-supported catalysts. All fresh catalysts show a broad peak around 3400 cm^{-1} assigned to the stretching vibrations of hydrogen-bonded silanols and O-H bonds of adsorbed moisture [76, 77]. A sharp band at 1630 cm^{-1} is also observed on fresh silica-supported catalysts and is associated to O-H deformation vibration of adsorbed moisture [78].

Figure 3. IR spectra of fresh and spent silica-supported catalysts (dotted lines are the fresh catalysts and solid lines are the spent catalysts)

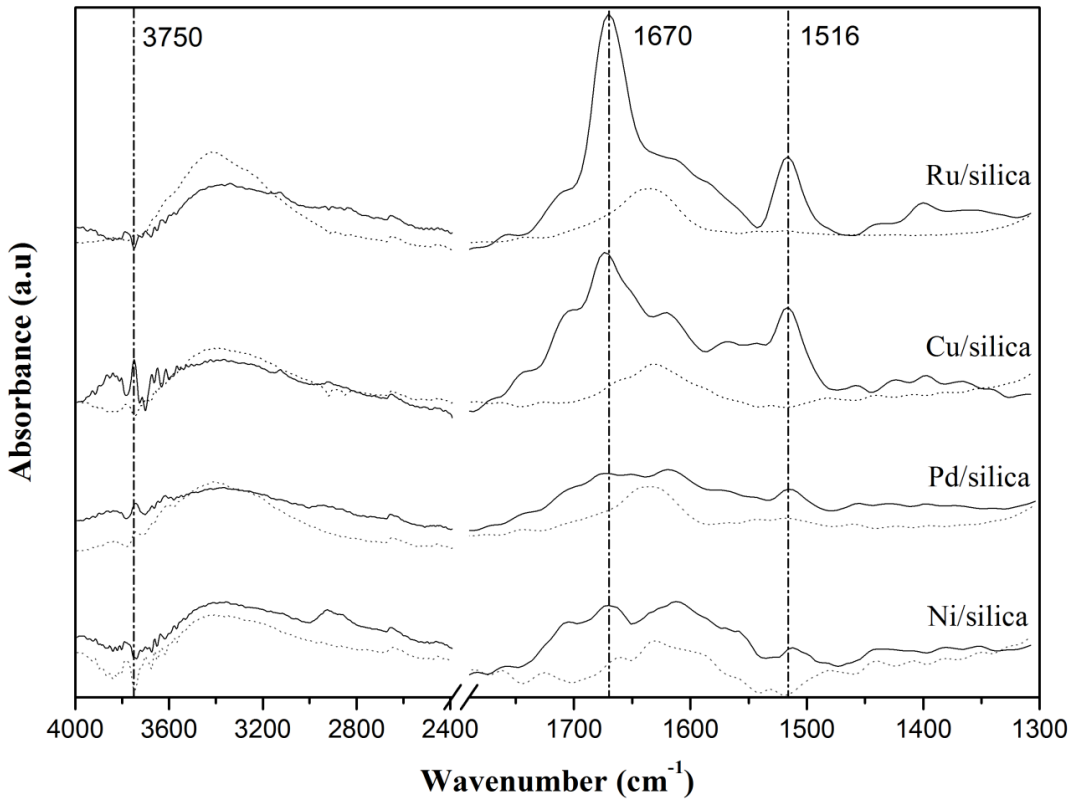

The ATR-IR spectra of the spent silica-supported catalysts reveal the appearance of a broad band between 3000 and 2800 cm^{-1}, which can be assigned to aliphatic C-H bands of the asymmetric and symmetric $–CH_2$ and CH_3 stretch modes. A band

centered at 1670 cm^{-1} appears on the spent catalysts and it has been ascribed to C=O stretching of aldehydes [79]. A band appearing at 1516 cm^{-1} has been associated to C=C bands in aromatic and highly conjugated structures, which is sometimes called as coke band [80, 81]. There is a more pronounced increase in the intensity of the bands located at 1516 cm^{-1} and at 1670 cm^{-1} on the Cu and Ru based catalysts as compared to those for the Ni and Pd based solids.

The intensive bands at 1516 cm^{-1} and 1670 cm^{-1} observed on the Cu and Ru based catalysts seem to indicate that an aromatic aldehyde structure is deposited on the spent solids. These peaks have been observed in the IR analysis of furan compounds adsorbed on supported catalysts [82,83]. Robinson and Ross [84] suggested that the interaction between furan compounds and silica is through the formation of hydrogen-bonds between the silanols of the silica and the aromatic ring or oxygen atom.

The fact that the bands situated at 1516 cm^{-1} and at 1670 cm^{-1} are not strong on the Ni/silica and Pd/silica catalysts, suggests that the nature of the carbonaceous material deposited on these solids is different from the “coke” deposited on the Cu and Ru based catalysts. Carbonaceous material obtained is more similar to the carbon type on spent silica-supported catalysts used in reactions with hydrocarbon feed [85, 86], that means it is less aromatic and with lower oxygen content.

In conclusion, all monometallic catalysts supported on silica used in this study show a drastic deactivation by deposition of considerable amounts of carbonaceous material. This carbonaceous material is suggested to be a compound with a high content of carbonyl functionalities on the Cu and Ru based catalysts and a compound less aromatic with lower oxygen content on the Ni and Pd based catalysts.

4. HYDRODEOXYGENATION OF 5-HYDROXYMETHYLFURFURAL OVER ALUMINA-SUPPORTED CATALYSTS IN AQUEOUS MEDIUM

As highlighted in the previous chapter, when HMF reacts with hydrogen using silica-supported catalysts, there is a significant carbon deposition and a strong catalyst deactivation. So it was thought to change the catalyst support by alumina. Although it is known that carbon is also deposited on this support, the use of alumina is expected to improve hydrogenolysis reactions due to the presence of acid sites and by this way stabilize the activity of the catalysts. The purpose of this chapter is to evaluate the reactivity of HMF on alumina-supported Ni, Pd, Cu and Ru catalysts in aqueous phase. The composition of each metal and the reaction conditions used to determine the HMF reactivity are similar to those reported for the silica-supported catalysts studied in the Chapter 3.

4.1 CATALYSTS CHARACTERIZATION

Table 8 presents the metal content, BET surface area, metal dispersion, active metal particle size and the total hydrogen consumption per active metal of the catalysts prepared in this work. The metal content of each catalyst measured by ICP-OES gave a concentration similar to the nominal value. Even though it has been reported that $RuCl_3$ can be oxidized by atmospheric air exposition [87], on calcined alumina-supported Ru catalyst a content of Cl less than 1 wt% is found. This indicates that at the calcination temperature used in this work the oxidation of $RuCl_3$ precursor is not completely reached.

It is worth to mention that the surface area of alumina reported in Table 8 corresponds to the surface area of the calcined alumina extrudates. The surface areas of the Ni, Cu and Ru-supported catalysts are 85%, 79% and 94% of the alumina surface area respectively, while the Pd-supported catalyst presents a

surface area similar to the alumina. Pd/alumina and Ru/alumina catalysts show a slight change in the total pore volume (TPV), where Ni/alumina and Cu/alumina catalysts display a drop in the TPV.

Table 8. Characterization of the monometallic Ni, Pd, Cu and Ru catalysts supported on alumina

Catalyst	Metal content (wt %)	Surface area (m^2/g)	TPV[a] (cm^3/g)	D[b] (%)	d_p[c] (nm)	H_2/Me[d] (mol/mol)
alumina	-	213	0.56	-	-	-
Ni/alumina	9.7	180	0.43	27.4	3.7	0.71
Pd/alumina	0.7	212	0.55	52.2	2.1	-
Cu/alumina	9.5	169	0.40	30.0	3.5	0.98
Ru/alumina	1.0	201	0.53	15.5	8.5	2.00

[a]TPV*:* Total pore volume (cm^3/g)
[b]*D*: metal dispersion (%)
[c]d_p: active metal particle size (nm)
[d]Hydrogen consumption per active metal (Me: Ni, Pd, Cu, Ru) based on TPR experiments

In the case of Ni and Cu-supported catalysts, these results provide evidence that the surface area of the catalysts decreases due to the partial blocking of the support pores by the metal particles. Other authors have observed a similar behavior with Ni/alumina catalyst prepared at high concentrations of Ni [88-90].The chemisorption data show that metals on the catalysts are well dispersed, presenting metal particle sizes smaller than 9 nm. Pd/alumina catalyst presents a higher metal dispersion. The dispersion measurements found in this work are similar to those reported elsewhere for catalysts of similar Ni [88, 91, 92], Pd [93-95], Cu [96, 97] and Ru [41] content.

Figure 4 shows the nitrogen adsorption-desorption isotherms and BJH pore size distributions of the calcined support and alumina-supported monometallic catalysts.

BJH pore size distributions were obtained from desorption branches of isotherms. The experimental data show that both alumina and monometallic catalysts exhibit typical IV-type isotherms with H2-type hysteresis loops, which are characteristics of mesoporous materials [98]. Ni and Cu-supported catalysts present porosities with narrow pore size distributions centered at 6.1 nm and 6.3 nm, respectively. Pd/alumina and Ru/alumina catalysts show a slightly wider pore size distribution than the other catalysts, suggesting that pores in the support are not blocked with the low content of the Pd and Ru metals.

Figure 4. Nitrogen adsorption-desorption isotherms and pore size distributions (inset) of support and alumina-supported monometallic catalysts

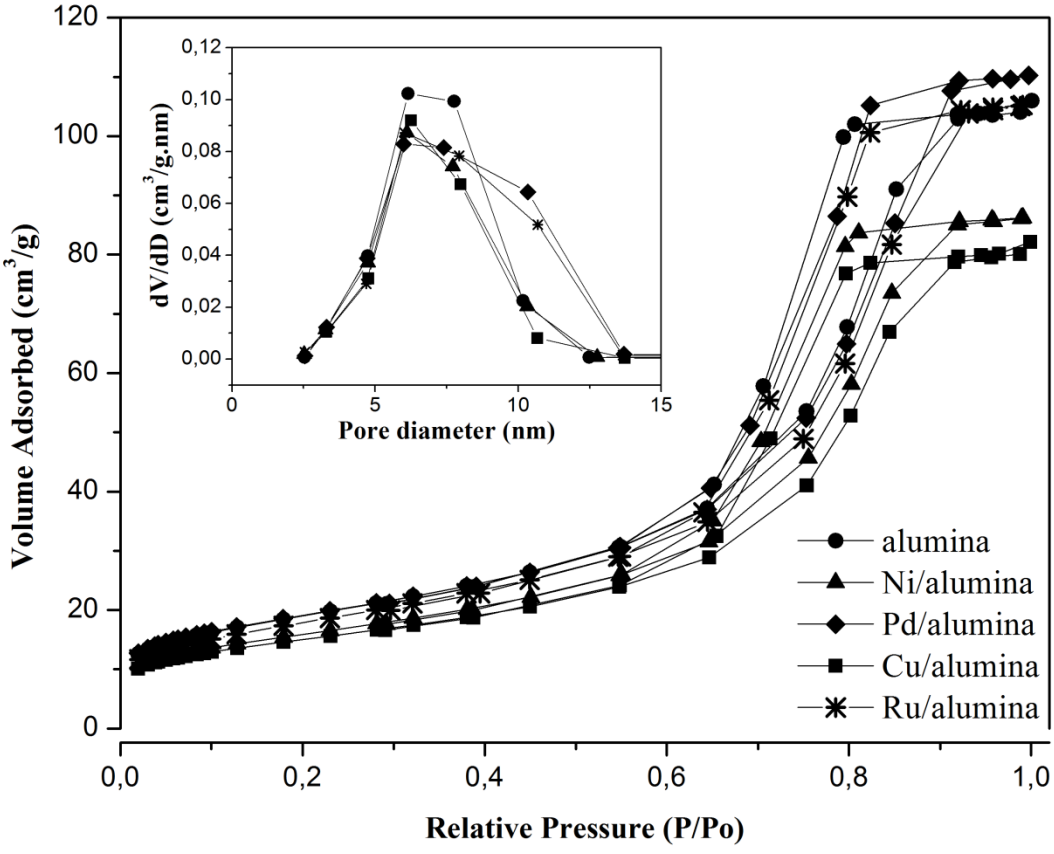

TPR profiles of the alumina-supported catalysts are shown in Figure 5. The profiles of Ni, Pd and Ru-supported catalysts were magnified 9, 30 and 7 times, respectively, for comparative purposes. Cu/alumina catalyst presents two overlapping peaks at 217 °C and 241 °C. In the literature the low temperature reduction peak is attributed to the reduction of highly dispersed amorphous CuO species and the high temperature peak to the reduction of highly dispersed bulk CuO [96, 99, 100].

Figure 5. TPR profiles of the calcined monometallic catalysts supported on alumina

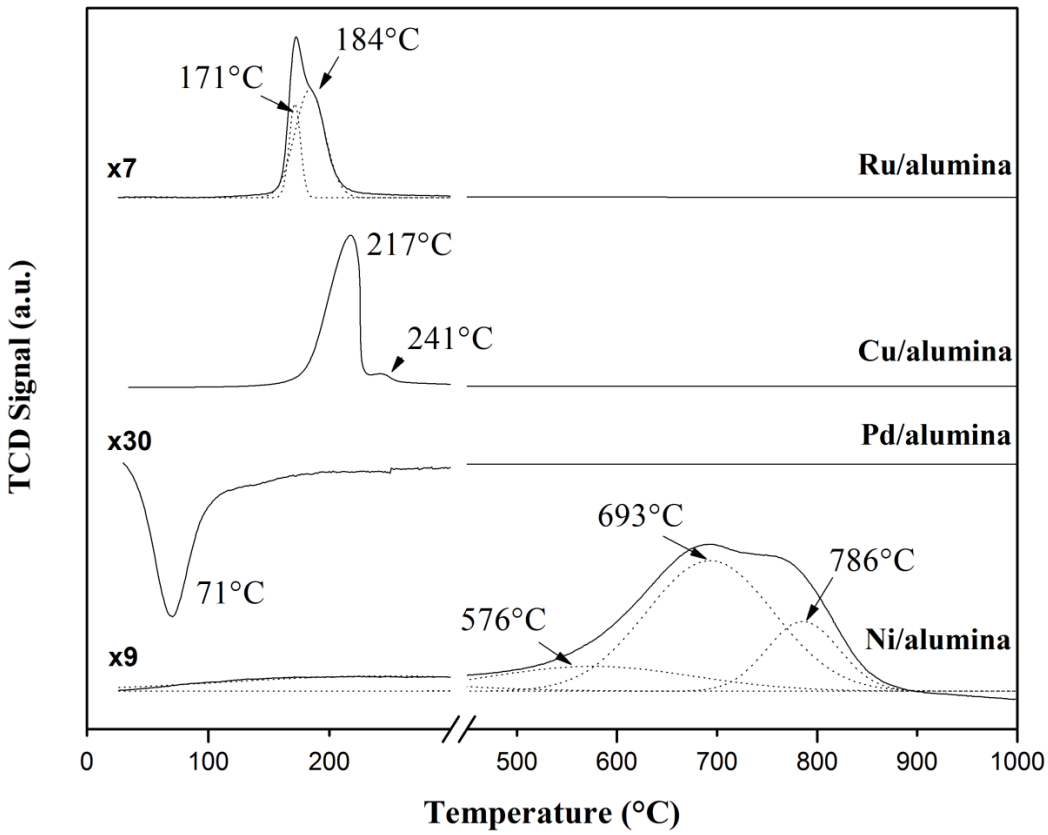

The TPR profile of Pd/alumina catalyst shows a small negative peak at 71 °C, assigned to the decomposition of the β-Pd hydride phase [45, 94, 101]. No reduction peak of PdO is detected at the conditions of the TPR experiment because the reduction of these particles has been reported to be achieved at temperatures below 20 °C [94].

Ni/alumina catalyst reduces between 400 and 900 °C. This broad region was deconvolved into three Gaussian-type peaks. The low temperature peak centered at 576 °C could be ascribed to the reduction of NiO with a strong interaction between metal and support [102-104]. The two high temperature peaks situated at 693 °C and at 786 °C have been related to Ni^{2+} ions occupying octahedral and tetrahedral sites in the Ni spinel structure, respectively [105-108].

Ru/alumina catalyst presents two reduction temperature peaks situated at 171 °C and at 184 °C. The lower temperature peak has been associated to the reduction of well-dispersed RuO_x species, whereas the higher temperature peak is assigned to the reduction of RuO_2 particles [109, 110]. Although chlorine is detected in the FRX analysis of the calcined Ru-supported catalysts, no temperature peaks attributed to the reduction of $RuCl_3$ or ruthenium oxychloride ($RuCl_xO_y$) were observed in Figure 5 [111]. Koopman et al. [111] have reported that the complete reduction of unsupported $RuCl_3$ is below 160 °C.

In Table 8, the amount of hydrogen consumed per mole of active metal was calculated from TPR data to evaluate the reducibility of the metals present on the alumina-supported catalysts. It was assumed that the active metals were present as divalent oxides in the calcined Ni and Cu catalysts and as tetravalent oxide in the calcined Ru catalyst. The hydrogen consumption per active metal was 0.71 and 0.98 for Ni and Cu based catalysts, respectively. The reduction degree of Ru-based catalyst is 100% according to the stoichiometry of the reduction of RuO_2. The hydrogen consumption of Pd/alumina is not calculated given that no reduction

peak of PdO is detected. Cu- and Ru-supported catalysts are totally reduced whereas Ni/alumina has a lower degree of reduction. These results are in agreement with those reported by other authors [112-114]. This low degree of reduction of nickel might be explained because some nickel species are incorporated within the support or can be blocked by other metal crystallites, thus making these species nonreactive toward hydrogen at the conditions of the TPR experiments [115-117].

In summary, the reducibility of supported transition metal oxide species depends on the interaction between metal and support. If the metal-support interaction is stronger then it will be more difficult to reduce the supported metal. It is the case of the Ni- and Cu-supported catalysts studied in this work. Ni/alumina shows higher reduction temperatures compared to Ni/silica catalyst studied in the Chapter 3. This result is in agreement with those reported by other authors [118-120]. On the contrary, Cu/alumina displays slightly lower reduction temperatures than the Cu/silica catalyst. Interestingly, TPR profiles of Pd and Ru based catalysts show similar reduction temperatures even though there are reports in the literature which show slight differences [41, 121, 122].

4.2 CATALYSTS EVALUATION

The influence of the nature of the metal supported on alumina in the reactivity of 5-hydroxymethylfurfural (HMF) in aqueous medium was studied in this chapter. The evolution of HMF conversion on alumina-supported catalysts as a function of time is presented in Figure 6. The reaction progress was monitored at 137 °C during the first 8 h in order to estimate the time necessary to approach the steady state.

The HMF conversion decreases during the first 180 min to achieve a steady-state value around 50 wt%, 44 wt% and 39 wt% for the Pd, Ni and Cu-supported

catalysts respectively. No conversion of HMF on Ru-based catalyst is observed at 137 °C. Consequently, the product sampling was established after 4 h of reaction, time required to reach steady state for all catalysts. The deactivation observed during the first minutes can be ascribed to carbonaceous material deposition on the surface or chemisorbed CO that accumulates on the surface and blocks a part of the active sites [123].

Figure 6. HMF conversion versus reaction time for the (▲) Ni/alumina, (♦) Pd/alumina and (■) Cu/alumina catalysts evaluated at 137 °C

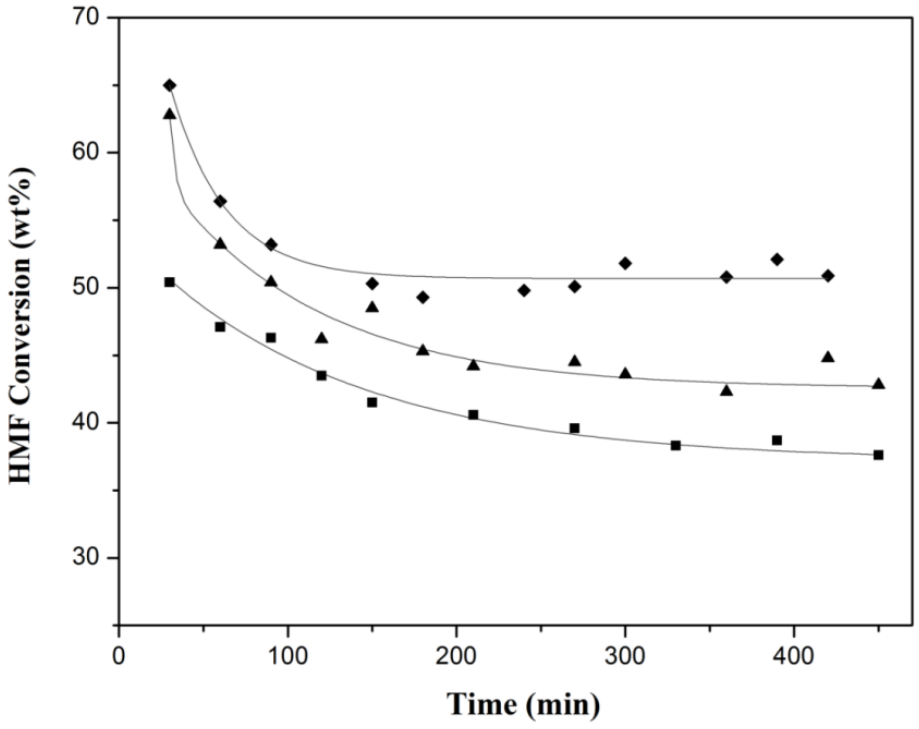

Conversion and product yields obtained at different reaction temperatures with Ni, Pd, Cu and Ru-supported catalysts are given in Table 9.

Table 9. Conversion and liquid product yield obtained over Ni, Pd, Cu and Ru supported on alumina as a function of temperature

Catalyst	Temp. (°C)	Conv. (wt%)	Product liquid yield (wt%)							
			BHF[a]	MFAL[b]	MFOL[c]	FOL[d]	THFOL[e]	DMF[f]	DMTHF[g]	Others
Ni/alumina	137	44	3.6	-	3.2	20.9	3.2	-	-	2.1
	155	100	-	-	27.3	41.0	7.6	1.0	0.3	7.7
	189	100	1.5	1.2	7.6	39.4	9.9	4.7	1.2	16.5
Pd/alumina	137	50	3.3	2.2	6.4	14.9	2.4	-	-	5.8
	155	100	4.3	-	3.5	8.7	48.6	4.2	1.1	13.6
	189	100	-	-	-	3.2	41.5	10.1	2.6	11.5
Cu/alumina	137	40	-	0.8	-	-	-	-	-	31.0
	155	94	5.2	21.3	17.7	2.9	-	-	-	37.8
	189	36	-	8.6	4.6	0.7	-	-	-	16.1
Ru/alumina	155	99	1.6	6.7	4.4	41.0	12.2	6.6	1.2	12.9
	189	5	-	0.6	-	0.6	-	-	-	1.2

[a]*BHF*: 2,5-bis(hydroxymethyl)furan
[b]*MFAL*: 5-methylfurfural
[c]*MFOL*: 5-methyl-2-furfuryl alcohol
[d]*FOL*: furfuryl alcohol
[e]*THFOL*: tetrahydrofurfuryl alcohol
[f]*DMF*: 2,5-dimethylfuran
[g]*DMTHF*: 2,5-dimethyltetrahydrofuran

Some preliminary tests were done charging the reactor with alumina extrudates and a very low conversion of HMF was obtained when alumina was evaluated at 137 °C (less than 3 wt%). As the temperature increased, the conversion of HMF became 19 wt% at 155 °C and 20 wt% at 189 °C. DFF and small amounts of 5-methylfurfural (MFAL) were observed. DFF yield was 7 wt% at 155°C and 189 °C. The MFAL yield did not exceed 1 wt% at both temperature levels. DFF is likely produced via dehydrogenation of HMF.

The previous result shows that alumina support itself has dehydrogenation sites able to promote this reaction. This result is consistent with Wang et al.'s results [124]. These authors have shown that acetone selectivity in the reaction of isopropanol decomposition is related to the presence of basic sites coming from Al vacancies [124]. DFF was only observed over alumina and was not detected on the catalysts studied.

HMF conversion on the alumina-supported Ni, Pd and Cu catalysts evaluated at 137 °C is in the range of 40 wt% to 50 wt%, with Pd-based catalyst being more active. At 155 °C, the HMF conversion is complete on Pd and Ni-supported catalysts and is 94 wt% and 99 wt% on Cu/alumina and Ru/alumina catalysts respectively. Unexpectedly, the conversion of HMF on Cu/alumina and Ru/alumina catalysts decreases to 36 wt% and 5 wt% at 189°C, respectively. This reduction in conversion is likely caused by partial deactivation of the catalyst after 13.5 h of reaction as it will be shown later.

Furfuryl alcohol (FOL) is the main product observed when the Ni/alumina catalyst is evaluated at the three reaction temperatures. This shows that Ni is able to catalyze the decarbonylation reaction of HMF. Sitthisa et al. [56] have obtained furan from furfural using Ni supported on silica at 250 °C and atmospheric pressure. However, some authors observed that HMF hydrogenation to 2,5-bis(hydroxymethyl)furan (BHF) and 2,5-bis(hydroxymethyl)tetrahydrofuran

(BHTHF) are the main reactions using Ni Raney under milder reaction conditions in aqueous medium [13, 125]. This might suggest that the activity of nickel for the decarbonylation reaction is faster than the hydrogenation reactions to BHF/BHTHF when the temperature is higher.

Previous studies related to the reactivity of aldehydes have shown that decarbonylation takes place on metals of Groups 8, 9 and 10 [58-61]. Barteau and co-workers [62-64] have suggested from isotopic labeling studies that decarbonylation reaction proceeds through a stable acyl species η^1(C)-acyl, as it was shown in Scheme 8(a). Thus it is likely that this acyl species leads to the formation of FOL and CO. The formation of carbon monoxide is also confirmed from analysis of the gas-phase reaction products at 189 °C and data are presented in Table 10. The main gas products from HMF conversion were CO, CO_2 and C^{6+} oxygenated products.

Table 10. Gas product yield (wt%) from hydrodeoxygenation of HMF evaluated on alumina-supported monometallic catalysts at 189 °C

Catalyst	Ni/alumina	Pd/alumina	Cu/alumina	Ru/alumina
CO_2	2.8	1.2	0.5	0.6
CO	13.2	15.4	0.1	0.2
C_3	0.1	-	-	-
nC_4	0.1	-	-	-
C_6^+	1.4	8.0	0.1	-

On Ni/alumina catalyst, as the reaction temperature is increased other compounds like 5-methyl-2-furfuryl alcohol (MFOL), tetrahydrofurfuryl alcohol (THFOL) and 2,5-dimethylfuran (DMF) are also observed. This shows that Ni has also active sites for hydrogenolysis and ring hydrogenation reactions.

Even though MFOL can be obtained through MFAL and BHF, the results herein suggest that BHF is the main intermediate in the production of MFOL. In fact, the absence of MFAL at low reaction temperatures indicates that hydrogenation of the HMF carbonyl group occurs faster than hydrogenolysis of the HMF hydroxyl group, as has also been suggested by Kumalaputri et al. [126]. Indeed, Nakagawa and Tomishige [125] have found that BHF is the main product when HMF is hydrogenated using Raney Ni and Ni/SiO_2 catalysts at 40 °C. Mavrikakis and Barteau [64] have previously pointed out that the preferential carbonyl compounds adsorption mode on the platinum group metals is the η^2(C,O)-aldehyde configuration (Scheme 10, a). In this way, from this η^2(C,O) species BHF could be formed and subsequently this compound could be hydrogenolyzed to MFOL.

Scheme 10. Proposed oxygenated intermediates species for the conversion of HMF on transition metals supported on alumina

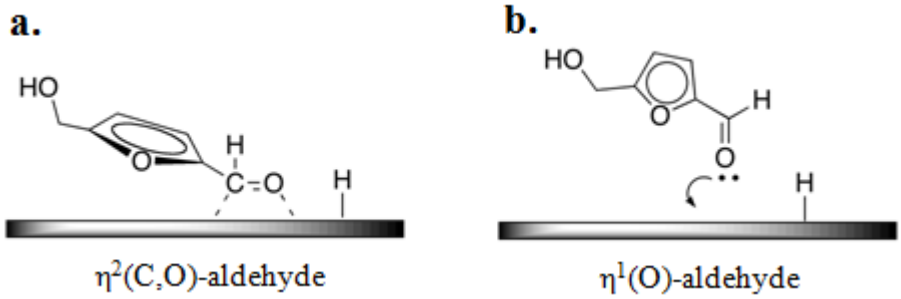

η^2(C,O)-aldehyde η^1(O)-aldehyde

It is important to note that the MFOL yield decreased from 27 wt% to 7 wt% as the temperature is increased from 155 °C to 189 °C. THFOL and DMF are probably obtained from the hydrogenation of FOL and the hydrogenolysis of MFOL, respectively. The decrease in MFOL yield and the increase in both DMF and other compounds when the temperature is increased can be explained by the MFOL hydrogenolysis. Shin and Keane [127] have shown from phenol hydrogenation reactions using Ni-supported catalysts that hydrogenolysis of phenol to benzene

was only initiated at temperatures as high as 250°C and were also favored by high nickel loadings. Therefore, the MFOL hydrogenolysis is promoted at high temperatures.

Additionally, a significant amount of other compounds was observed on Ni/alumina at the highest temperature. These compounds correspond to secondary reaction products like 2,5-hexanedione (HD), 2-pentanone and 1,2-pentanediol, among others, which were confirmed by MS (quality index higher than 83%) and their presence indicates that Ni supported on alumina breaks the ether C-O bond of the furan ring [56]. Sitthisa et al. [56] discussed that these ring-opening compounds are obtained from C-O-C cleavage of the ring because the interaction between furan ring and the Ni atoms is so strong that the ether C-O bond in the ring weakens and then opens the ring. Zhang et al. [128] also observed the formation of these compounds in the FOL conversion over a Ru/MnO_x catalyst in the aqueous phase. They have proposed that the formation of these ring-opening compounds is through the FOL hydrogenolysis to obtain 1-hydroxy-2-pentanone, which is subsequently hydrogenated and hydrogenolyzed to 1,2-pentanediol and 2-pentanone respectively [128]. It is also important to mention that the ring-opening compounds are favored with high temperatures.

The main products observed over Pd/alumina catalyst are FOL at low temperature and THFOL at higher temperatures, and their yields are shown in Table 9. As it is known from the literature, Pd-based catalyst favors the hydrogenation of the furan ring [71, 129]. For example, the formation of tetrahydrofuran (THF) has been reported when the hydrogenation of furfural was carried out using Pd catalysts supported on silica, alumina and activated carbon [130-133].

It has been suggested elsewhere that the tendency of Pd to hydrogenate the unsaturated furan ring is a result of the strong interaction between the Pd and the π bonds in the furan [56]. This strong interaction is caused apparently by the small *d*

bandwidth of Pd [134]. Moreover, Bradley et al. [135] showed that the rehybridization of the C bonding in the furan from sp^2 to sp^3 pushes the O atom sufficiently far from the Pd surface such that the O-Pd interaction is very small. Because of this repulsion, it is unlikely that the C-O-C cleavage of the ring and subsequent ring-opening reactions are observed on Pd/alumina. This is in agreement with our results whereby small amounts of 2,5-hexanedione (HD) with yields less than 3 wt% were found in the hydrogenation/hydrogenolysis reactions of HMF on Pd/alumina catalyst.

Unlike the Ni-based catalyst, on Pd/alumina the formation of THFOL is remarkably enhanced as the temperature is increased, while the amount of FOL decreases significantly. It suggests that THFOL is obtained from the consecutive hydrogenation reaction of FOL and Pd is active for decarbonylation and the subsequent ring hydrogenation reaction. The other two compounds observed in high concentration are MFOL and DMF. The presence of BHF and MFAL at low temperature indicates these compounds are the intermediates to produce MFOL. Other compounds like 2,5-dimethyltetrahydrofuran (DMTHF) and 5-methyltetrahydrofuran-2-methanol (MTHFOL) were observed at 155 °C and 189 °C. DMTHF and MTHFOL are likely obtained through the furan-ring hydrogenation of DMF and MFOL, respectively. In summary, Pd favors decarbonylation, ring hydrogenation and hydrogenolysis reactions.

Regarding Cu/alumina, Table 9 provides the major products obtained on this catalyst. The main compounds observed in the liquid reaction product are 5-methylfurfural (MFAL) and 5-methyl-2-furfuryl alcohol (MFOL). This result shows that Cu has the ability to promote hydrogenolysis and hydrogenation reactions. There are numerous reports in the literature showing that Cu is effective in the C=O bond hydrogenation using furfural and HMF as reactants [136-139]. In fact, Deutsch and Shanks [140] have shown that copper mixed metal oxide catalysts were selective to DMF from MFOL and Bienholz et al. [141] and Vasiliadou et al.

[142] have also reported that this metal is selective to glycerol hydrogenolysis giving rise to propylenglycol.

Even though a BHF yield of 5 wt% is obtained at 155 °C, MFOL seems to be produced through reactions involving both the cleavage of the HMF hydroxyl group to obtain MFAL and the hydrogenation of this compound. Barteau [143] suggested from isotopic labeling experiments that aldehydes tend to preferentially adsorb in the η^1(O) configuration on Group 11 metals (Scheme 10, b), which would allow the interaction between the Cu surface and the oxygen in the HMF carbonyl group to yield BHF.

Several studies have suggested that the methanol decomposition pathway on Cu surfaces involves first the O-H bond scission to form stable alkoxide (CH_3O) intermediates [64, 144-146]. In the case of HMF, it is possible that the first step involves the hydrogen abstraction from the hydroxyl group leading to an adsorbed furoxy intermediate (Scheme 8, b). From this adsorbed furoxy intermediate the formation of MFAL is presumed to occur. Then MFAL might be hydrogenated to MFOL through the η^1(O) aldehyde adsorption configuration. Additionally, the low yields to FOL (up to 2.9 wt%) would confirm the affinity of Cu by both the η^1(O) and the furoxy adsorption modes, whereby decarbonylation reaction is not favored on Cu/alumina.

Unlike previous reports in which only hydrogenation and hydrogenolysis reaction products are observed on Cu-based catalysts [9, 13, 140, 142], in this work other behavior is observed. At 137 °C a large amount of 1-hydroxy-2,5-hexanedione (yield of 27 wt%) is attained, although this compound disappears at higher reaction temperatures. Schiavo et al. [13] and Nakagawa et al. [147] have reported the formation of 1-hydroxy-2,5-hexanedione (HHD) through the rearrangement of HMF using noble-metal catalysts in aqueous medium catalyzed by acids. When the temperature is increased at 155 °C and 189 °C, the formation of other compounds

like furfural, 2,5-hexanedione (HD), 1,2-pentanediol (1,2-Pdiol), 2-hydroxy-3-methyl-2-cyclopenten-1-one, 3-methyl-2-cyclopenten-1-one and 3-methyl-cyclopentanone (m-C5one) is observed. These compounds are presented as “others” in Table 9. The cyclic-compounds (yield goes up to 15 wt%) were detected by GC-MS, presenting a quality index higher than 91%.

Previous studies reported by Hronec et al. [148, 149] revealed the formation of cyclic-compounds from FOL using Pt, Pd, Ru or Ni catalysts under similar reaction conditions used herein. They suggested that these cyclic-compounds are the result of the water effect in the reaction medium [148, 149]. In addition, Ohyama et al. [69] pointed out that cyclopentanone derivatives are obtained through intramolecular aldol-condensation of 1-hydroxy-2,5-hexanedione, this latter intermediate compound observed in large amounts at 137 °C. In this study, large amounts of cyclic-compounds were only detected over Cu/alumina catalyst and these results show that copper has also the capacity to catalyze the formation of cyclic-compounds.

The product distribution from the HMF conversion over the alumina-supported Ru catalyst is summarized in Table 9. No reaction products are observed at 137 °C. FOL is the main product obtained on Ru/alumina catalyst at 155 °C, probably from decarbonylation of the HMF carbonyl group as was aforementioned. Small yields of furan have been reported in the conversion of furfural on Ru/C catalyst in 2-propanol, occurring in parallel to the dominant reaction of hydrogenation of the aldehyde group [150]. In the case of the conversion of HMF on Ru/alumina catalyst the decarbonylation reaction occurs much more readily than the hydrogenolysis/hydrogenation reactions.

A low yield of MFOL is also obtained on Ru/alumina catalyst at 155 °C. BHF and MFAL are detected among the reaction products, suggesting that they are the intermediate compounds in the hydrogenolysis of HMF to MFOL. Considerable

amounts of ring-hydrogenated products like THFOL, DMTHF and MTHFOL are obtained on alumina-supported Ru catalyst. THFOL, DMTHF and MTHFOL are probably obtained from the ring hydrogenation of FOL, DMF and MFOL, respectively. Other compounds like HD, 1-pentanol and 2-hexanol are also formed at 155 °C.

The ring-opening compounds are probably obtained from C-O-C cleavage of the furan ring of either HMF or its hydrogenated intermediates. The amount of these ring-opening products is slightly higher than that obtained on Ni/alumina catalyst evaluated at the same reaction temperature. These results are consistent with Jacquin et al. results [151]. These authors showed that the Ru-containing catalyst has higher selectivity towards ring-opening products than the Pt-containing catalyst in the hydrogenation of naphthalene on mesoporous aluminosilicates monometallic catalysts.

The above results indicate that the catalytic behavior of the Ru/alumina catalyst is similar to the Ni/alumina catalyst, noteworthy amounts of decarbonylated, ring-hydrogenated and ring-opening products are formed. However they also differ somewhat in the catalytic behavior, the reaction becomes less selective towards hydrogenolysis products on alumina-supported Ru catalyst.

These previous results show that the reactions' network on alumina-supported monometallic catalysts is even wider than that obtained on silica-supported catalysts. All of the results of this chapter can be rationalized according to the chemical reactions' network presented in Scheme 11.

In conclusion, decarbonylation of the HMF carbonyl group is the dominant reaction on alumina-supported Ni, Pd and Ru catalysts. Additionally, Pd/alumina catalyst tends to hydrogenate the furan ring, especially at high temperatures. Ring-opening compounds are also obtained on Ni/alumina and are likely formed from

hydrogenolysis of FOL. On the contrary, Cu/alumina catalyst is active for both hydrogenolysis and hydrogenation reactions. Cyclic-compounds are also observed on Cu/alumina and are likely obtained through 1-hydroxy-2,5-hexanedione.

Scheme 11. Hydrodeoxygenation reaction pathways of HMF over alumina-supported catalysts

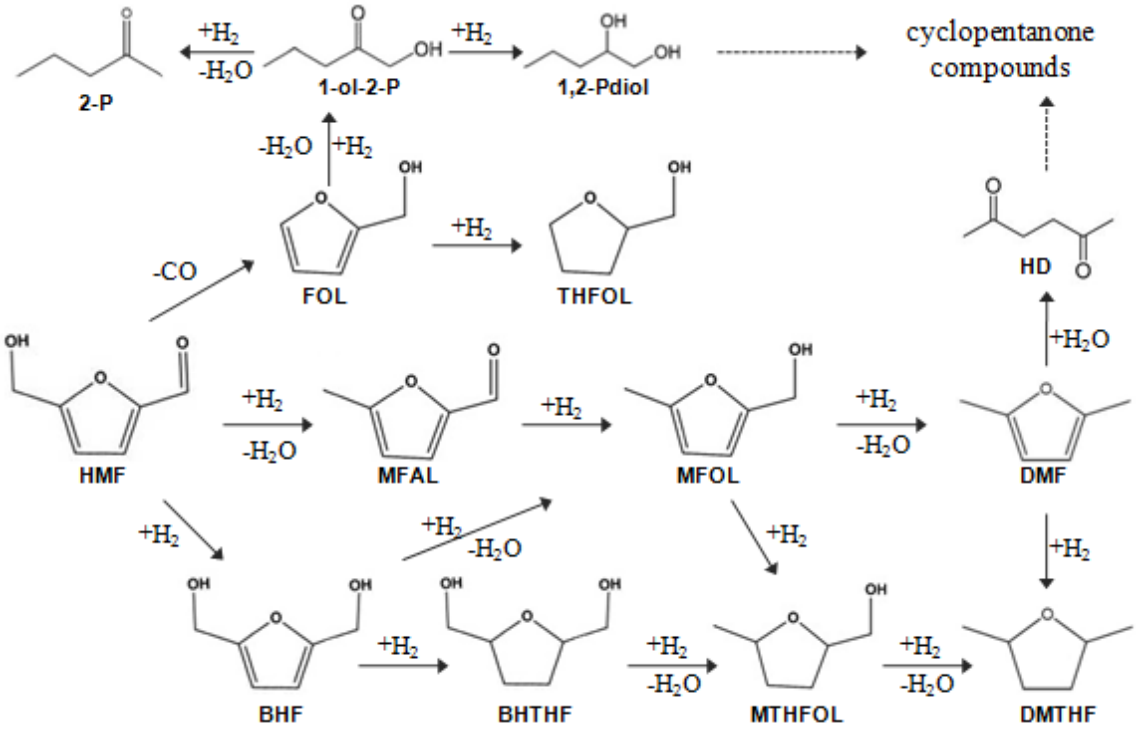

In comparison to previous results of the silica-supported catalysts, a higher amount of ring-hydrogenated, ring-opening and cyclic products are obtained on alumina-supported catalysts.

It is worth to note that the alumina-supported Cu and Ru catalysts have a drastic deactivation at 189 °C. It is therefore important to know the characteristics of the

carbonaceous material deposited on the spent catalysts in order to understand the possible causes of their deactivation.

4.3 CARBONACEOUS MATERIAL DEPOSITION ON THE ALUMINA-SUPPORTED CATALYSTS

The concentration of carbonaceous material deposited on the spent supported Ni, Pd, Cu and Ru catalysts is presented in Table 11. As the catalyst samples were evaluated at three consecutive temperature conditions without catalyst discharge then the amount of this carbonaceous material corresponds to the total amount deposited during the 13.5 h of contact between HMF and the catalyst. A substantial amount of carbon is found on all catalysts, especially on the alumina support and the Ru-based catalyst. It is in agreement with other studies showing that alumina support favors coke formation due to the presence of acid sites on the surface of the support [152-154].

Table 11. Carbonaceous material concentration on spent catalysts and alumina support

Support/Catalyst	alumina	Ni	Pd	Cu	Ru
g carbon/ g cat	0.231	0.173	0.129	0.176	0.239

The presence of metal in the catalyst decreases the amount of carbon deposited on the surface, except for the Ru/alumina catalyst. These high values of carbonaceous deposit might be explained by coke deposition and/or adsorbed HMF/products. Previous studies have shown that furfural and/or furfuryl alcohol have a strong adsorption on copper-based catalysts and these adsorbed compounds are thought to cause deactivation of the catalyst [155-157].

Consequently, ATR-IR studies were performed with the aim of clarifying the nature of this carbonaceous material.

ATR-IR spectra of the spent and fresh alumina-supported catalysts are depicted in Figure 7. The broad band centered at 3400 cm^{-1} present in all calcined and spent catalysts is assigned to the O-H bonds vibrations of adsorbed moisture and OH groups of the alumina support. Likewise, the band at 1640 cm^{-1} is attributed to O-H deformation modes of water.

Figure 7. ATR-IR spectra of fresh and spent alumina-supported catalysts (dotted lines are the fresh catalysts and solid lines are the spent catalysts)

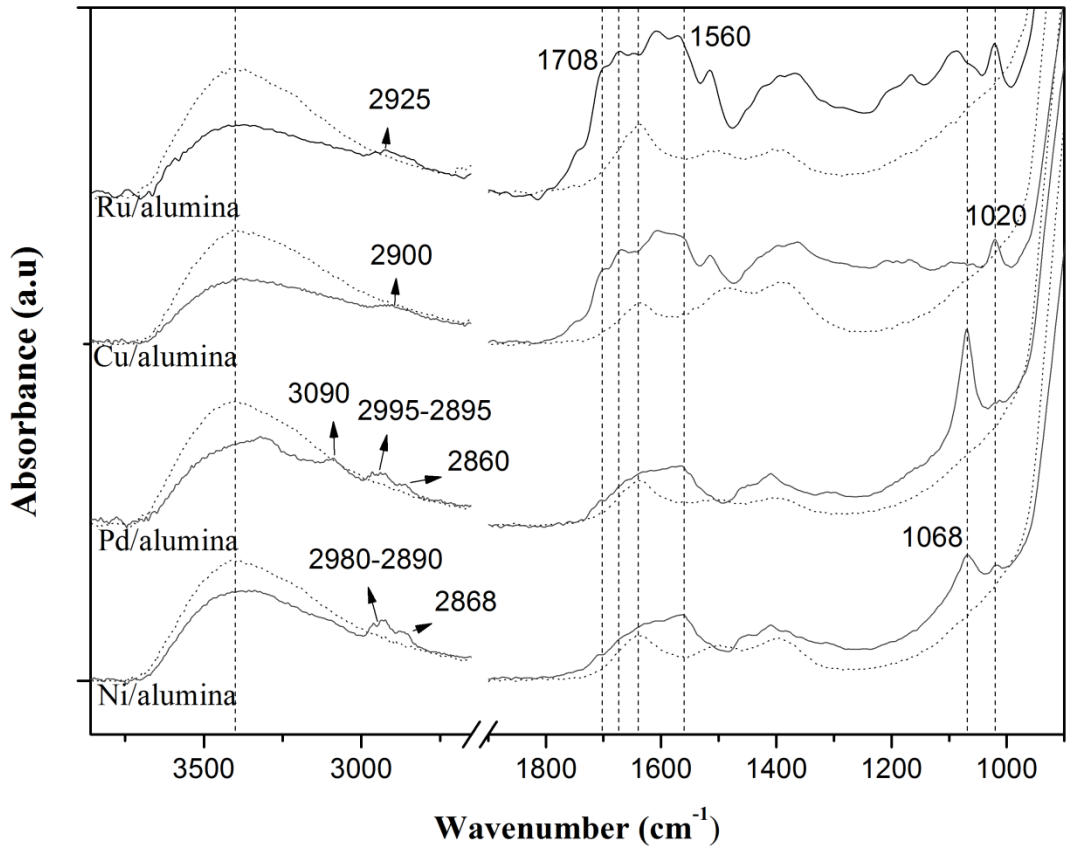

The ATR-IR spectra of the spent catalysts reveal the appearance of bands between 3000 and 2890 cm^{-1} attributed to aliphatic C-H bands of the asymmetric and symmetric $-CH_2$ and $-CH_3$ stretch modes. In the case of spent supported Ni and Pd catalysts, the band located at 2860 cm^{-1} corresponds to the C-H stretching vibration on a CHO group [158]. New bands appear at 1708 cm^{-1} and at 1670 cm^{-1} on the spent alumina-supported Cu and Ru catalysts and are assigned to stretching vibrations of conjugated and non-conjugated carbonyl groups with the aromatic ring [159]. The band at around 1560 cm^{-1} on the spent catalysts has been ascribed to C=C bands in aromatic and highly conjugated structures, which some authors have called the “coke band” [80, 160]. In the region from 1470 to 1250 cm^{-1}, small bands appear on the spent catalysts attributed to C-H deformation modes.

In the ATR-IR spectra of the spent catalysts, intense bands at 1068 cm^{-1} and at 1020 cm^{-1} are also observed. The band situated at 1068 cm^{-1} is stronger on spent Ni and Pd-supported catalysts while it is weak on the spent Cu/alumina. On the contrary, the band at 1020 cm^{-1} is prominent on spent Cu and Ru based catalyst.

Aoshima et al. [161] assigned the bands appearing in the region 1030-1070 cm^{-1} to C-O-C stretching vibration of the tetrahydrofuran ring in interaction with acid catalysts. Barsberg and Thygesen [162] assigned the band at 1020 cm^{-1} to furan ring C-H wag vibration of polyfurfuryl alcohol. This suggests that the type of carbonaceous material deposited on the surface of the spent catalysts depends on the active metal. On spent Ni and Pd based catalysts, this carbonaceous material might be a hydrogenated furan ring oligomer whereas on spent Cu and Ru based catalysts this material might be of polyfuran type.

At this point, it is worth comparing our IR results to those obtained on spent catalysts from petroleum fractions hydrotreatment [163, 164]. On spent petroleum hydrotreatment catalysts, bands have been observed in the regions of 3000-2800 cm^{-1} and 1700-1300 cm^{-1} [164]. The bands in the region of 3000-2800 cm^{-1} were

assigned to the C-H stretch vibrations of hydrogen bonded to aliphatic carbon and the bands in the region of 1700-1300 cm^{-1} were attributed to C-H, O-H and N-H deformations and C=O and C=C stretch vibrations [164].

Also, a band at 1560 cm^{-1} ascribed to C=C vibrations in highly conjugated structures known as coke band has been observed [165]. The intensive bands observed in this work at 1068 cm^{-1} and 1020 cm^{-1} (Figure 7) have not been reported on spent petroleum hydrotreatment catalysts. This indicates that the nature of the carbonaceous deposits obtained on the catalyst in rich oxygenated compound environments is different from that obtained in hydrocarbon environments and the former material contains significant amounts of the oxygenated compounds.

As it was shown previously, both HMF conversion and product yields decrease on Cu/alumina and Ru/alumina catalysts when the temperature is increased from 155 °C to 189 °C. It has been reported elsewhere that the Cu-based catalysts are susceptible to deactivation not only by the formation of coke, but also by catalyst poisoning due to adsorption of either reactant or byproducts and/or changes in the oxidation state of the copper during the reaction [166-168]. The ATR-IR spectra of the spent alumina-supported Cu and Ru catalysts have shown the deposition of compounds with both carbonyl and aromatic functionalities on the surface. These compounds, which are probably produced by oligomerization, might be the main cause of deactivation.

Although Ni/alumina also presents high carbon content, no loss of conversion was observed on this catalyst when the temperature was increased. This difference in susceptibility of the catalytic activity toward carbon deposition might be explained by the chemical nature of the deposited carbonaceous material. Polyfuran ring oligomers present on Cu and Ru based catalysts should be more strongly adsorbed on the surface and therefore cause more deactivation.

Moreover, as it is shown in Table 12, the spent Cu-based catalyst has a lower mass ratio of active metal to aluminum than the fresh catalyst, whereas the fresh and spent Ni, Pd and Ru based catalysts have similar mass ratios after reaction. These results indicate that no leaching of the Ni, Pd and Ru metals had occurred during the reaction, whereas a small amount of Cu is leached into the aqueous phase. The slight decrease of copper content on the spent Cu/alumina catalyst might be another factor that causes the loss of activity observed on this catalyst.

Table 12. Mass ratio of active metal to aluminum for both fresh and spent monometallic alumina-supported catalysts

Catalyst (%wt Me/%wt Al)	Ni/alumina Ni/Al	Pd/alumina Pd/Al	Cu/alumina Cu/Al	Ru/alumina Ru/Al
Fresh	0.245	0.014	0.273	0.018
Spent	0.241	0.014	0.248	0.018

In summary, the Cu and Ru based catalysts are prone to deactivation by the carbonaceous material deposited on the catalyst surface. All spent alumina monometallic catalysts have high carbon content, however the Ni and Pd based catalysts are less susceptible to deactivation by carbon deposition. The ATR-IR results indicate that the deposited carbonaceous material type of the alumina-supported Ni and Pd catalysts is different from the alumina-supported Cu and Ru catalysts. Hydrogenated furan ring oligomer species are likely deposited on the Ni and Pd based catalysts whereas polyfuran compounds are deposited on the Cu and Ru based catalysts.

5. BIMETALLIC Ni-Cu CATALYSTS SUPPORTED ON ALUMINA: INFLUENCE OF THE IMPREGNATION SEQUENCE ON THE HYDRODEOXYGENATION OF 5-HYDROXYMETHYLFURFURAL

In the Chapter 3 it was found that the silica-supported monometallic catalysts are drastically deactivated. On the other hand, the alumina-supported monometallic catalysts studied in Chapter 4 are more active and have a better stability than those supported on silica, despite a high amount of carbonaceous material is deposited on the surface. In Chapter 4 it was also shown from TPR that some of the nickel was not reducible because it was associated as nickel aluminate spinel. It was thought that reducing this interaction the activity of the catalyst might be increased. This chapter presents then the effect of the addition of copper to the formulation of the catalyst and the effect of the order of impregnation.

In the literature, it has been reported that bimetallic solids may present reaction selectivity and even catalytic properties completely different from the corresponding monometallic catalysts as a result of both electronic and structural effects [169, 170].

In this chapter, bimetallic Ni-Cu catalysts supported on alumina with three different impregnation sequences were investigated in the HDO of HMF in aqueous medium. All bimetallic catalysts were prepared by incipient wetness impregnation with the nominal contents of 8 wt% Ni and 2 wt% Cu. The reactions were carried out at a hydrogen pressure of 0.41 MPa and a temperature range of 137-189 °C.

5.1 CATALYSTS CHARACTERIZATION

5.1.1 N_2-physisorption, chemical composition and metal dispersion

The metal content, surface area, total pore volume (TPV) and average pore diameter (APD) of the prepared material are presented in Table 13. All catalysts have a total metallic Ni+Cu content about 10 wt%, which is close to the nominal metallic contents.

Table 13. Characterization of the supported monometallic and bimetallic Ni-Cu catalysts

Catalyst	Bulk content (wt%)		S_{BET}[b] (m^2/g)	TPV[c] (cm^3/g)	APD[d] (nm)	D[e] (%)	Ni Red.[f] (mol/mol)
	Ni	Cu					
alumina	-	-	213	0.57	7.8	-	-
Ni/alumina	9.7	-	180	0.43	6.6	4.9	0.11
Cu/alumina	-	9.5	169	0.40	6.7	-	-
CuNi/A-Int.cal	7.7	2.3	170	0.43	6.5	51	0.10
NiCu/A-Int.cal	8.0	2.3	175	0.44	6.7	73	0.21
CuNi/A-CoImp	7.5	2.2	160	0.41	6.6	54	0.04

[a]Bulk metallic content (wt%) measured by ICP-OES
[b]*S_{BET}*: surface area calculated from BET method
[c]*TPV*: total pore volume calculated from BJH desorption
[d]*APD*: average pore diameter calculated from BJH desorption
[e]*D*: metal dispersion using H_2 as reactant gas
[f]Nickel reducibility at reaction conditions calculated from molecular hydrogen consumption per mole nickel present on the catalyst from TPR

For the bimetallic solids, the BET surface areas (SA_{BET}), the total pore volume and the average pore diameter are lower when compared to the properties of the alumina support (Table 13). Among the catalysts, CuNi/A-CoImp catalyst has the lowest SA_{BET} (160 m^2/g) and total pore volume (0.41 cm^3/g). These results are in

agreement with other authors [171, 172] and indicate that there is a partial blocking of the support pores by the metal particles.

It is well known that copper does not chemisorb hydrogen at room temperature [173]. Metal dispersion was then calculated assuming that all the hydrogen was chemisorbed on nickel. The metal dispersion is then between 51% and 73% (Table 13). These metal dispersion values are significantly higher than that for Ni/alumina, and indicate that the addition of copper to the Ni-supported catalyst increases the nickel dispersion on the surface. These metal dispersion values are higher than those reported by Gandarias et al. [174] for bimetallic Ni-Cu catalysts measured by H_2 chemisorption, but those catalysts have a higher metal content.

5.1.2 TPR measurements

TPR profiles of the catalysts are shown in Figure 8. The monometallic Cu catalyst profile was adjusted, its signal intensity value multiplied by 0.125, for comparative purposes.

The reduction pattern of Cu/alumina shows two reduction peaks at 217 °C and 241 °C, which are attributed to the reduction of amorphous CuO species and bulk CuO, respectively [96, 99, 100]. The reduction pattern of Ni/alumina consists of a broad peak extending from 450 °C to 900 °C with two prominent peaks (Figure 8). The peak centered at 576 °C can be assigned to the reduction of NiO interacting strongly with the support [102-104]. The peaks at 693 °C and 786 °C have been respectively associated to Ni^{2+} ions occupying octahedral and tetrahedral sites in the Ni spinel structure [105-108].

TPR profiles of the bimetallic Ni-Cu catalysts are significantly different from those of the monometallic solids. For all the bimetallic catalysts a low temperature peak

is observed around 260 °C. A similar peak has been observed by Kang et al. [175], which assigned to the reduction of highly dispersed bulk CuO. Copper in the bimetallic catalysts is being reduced at a higher temperature than the monometallic solid. This result shows that due to the presence of nickel the reducibility of copper decreases.

Figure 8. Temperature-programmed reduction profiles of the supported monometallic and bimetallic Ni-Cu catalysts

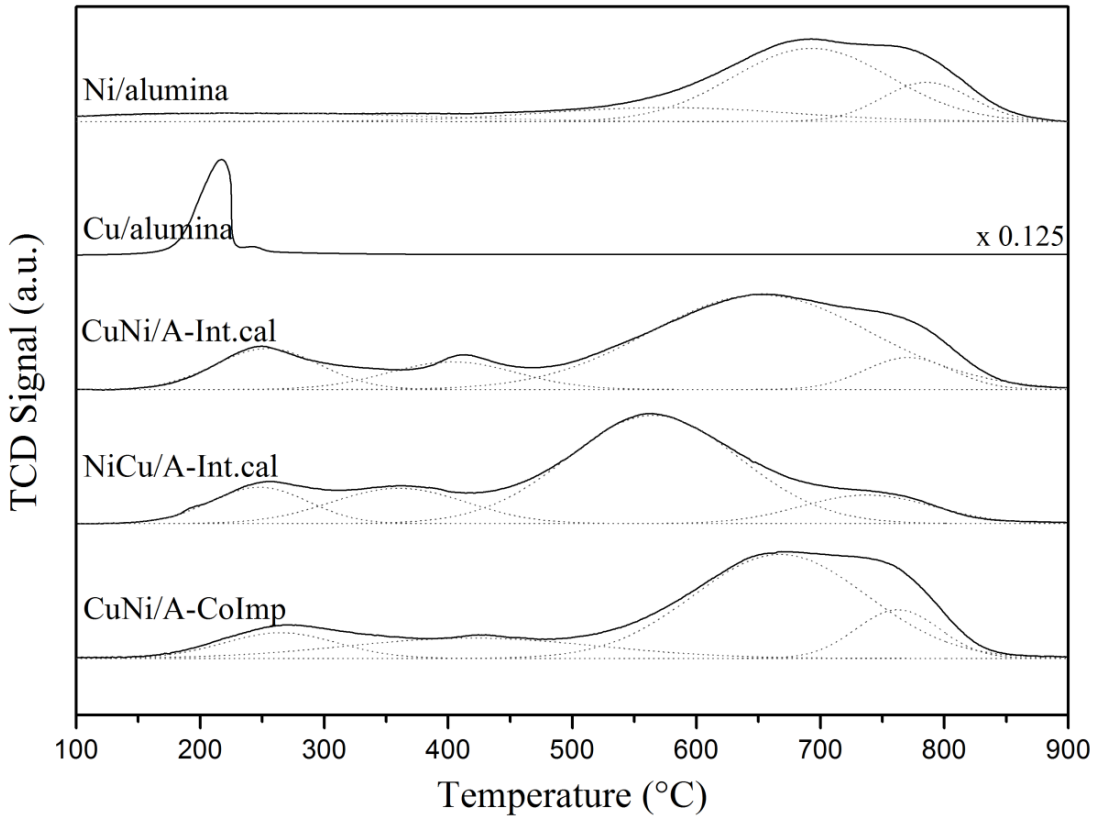

A second reduction peak is observed for the bimetallic catalysts situated between 360 °C and 485 °C. Other authors have observed this peak and they have suggested that it corresponds to reduction of NiO [176] or nickel species more

easily reduced by the interaction of Ni with the surface of copper oxide (Ni-Cu alloy particles) [175].

The other two high temperature peaks exhibit a remarkable shift towards lower reduction temperatures in comparison to Ni/alumina catalyst. Indeed, NiCu/A-Int.cal is the catalyst with lower reduction temperature peaks. These high temperature peaks, centered around 640 °C and 760 °C, could be related to Ni spinel species.

In general, the TPR profiles show that the addition of Cu to the Ni-supported catalyst promotes the reduction of the Ni-based species to lower temperatures. In the literature has been suggested that this change in the reduction temperature is due to an interaction between the Ni and Cu particles or an alloy effect [175, 177].

To determine the amount of nickel reduced at reaction conditions, TPR were run following the activation procedure, it means, heating at 500 °C at a rate of 2 °C/min, staying at this temperature for 4 hours and using the TCD to evaluate the quantity of hydrogen consumed (Table 13). These experiments show that copper is totally reduced as expected whereas Ni/alumina catalyst has a low degree of reduction (11 mole%). This behavior has been explained due to nickel ions that are incorporated within the support are not exposed to the hydrogen molecules [28].

For the bimetallic catalyst, it was then assumed that all copper is reduced and the extent of the reduction was calculated for nickel. The degree of nickel reduction in the bimetallic catalysts depends on the impregnation sequence. CuNi/A-Int.cal shows a similar reducibility of Ni as compared to Ni/alumina, where CuNi/A-CoImp presents a lower degree of reduction. NiCu/A-Int.cal has a higher degree of reduction of Ni than that achieved for the monometallic Ni catalyst. This indicates that the reduction of nickel species is favored when copper is impregnated and calcined in the first step. Similar results have been observed by Juszczyk et al.

[178]. It has also being suggested that the enhancement of Ni reducibility is possibly due to a hydrogen spillover effect from a more readily reducible copper site [178].

5.1.3 XPS measurements

The Ni $2p_{3/2}$ spectra for calcined Ni/alumina and Ni-Cu/alumina are presented in Figure 9. In general, the Ni $2p_{3/2}$ peak is centered at ca. 856.1 eV with the corresponding Ni $2p_{1/2}$ satellite at 862.2 eV. Such binding energies correspond to Ni^{2+} species in the nickel aluminate spinel phase [179, 180].

Figure 9. XPS Ni 2p region for calcined Ni/alumina and Ni-Cu/alumina catalysts

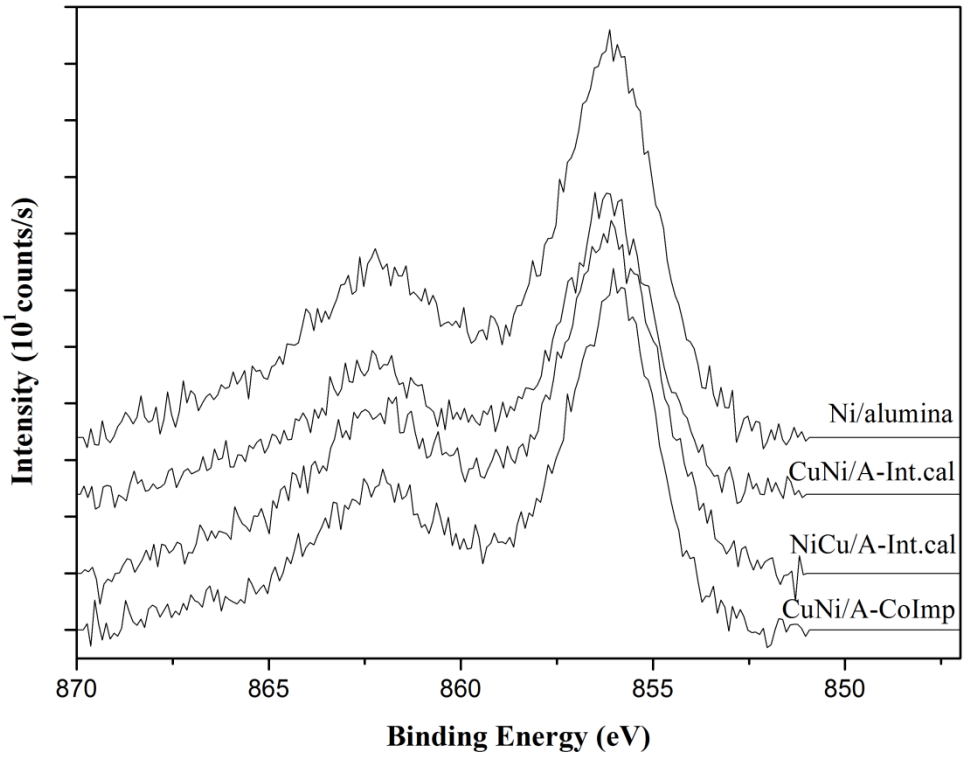

Results of Ni $2p_{3/2}$ in the alumina-supported Ni-Cu catalysts show that the binding energy shifts slightly with the addition of copper to the monometallic Ni catalyst. Only NiCu/A-Int.cal does not present a shift with the incorporation of copper. A slight increase of the binding energies for the CuNi/A-Int.cal and CuNi/A-CoImp catalysts is observed, $\Delta BE \approx 0.29$ and $\Delta BE \approx 0.08$ respectively. It is likely due to a decrease in electron density of Ni aggregates or a higher reduction degree of Ni particles caused by the interaction between Ni and Cu [181].

For Cu/alumina and alumina-supported Ni-Cu catalysts, the Cu $2p_{3/2}$ peak is found at BE ≈ 932.9 eV and the Cu $2p_{1/2}$ peak at BE ≈ 952.5 eV (Figure 10). The Cu $2p_{3/2}$ peak has been associated to Cu^{2+} or Cu^{0} species [182, 183]. There is not a significant change in the Cu $2p_{3/2}$ binding energy with the modification of the impregnation sequence of copper in the bimetallic Ni-Cu catalysts.

Figure 10. XPS Cu 2p region for calcined Cu/alumina and Ni-Cu/alumina catalysts

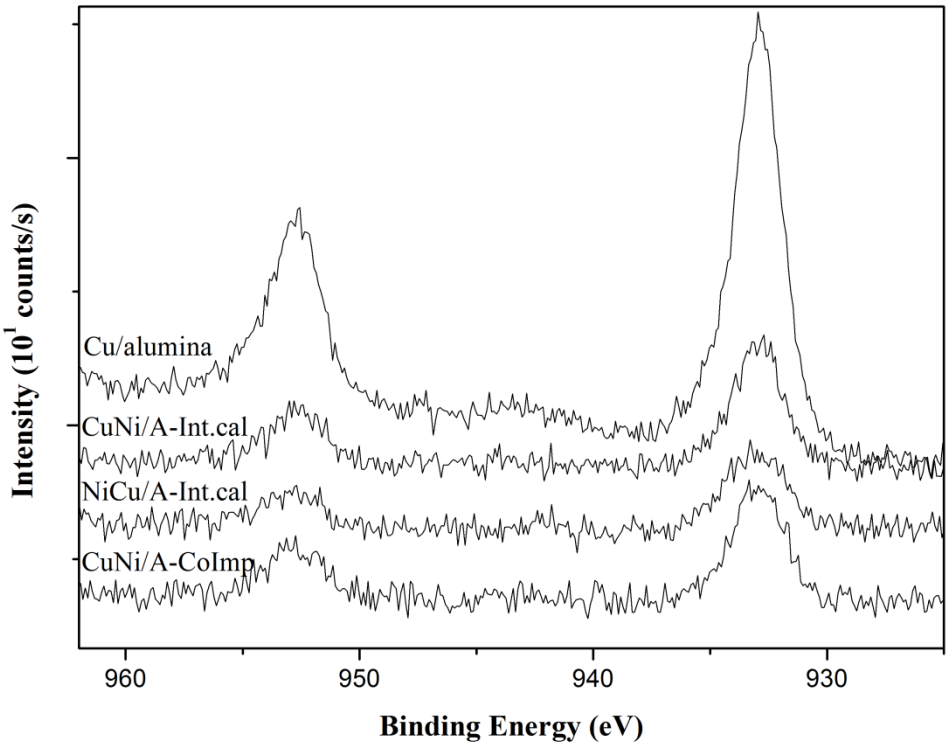

The surface atomic metal/Al and Ni/Cu ratios are compiled in Table 14. The surface concentration of Ni and Cu is lower in the bimetallic Ni-Cu catalysts than in the monometallic solids due to lower metal contents in the bimetallic solids.

Table 14. Surface atomic composition (wt%) and atomic ratio of calcined alumina-supported Ni-Cu catalysts by XPS

Catalyst	Bulk atomic ratio	Surface atomic ratios		
	Ni/Cu	Ni/Al	Cu/Al	Ni/Cu
Ni/alumina	-	0.108	-	-
Cu/alumina	-	-	0.073	-
CuNi/A-Int.cal	3.6	0.074	0.021	3.5
NiCu/A-Int.cal	3.8	0.105	0.012	8.9
CuNi/A-CoImp	3.7	0.075	0.014	5.2

For the bimetallic catalyst, the surface atomic concentration of nickel and copper depends on the impregnation sequence. When nickel is impregnated in the first step (CuNi/A-Int.cal) or at the same time than copper (CuNi/A-CoImp), its surface concentration is low. The same is true for copper, NiCu/A-Int.cal and CuNi/A-CoImp present a lower surface concentration of this metal.

This result suggests that some of the metal that is impregnated and calcined first gets into the lattice of alumina and forms the corresponding aluminate spinel and this spinel is present in crystallites larger than about 4 nm, the XPS inelastic electron mean free path. As a consequence of this, the metal being impregnated in the second place is less prone to get into the alumina lattice and will have a higher concentration on the surface.

This might also explain the difference in the atomic Ni/Cu surface ratio. NiCu/A-Int.cal presents a Ni/Cu atomic surface ratio higher than the bulk material while

CuNi/A-Int.cal has a ratio of 3.5. Interestingly when both metals are coimpregnated the atomic surface ratio is higher than the bulk suggesting that when both metals compete copper has a higher tendency to occupy vacant sites in the alumina lattice.

5.2 CATALYSTS EVALUATION

The hydrodeoxygenation of HMF over supported bimetallic Ni-Cu catalysts was evaluated under a hydrogen atmosphere of 0.41 MPa at a temperature range between 137 °C and 189 °C. The results of catalytic activity are shown in Table 15.

The bimetallic Ni-Cu catalysts present a conversion of HMF between 28 wt% and 56 wt% at 137 °C. The CuNi/A-Int.cal and NiCu/A-Int.cal catalysts have similar conversions of HMF, 54 wt% and 56 wt% respectively. CuNi/A-CoImp gave the lowest conversion as compared to the other bimetallic catalysts. In general, these results show that the bimetallic Ni-Cu catalysts exhibit a significantly higher catalytic activity for the conversion of HMF at 137 °C as compared to the corresponding monometallic catalysts and also their catalytic activity is influenced by the used impregnation sequence.

The changes in the catalytic activity of the bimetallic Ni-Cu catalysts can be caused by changes in the metal dispersion on the catalyst surface, in the electronic properties of the Ni particles and in the total pore volume of catalyst, which are affected by the application of different impregnation sequences.

Higher conversions of HMF on bimetallic catalysts, as compared to Ni/alumina, are achieved with the higher metal dispersion measured by H_2 chemisorption. However CuNi/A-CoImp does not follow this trend, it presents the lower conversion of HMF at 137 °C having a good metal dispersion (54%). Pudi et al. [184] also showed that

conversion of glycerol on several bimetallic Ni-Cu catalysts is directly related to their metal dispersion; however they observed a higher metal dispersion and a low conversion of glycerol on the Ni/alumina catalyst as compared to the bimetallic catalysts.

Table 15. Conversion and liquid product yield obtained over both monometallic and bimetallic Ni-Cu catalysts as a function of temperature

Catalyst	Temp. (°C)	Conv. (wt%)	Product liquid yield (wt%)					
			BHF[a]	MFAL[b]	MFOL[c]	FOL[d]	THFOL[e]	Others
Ni/alumina	137	44	3.6	-	3.2	20.9	3.2	2.1
	155	100	-	-	27.3	41.0	7.6	9.0
	189	100	1.5	1.2	7.6	39.4	9.9	22.4
Cu/alumina	137	40	-	0.8	-	-	-	31.0
	155	94	5.2	21.3	17.7	2.9	-	37.8
	189	36	-	8.6	4.6	0.7	-	16.1
CuNi/A-Int.cal	137	54	-	2.7	4.2	24.1	-	6.4
	155	100	-	-	44.2	39.6	-	3.6
	189	100	-	2.9	19.7	49.5	-	12.2
NiCu/A-Int.cal	137	56	-	-	6.9	30.6	-	5.1
	155	100	-	2.0	22.4	49.1	-	10.5
	189	100	-	1.8	4.6	49.6	-	30.8
CuNi/A-CoImp	137	28	-	-	1.8	8.7	-	4.4
	155	100	-	1.4	43.7	29.7	-	5.0
	189	100	-	2.9	23.9	44.9	-	8.9

[a]*BHF*: 2,5-bis(hydroxymethyl)furan
[b]*MFAL*: 5-methylfurfural
[c]*MFOL*: 5-methyl-2-furfuryl alcohol
[d]*FOL*: furfuryl alcohol
[e]*THFOL*: tetrahydrofurfuryl alcohol

On the other hand, a similar correlation can also be made from the reducibility degree of nickel from TPR. HMF conversion on NiCu/A-Int.cal increases due to its higher Ni reducibility; on the contrary the conversion decreases on CuNi/A-CoImp due to its lower Ni reducibility. It is well known that catalyst activity in hydrotreatment reactions depend on the amount of reduced metallic sites, so an increase of the amount of reduced nickel particles promotes an increase in the conversion of HMF. In the case of CuNi/A-Int.cal, the addition of copper promotes the conversion of HMF on this catalyst since its nickel reducibility is similar to Ni/alumina.

HMF conversion seems to be influenced by the Ni surface content; a higher conversion is obtained with the higher content of surface nickel. However, CuNi/A-CoImp does not follow this trend. A relationship between the HMF conversion and the change of binding energy of Ni on the bimetallic Ni-Cu catalysts is not observed. Kang et al. [175] have also pointed out that a correlation between conversion of 1,3-butadiene and the structural parameters of Ni-Cu catalysts is difficult and that the only indication is the decrease of the activity with the addition of Cu, likely caused by the increase of the electron density of nickel. HMF conversion does not follow a clear tendency with the change of electron density of Ni. Nonetheless, the TPR results suggest an interaction between the Ni and Cu particles. Other authors have suggested that the interaction between the Ni and Cu particles modifies the catalytic activity of the bimetallic Ni-Cu catalysts [175, 177, 185].

A direct relationship between the HMF conversion and the total pore volume of the catalysts is also observed. The higher conversions are obtained with the catalysts with larger total pore volumes, being NiCu/A-Int.cal the catalyst with higher conversion of HMF and larger total pore volume. The larger pores allow the higher diffusion of the reactant and its derivatives products.

In summary, the metal dispersion, reducibility degree of Ni, nickel surface contents and total pore volume can have an impact on the catalytic activity of the bimetallic catalysts as compared to Ni/alumina. Most of researches have only discussed the influence of one factor, usually the changes of electron density of Ni. In this work, various factors were shown to have influence on the catalytic activity of the bimetallic Ni-Cu catalysts.

As the temperature increases, the HMF conversion on Ni/alumina and the bimetallic Ni-Cu catalysts becomes complete, except for Cu/alumina at 189 °C, whose catalytic activity decreases at the higher temperature. In Chapter 4 this behavior on Cu/alumina was discussed.

The product yields on bimetallic Ni-Cu catalysts are also summarized in Table 15. As it was mentioned in Chapter 4, a predominant decarbonylation reaction of HMF is observed on Ni/alumina, whereas hydrogenolysis and cyclization reactions were favored on Cu/alumina. On all bimetallic catalysts HMF is converted mainly to FOL. This decarbonylation reaction is also favored at the higher temperatures.

NiCu/A-Int.cal is the catalyst with the higher formation of FOL at all reaction conditions. From the results of hydrogen consumption per mole nickel can be observed that NiCu/A-Int.cal has a higher amount of reduced nickel species in comparison to the other bimetallic catalysts. These results are coherent with those obtained by XPS showing that this catalyst has also higher amounts of surface nickel. As it was shown previously that Ni has an overall promoting effect to decarbonylate HMF, a higher amount of reduced nickel species on NiCu/A-Int.cal might explain the higher conversion of HMF to FOL on this catalyst. Therefore, the addition of Cu to Ni/alumina produces more easily reducible surface nickel species, which promote the higher formation of FOL on the bimetallic Ni-Cu catalysts.

The main product from hydrogenolysis of HMF, MFOL, is attained in a yield between 1.8 wt% and 6.9 wt% on the bimetallic Ni-Cu catalysts at 137 °C. Higher amounts of MFOL are achieved at 155 °C. At this mild reaction condition, the CuNi/A-Int.cal and CuNi/CoImp catalysts have the higher concentrations of MFOL, whereas NiCu/A-Int.cal produces the lower MFOL yield. MFOL can be obtained from hydrogenolysis of BHF and hydrogenation of MFAL. However in the reaction products on the bimetallic catalysts only MFAL is detected at the used reaction conditions.

A clear trend of the MFOL yield with the amount of reduced Ni species can not be observed on the bimetallic Ni-Cu catalysts, but these results highlight that the presence of Cu on the bimetallic catalysts promotes the hydrogenolysis of HMF to MFOL, except for NiCu/A-Int.cal. The review of the literature reveals that few studies have been conducted on Ni-Cu alloys for the hydrogenolysis of aldehydes.

Gandarias and co-workers [186] shown that the Ni-Cu/Al_2O_3 catalysts promote the activity for the C-O bond cleavage in the hydrogenolysis of glycerol to 1,2-propanediol at a N_2 atmosphere and using formic acid as hydrogen donor molecule. It is possible that the formation of Ni-Cu alloys on the bimetallic catalyst surface supported on alumina can be responsible of the beneficial effect on both the conversion and hydrogenolysis of the C-OH bond of HMF. It can be supported with the results reported herein, where it is observed that the CuNi/A-Int.cal catalyst has the higher yield of MFOL. This catalyst shows a significant decrease of the electron density of Ni as it was aforementioned in section 5.2.3, suggesting an interaction between Ni and Cu, as it was also suggested by the TPR results.

In regard to the hydrogenolysis of HMF on NiCu/A-Int.cal catalyst, a different behavior was observed as compared to the other bimetallic Ni-Cu catalysts. In Table 15 is shown that only 22.4 wt% of MFOL yield is achieved on NiCu/A-Int.cal catalyst a 155 °C. Besides, this catalyst has the higher yield to FOL. This result

might be directly influenced by the impregnation sequence applied, in the case of this catalyst Cu is first impregnated and, after a calcination step, it is again impregnated with Ni. As it was aforementioned in section 5.2.2, when the Ni precursor is impregnated first on the alumina support, a fraction of the Ni^{2+} ions occupy the octahedral and tetrahedral sites to form a nickel aluminate of spinel-like structure. On the contrary, when the Cu precursor is impregnated first, it is possible that Cu is dispersed on the surface, thus preventing the diffusion of the Ni^{2+} ions into the cavities of the alumina support. For this reason, the availability of the Ni ions on the NiCu/A-Int.cal catalyst surface is greater than that of the other bimetallic Ni-Cu catalysts. It can be supported from XPS results presented in section 5.2.3, where it is shown that the NiCu/A-Int.cal catalyst has higher surface ratios of Ni/Al and Ni/Cu. Therefore, it can be inferred that Ni is the main active metal on the NiCu/A-Int.cal catalyst, which catalyzes the preferential decarbonylation reaction instead of the hydrogenolysis reaction.

THFOL is a secondary product obtained from ring-hydrogenation reaction of FOL. On Ni/alumina, THFOL is reached in considerable amounts. However, THFOL is not detected on the bimetallic Ni-Cu catalysts studied herein. This result indicates that the addition of Cu suppresses the ring-hydrogenation reaction of HMF.

On supported bimetallic Ni-Cu catalysts, only DMF, 2,5-hexanedione (HD), 1-hydroxy-2,5-hexanedione (HHD) and 3-methyl-cyclopentanone (m-C5one) are observed at the two lower temperatures. The ring-opening compounds are also observed on Ni/alumina, whereas m-C5one is observed on Cu/alumina. These compounds can be produced through ring-opening and cyclization reactions of DMF [187]. These results seem to indicate that the formation of secondary compounds on bimetallic catalysts is through the combined effect between Ni and Cu metals.

As the temperature rises at 189 °C, other compounds like FAL, MTHFOL, 1,2-pentanediol and 5-methyl-2-hexanone also appear. NiCu/A-Int.cal presents the higher concentration of other compounds as compared to the other bimetallic catalysts, whereas CuNi/A-CoImp shows the lower value. In general, secondary products from hydrogenolysis, ring-hydrogenation, ring-opening and cyclization reactions of HMF and/or its derivative compounds are observed on bimetallic Ni-Cu catalysts.

6. OVERALL DISCUSSION

Four reduced metals supported on silica were studied in Chapter 3 for the hydrodeoxygenation of 5-hydroxymethylfurfural (HMF) in aqueous medium. Silica-supported catalysts show almost complete reduction of the metals at temperatures below 600 °C. Metal dispersion of the silica-supported catalysts is in the range of 2% and 31%. The previous results show that the apparent order of activity for the conversion of HMF is:

$$Pd \geq Ni \geq Cu \approx Ru$$

The silica-supported catalysts present a drastic deactivation that can be explained for a significant deposition of carbonaceous material. Carbon deposited on both spent Ni and Pd catalysts seems to be less aromatic, whereas the silica-supported Cu and Ru catalysts contain more aromatic aldehyde structures. It is possible that these latter compounds are strongly adsorbed on the surface thereby are blocking the access to the active sites of the catalyst.

On the other hand, Ni/alumina shows a degree of reduction around 71% at the TPR analysis conditions, whereas alumina-supported Pd, Cu and Ru catalysts are completely reduced. Metal dispersion of the alumina-supported catalysts is between 15% and 52%. The apparent order of activity for the conversion of HMF on alumina-supported catalysts is similar to that observed on silica-supported catalysts. However, the alumina-supported catalysts have a higher conversion of HMF than the silica-supported catalysts. In addition, the use of alumina as catalyst support resulted in less deactivation as compared to silica support.

In the literature has also been pointed out that the alumina-supported Mo and CoMo catalysts have a higher activity than the silica-supported catalysts for the

conversion of guaiacol [188, 189]. This difference in catalytic activity using the two supports has been explained by the density of their acid sites [189]. From metal dispersion data pointed out previously, it is concluded that the alumina-supported catalysts have a higher metal dispersion than silica-supported catalysts. Therefore, both the enhanced metal dispersion and the higher amount of acid sites on alumina-supported catalysts might promote the conversion of HMF as compared to the silica-supported catalysts.

A comparison of the catalytic activity results of the catalysts supported on both silica and alumina reveals that even though the nature of the support has an influence on the catalyst activity and its stability, the nature of the reaction products depends strongly on the kind of supported metal. For the Ni, Pd and Ru based catalysts, the decarbonylation of the HMF carbonyl group proceeds predominantly to form FOL. Significant amounts of ring-hydrogenated products are observed with Pd and Ru based catalysts. In the case of the Cu-based catalysts, although a very low conversion of HMF is obtained over Cu/silica, it was possible to determine that Cu favors the hydrogenolysis and cyclization reactions.

As it was mentioned previously, Ni metal is responsible for the selective decarbonylation of HMF. In the case of the Ni/silica catalyst, a lower interaction between Ni particles and the silica support is suggested from TPR results as compared to Ni/alumina. This lower interaction could enhance the reducibility of a large amount of nickel particles dispersed on the catalyst surface. Thus the higher amount of reduced nickel particles exposed on the silica-supported Ni catalyst compared to Ni/alumina could contribute to the higher decarbonylation of HMF to FOL at 155 °C.

Hydrogenolysis reaction products are more favored on Ni/alumina than Ni/silica catalyst. Yang et al. [190] have shown that strong acid sites may influence the hydrogenolysis of anisole, while metallic sites hydrogenate the intermediate

compounds to obtain cyclohexane, when the hydrodeoxygenation of anisole is evaluated over Ni-supported catalysts. This suggests that the nature of the alumina support favors the hydrogenolysis reaction of HMF to produce mainly MFOL and DMF, which occurs in parallel to the dominant reaction of decarbonylation. Additionally, Ni/alumina also promotes the formation of ring-opening products like 2-pentanone, 1,2-pentanediol, 1-hydroxy-2-pentanone, among others, which are likely formed through hydrogenolysis reactions of FOL and are not observed on Ni/silica.

Pd/alumina produces markedly more THFOL than FOL, while Pd/silica catalyst produces more FOL than THFOL. In other words, Pd metal has the capacity for decarbonylate the HMF carbonyl group, whereas the subsequent furan ring hydrogenation is indirectly promoted by the nature of the alumina support. These results seem to indicate that selectivity is influenced by the interaction of metal-support, since no FOL or THFOL were obtained when the reaction was evaluated using the bare supports.

It is possible that the alumina support promotes the adsorption of HMF on the catalyst surface since it can be considered as a Lewis base due to the π-electron-rich nature of the furan ring, such as it has been suggested for other aromatic rings [191]. On the other hand, it has been suggested that the metal-support interaction between Pd and alumina support facilitates the electron transfer from Pd to acidic sites on alumina, which leads to the electron-deficient character of the palladium atoms [192-194]. Thus, the adsorption of HMF on the electron-deficient palladium atoms might be promoted due to the enhanced electron donor from the furan ring to the electron-deficient palladium atoms [191].

An interesting behavior is observed with the Cu-based catalysts. In addition to hydrogenation and hydrogenolysis reactions, the formation of cyclic compounds was highlighted. In the literature has been reported that cyclic compounds are

formed as a result of water presence in the reaction medium [148]. However, the results reported herein clearly indicate that copper is required to form this type of compounds. Cyclic compounds are produced in relatively high amounts only on Cu/alumina catalyst.

One prominent decarbonylation reaction of HMF is also observed on Ru/alumina. This catalyst displayed a catalytic behavior similar to Ni/alumina. Notable amounts of decarbonylated and ring-opening products are obtained at 155 °C. However, the reaction is less selective towards hydrogenolysis products and more selective towards ring-hydrogenated products on Ru/alumina as compared to Ni/alumina.

The alumina-supported Cu and Ru catalysts suffer from poor stability during the reaction. Unlike the spent silica-supported catalysts, ATR-IR results showed the appearance of bands at 1020 cm^{-1} and 1068 cm^{-1} on spent alumina-supported catalysts. These bands were prominent and indicate that the carbonaceous material deposited on the Ni and Pd based catalysts could be a hydrogenated furan ring oligomer, whereas on the Cu and Ru based catalysts could be polyfuran compounds.

It is worth to note that the deposition of carbonaceous material is higher on Ni, Pd and Cu catalysts supported on silica than those deposited on alumina. This result seems to indicate that the formation of hydrogenolysis products on alumina-supported catalysts diminishes the possibility of production of carbonaceous material precursor. Barbier and Marecot [195] have suggested that the same metallic reactive sites are responsible for hydrogenolysis and carbonaceous material formation. So, the decrease of the carbonaceous material deposits on alumina-supported catalyst might be a result of the competition between the hydrogenolysis and coke formation reactions for the same metallic sites.

On the other hand, Parera and co-workers [196, 197] have shown that the precursors of carbonaceous material or coke are polymeric unsaturated compounds and that the hydrogenolysis reaction destroys coke precursors producing lighter and more hydrogenated products. Therefore, a carbonaceous material more hydrogenated that is less toxic for the metallic function might be produced from hydrogenolysis reaction of HMF on the alumina-supported catalysts.

On Ru/alumina, it is deposited a higher amount of carbonaceous material than Ru/silica. As it was aforementioned, Ru/alumina does not favor the hydrogenolysis reaction so lower amounts of coke precursors are destroyed, favoring the deposition of these precursors.

In the chapter 5, it is shown that the addition of Cu to the monometallic Ni catalyst modifies the nickel reducibility in the bimetallic catalysts. The degree of nickel reduction in the bimetallic Ni-Cu catalysts is also changed with the variation of the impregnation sequence. CuNi/A-Int.cal shows similar nickel reducibility than the Ni/alumina catalyst, whereas the CuNi/A-CoImp and NiCu/A-Int.cal catalysts have a higher and a lower degree of reducibility respectively.

The catalytic activity and the product yields in the hydrodeoxygenation of HMF are influenced by the addition of copper to Ni/alumina. At 137 °C, the conversion of HMF is proportional to the content of reduced nickel for the bimetallic catalysts. Conversion of HMF is complete at the higher temperatures. MFOL and FOL are the main products observed on the bimetallic Ni-Cu catalysts.

The effect of the reducibility degree of nickel on the MFOL/FOL yield ratio at 155 °C is presented in Figure 11 in order to correlate the reduction of nickel with the preferential reaction in each bimetallic Ni-Cu catalyst. It is found that there is a tendency between the Ni reducibility and the MFOL/FOL ratio on the bimetallic Ni-

Cu catalysts. This tendency is influenced by the addition of Cu since the point corresponding to Ni/alumina does not fit into the trendline. From this figure can be easily understood the catalytic behavior of the bimetallic catalysts. At higher values of Ni reducibility, the conversion of HMF leads to decarbonylation reactions on the bimetallic Ni-Cu catalysts. On the contrary, at lower values of Ni reducibility the hydrogenolysis reactions occur preferentially on the bimetallic catalyst.

Figure 11. Effect of nickel reducibility on the MFOL/FOL yield ratio at 155 °C

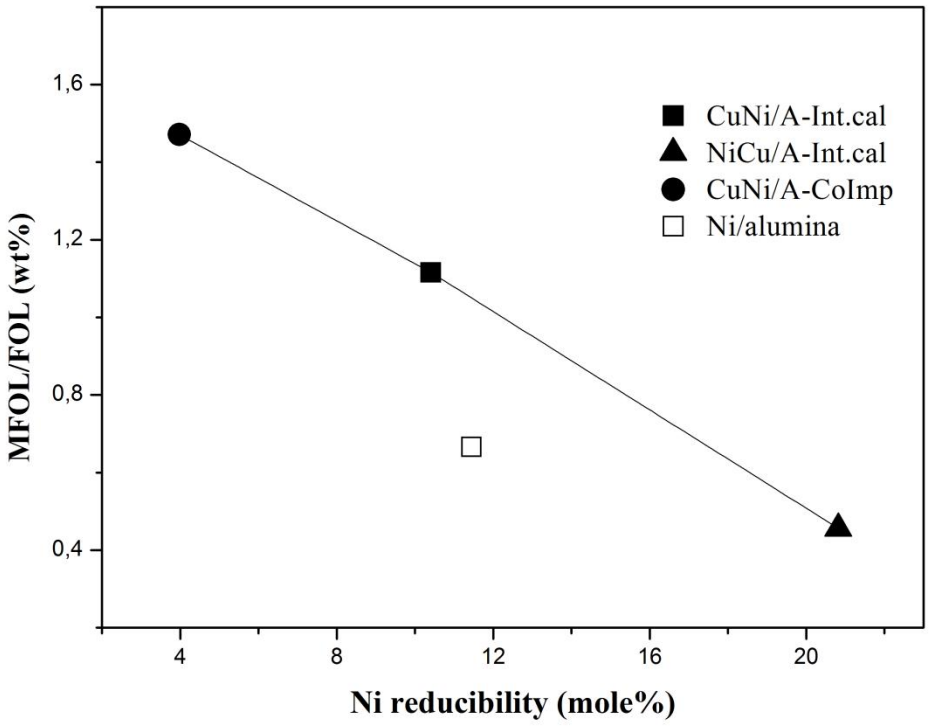

7. CONCLUSIONS

The nature of the reaction products in the conversion of 5-hydroxymethylfurfural depends strongly upon the kind of supported metal on catalyst, regardless of the nature of the support. The Ni, Pd and Ru based catalysts promote decarbonylation reaction of HMF to furfuryl alcohol. The decarbonylated products are also promoted by the high temperatures. Cu-based catalysts favor both the hydrogenolysis of HMF to 5-methyl-2-furfuryl alcohol and the formation of cyclic-compounds.

Regarding the influence of the support nature, the alumina-supported catalysts possess a higher metal dispersion than the silica-supported catalysts. These results might be influenced by the stronger interaction between the metal particles and the alumina support. In fact, the degree of reducibility of the supported transition metals is observed to depend on the metal-support interaction. If the interaction is stronger then it will be more difficult to reduce the supported metal.

For alumina-supported catalysts, higher conversions of HMF are obtained as compared to silica-supported catalyst. Ni- and Pd-based catalysts are the most active catalysts in the hydrodeoxygenation of HMF. The formation of hydrogenolysis, ring-hydrogenated and ring-opening products in the conversion of HMF is strongly influenced by the nature of the support. A higher amount of these compounds are obtained on alumina-supported catalysts as compared to the silica-supported catalysts.

Nevertheless, all silica-supported catalysts and the Cu/alumina and Ru/alumina catalysts exhibit a drastic deactivation caused by the deposition of carbonaceous material on the surface. Even though a high content of carbonaceous material is deposited on the surface of the Ni/alumina and Pd/alumina catalysts, these

catalysts are more stable than the silica-supported catalysts. The promotion of hydrogenolysis reactions on alumina-supported catalysts seems also to favor the hydrogenolysis of coke precursors, thus producing lighter and more hydrogenated carbonaceous material compounds.

The addition of Cu to the alumina-supported Ni catalyst improves the conversion of HMF. This enhanced conversion is favored by the higher amount of nickel reduced on the bimetallic Ni-Cu catalysts. Besides, a change in the nickel reducibility degree is caused by the different impregnation sequences applied during the catalyst preparation. MFOL and FOL are the main products observed in the conversion of HMF. The concentration of these compounds can be modified with the amount of nickel reduced on the bimetallic Ni-Cu catalysts. Much higher yields of decarbonylated compounds are obtained on the bimetallic catalyst with higher nickel reduction degree (NiCu/A-Int.cal). On the contrary, a higher yield of hydrogenolyzed compound is obtained on the bimetallic catalyst with lower nickel reduction degree (CuNi/A-CoImp).

The results of this work show that a mixture of different kinds of molecules is produced in the hydrodeoxygenation of HMF in aqueous phase. Therefore, multiple processes for multiple types of raw materials should be considered within a biorefinery concept as it happens in the petroleum industry.

CITATIONS

[1] WYMAN, CE. Biomass ethanol: Technical Progress, Opportunities, and Commercial Challenges. In: *Annual Review of Energy and the Environment* 1999. Vol. 24. p. 189-226.

[2] KLASS, DL. Chapter 3 - Photosynthesis of Biomass and Its Conversion-Related Properties. In: *Biomass for Renewable Energy, Fuels, and Chemicals*. KLASS, DL. Ed. First ed. San Diego: Academic Press; 1998. p. 51-90.

[3] DE, S, et al. Hydrodeoxygenation processes: Advances on catalytic transformations of biomass-derived platform chemicals into hydrocarbon fuels. In: *Bioresource Technology* 2015. Vol. 178. p. 108-118.

[4] VASILAKOS, NP and BARREIROS, MT. Homogeneous catalytic hydrogenolysis of biomass. In: *Ind. Eng. Chem. Process Des. Dev.* 1984. Vol. 23. p. 755-763.

[5] BOZELL, JJ and PETERSEN, GR. Technology development for the production of biobased products from biorefinery carbohydrates-the US Department of Energy's "Top 10" revisited. In: *Green Chemistry* 2010. Vol. 12. p. 539-554.

[6] LEWKOWSKI, J. Synthesis, chemistry and applications of 5-hydroxymethylfurfural and its derivatives. In: *Arkivoc* 2001. Vol. 1. p. 17-54.

[7] ANTAL JR, MJ, et al. Mechanism of formation of 5-(hydroxymethyl)-2-furaldehyde from d-fructose and sucrose. In: *Carbohydrate research* 1990. Vol. 199. p. 91-109.

[8] ANET, EFLJ. 3-Deoxyglycosuloses (3-Deoxyglycosones) and the Degradation of Carbohydrates. In: *Advances in Carbohydrate Chemistry*. MELVILLE, LW. Ed. First ed. London: Academic Press; 1964. p. 181-218.

[9] ROMÁN-LESHKOV, Y, et al. Production of dimethylfuran for liquid fuels from biomass-derived carbohydrates. In: *Nature* 2007. Vol. 447. p. 982-985.

[10] JAMES, OO, et al. Towards the conversion of carbohydrate biomass feedstocks to biofuels via hydroxylmethylfurfural. In: *Energy and Environmental Science* 2010. Vol. 3. p. 1833-1850.

[11] GANDINI, A and BELGACEM, MN. Furans in polymer chemistry. In: *Progress in Polymer Science* 1997. Vol. 22. p. 1203-1379.

[12] WILSENS, CHRM, et al. Thermotropic Polyesters from 2,5-Furandicarboxylic Acid and Vanillic Acid: Synthesis, Thermal Properties, Melt Behavior, and Mechanical Performance. In: *Macromolecules* 2014. Vol. 47. p. 3306-3316.

[13] SCHIAVO, V, et al. Hydrogénation catalytique du 5-hydroxyméthylfurfural en milieu aqueux. In: *Bulletin de la Société chimique de France* 1991. Vol. 128. p. 704-711.

[14] BUNTARA, T, et al. Caprolactam from Renewable Resources: Catalytic Conversion of 5-Hydroxymethylfurfural into Caprolactone. In: *Angewandte Chemie International Edition* 2011. Vol. 50. p. 7083-7087.

[15] ALAMILLO, R, et al. The selective hydrogenation of biomass-derived 5-hydroxymethylfurfural using heterogeneous catalysts. In: *Green Chemistry* 2012. Vol. 14. p. 1413-1419.

[16] LUIJKX, GC, et al. Ether formation in the hydrogenolysis of hydroxymethylfurfural over palladium catalysts in alcoholic solution. In: *Heterocycles* 2009. Vol. 77. p. 1037-1044.

[17] CHIDAMBARAM, M and BELL, AT. A two-step approach for the catalytic conversion of glucose to 2,5-dimethylfuran in ionic liquids. In: *Green Chemistry* 2010. Vol. 12. p. 1253-1262.

[18] Process for producing 5-methylfurfural. HAMADA, K, et al. US Patent No. 4,335,049. 30-June-1982. USA. Utility patent.

[19] ZU, Y, et al. Efficient production of the liquid fuel 2,5-dimethylfuran from 5-hydroxymethylfurfural over Ru/Co3O4 catalyst. In: *Applied Catalysis B: Environmental* 2014. Vol. 146. p. 244-248.

[20] NISHIMURA, S, et al. Selective hydrogenation of biomass-derived 5-hydroxymethylfurfural (HMF) to 2,5-dimethylfuran (DMF) under atmospheric

hydrogen pressure over carbon supported PdAu bimetallic catalyst. In: *Catalysis Today* 2014. Vol. 232. p. 89-98.

[21] WANG, G-H, et al. Platinum–cobalt bimetallic nanoparticles in hollow carbon nanospheres for hydrogenolysis of 5-hydroxymethylfurfural. In: *Nature Materials* 2014. Vol. 13. p. 293-300.

[22] HU, L, et al. Selective Transformation of 5-Hydroxymethylfurfural into the Liquid Fuel 2,5-Dimethylfuran over Carbon-Supported Ruthenium. In: *Industrial and Engineering Chemistry Research* 2014. Vol. 53. p. 3056-3064.

[23] HUANG, YB, et al. Nickel–Tungsten Carbide Catalysts for the Production of 2,5-Dimethylfuran from Biomass-Derived Molecules. In: *ChemSusChem* 2014. Vol. 7. p. 1068-1072.

[24] SAHA, B, et al. Zinc-Assisted Hydrodeoxygenation of Biomass-Derived 5-Hydroxymethylfurfural to 2,5-Dimethylfuran. In: *ChemSusChem* 2014. Vol. 7. p. 3095-3101.

[25] KONG, X, et al. Switchable synthesis of 2,5-dimethylfuran and 2,5-dihydroxymethyltetrahydrofuran from 5-hydroxymethylfurfural over Raney Ni catalyst. In: *RSC Advances* 2014. Vol. 4. p. 60467-60472.

[26] BRUNAUER, S, et al. Adsorption of Gases in Multimolecular Layers. In: *Journal of the American Chemical Society* 1938. Vol. 60. p. 309-319.

[27] BOSS, CB and FREDEEN, KJ. *Concepts, Instrumentation and Techniques in Inductively Coupled Plasma Optical Emission Spectrometry*. Third edition ed. USA: Perkin Elmer; 2004.

[28] LI, G, et al. Comparison of reducibility and stability of alumina-supported Ni catalysts prepared by impregnation and co-precipitation. In: *Applied Catalysis A: General* 2006. Vol. 301. p. 16-24.

[29] BECK, A, et al. Pd nanoparticles prepared by “controlled colloidal synthesis” in solid/liquid interfacial layer on silica. I. Particle size regulation by reduction time. In: *Catalysis Letters* 2000. Vol. 65. p. 33-42.

[30] DANDEKAR, A and VANNICE, MA. Determination of the dispersion and surface oxidation states of supported Cu catalysts. In: *Journal of Catalysis* 1998. Vol. 178. p. 621-639.

[31] KOBAYASHI, M and SHIRASAKI, T. The chemisorption of CO on ruthenium metals and ruthenium-silica catalysts. In: *Journal of Catalysis* 1973. Vol. 28. p. 289-295.

[32] SCANLON, JT and WILLIS, DE. Calculation of Flame Ionization Detector Relative Response Factors Using the Effective Carbon Number Concept. In: *Journal of Chromatographic Science* 1985. Vol. 23. p. 333-340.

[33] JORGENSEN, AD, et al. Prediction of gas chromatography flame ionization detector response factors from molecular structures. In: *Analytical Chemistry* 1990. Vol. 62. p. 683-689.

[34] CAÑIZARES, P, et al. Characterization of Ni and Pd supported on H-mordenite catalysts: Influence of the metal loading method. In: *Applied Catalysis A: General* 1998. Vol. 169. p. 137-150.

[35] CHEN, C-S, et al. Synthesis of Cu nanoparticles in mesoporous silica SBA-15 functionalized with carboxylic acid groups. In: *Chemical Communications* 2011. Vol. 47. p. 2288-2290.

[36] ALOTHMAN, Z. A Review: Fundamental Aspects of Silicate Mesoporous Materials. In: *Materials* 2012. Vol. 5. p. 2874-2902.

[37] SIETSMA, JRA, et al. Ordered Mesoporous Silica to Study the Preparation of Ni/SiO2 ex Nitrate Catalysts: Impregnation, Drying, and Thermal Treatments. In: *Chemistry of Materials* 2008. Vol. 20. p. 2921-2931.

[38] PANPRANOT, J, et al. Effects of Pd precursors on the catalytic activity and deactivation of silica-supported Pd catalysts in liquid phase hydrogenation. In: *Applied Catalysis A: General* 2005. Vol. 292. p. 322-327.

[39] PAN, Y-X, et al. Preparation and characterization of coke resistant Ni/SiO2 catalyst for carbon dioxide reforming of methane. In: *Journal of Power Sources* 2008. Vol. 176. p. 46-53.

[40] TOUPANCE, T, et al. Conditions of Formation of Copper Phyllosilicates in Silica-Supported Copper Catalysts Prepared by Selective Adsorption. In: *The Journal of Physical Chemistry B* 2002. Vol. 106. p. 2277-2286.

[41] VASILIADOU, ES, et al. Ru-based catalysts for glycerol hydrogenolysis—Effect of support and metal precursor. In: *Applied Catalysis B: Environmental* 2009. Vol. 92. p. 90-99.

[42] HE, S, et al. Characterization and catalytic properties of Ni/SiO2 catalysts prepared with nickel citrate as precursor. In: *Materials Research Bulletin* 2014. Vol. 49. p. 108-113.

[43] ERMAKOVA, MA and ERMAKOV, DY. High-loaded nickel–silica catalysts for hydrogenation, prepared by sol–gel: Route: structure and catalytic behavior. In: *Applied Catalysis A: General* 2003. Vol. 245. p. 277-288.

[44] ZHU, Y-Y, et al. The Influence of Copper Particle Dispersion in Cu/SiO2 Catalysts on the Hydrogenation Synthesis of Ethylene Glycol. In: *Catalysis Letters* 2010. Vol. 135. p. 275-281.

[45] MUSOLINO, MG, et al. Supported palladium catalysts for the selective conversion of cis-2-butene-1,4-diol to 2-hydroxytetrahydrofuran: effect of metal particle size and support. In: *Applied Catalysis A: General* 2007. Vol. 325. p. 112-120.

[46] FAGHERAZZI, G, et al. Structural investigation on the stoichiometry of β-PdHx in Pd/SiO2 catalysts as a function of metal dispersion. In: *Catalysis Letters* 1995. Vol. 32. p. 293-303.

[47] NEYERTZ, C, et al. Palladium–vanadium interaction in binary supported catalysts. In: *Catalysis Today* 2000. Vol. 57. p. 255-260.

[48] KOOPMAN, PGJ, et al. Characterization of ruthenium catalysts as studied by temperature programmed reduction. In: *Journal of Catalysis* 1981. Vol. 69. p. 172-179.

[49] NURUNNABI, M, et al. Effect of Mn addition on activity and resistance to catalyst deactivation for Fischer–Tropsch synthesis over Ru/Al2O3 and Ru/SiO2 catalysts. In: *Catalysis Communications* 2007. Vol. 8. p. 1531-1537.

[50] SEPÚLVEDA, J and FÍGOLI, NS. Ni/SiO2 catalysts, effect of Ni reduction on activity and thiotolerance during ethylbenzene hydrogenation. In: *Reaction Kinetics and Catalysis Letters* 1995. Vol. 55. p. 383-389.

[51] MARTIN, GA, et al. Chemistry of silica-supported catalysts: preparation activation and reduction. In: *Applied Catalysis* 1981. Vol. 1. p. 367-382.

[52] DÍAZ, A, et al. Characterization of Alkali-Doped Ni/SiO2 Catalysts. In: *Journal of Physical Chemistry B* 1997. Vol. 101. p. 1782-1790.

[53] GALLO, A, et al. Size controlled copper nanoparticles hosted in mesoporous silica matrix: Preparation and characterization. In: *Applied Catalysis B: Environmental* 2012. Vol. 126. p. 161-171.

[54] MATSUMURA, Y, et al. Selective dehydrogenation of ethanol over highly dehydrated silica. In: *Journal of Catalysis* 1989. Vol. 117. p. 135-143.

[55] JAE, J, et al. Production of Dimethylfuran from Hydroxymethylfurfural through Catalytic Transfer Hydrogenation with Ruthenium Supported on Carbon. In: *ChemSusChem* 2013. Vol. 6. p. 1158-1162.

[56] SITTHISA, S and RESASCO, DE. Hydrodeoxygenation of furfural over supported metal catalysts: A comparative study of Cu, Pd and Ni. In: *Catalysis Letters* 2011. Vol. 141. p. 784-791.

[57] DUAN, Y, et al. Towards conversion of octanoic acid to liquid hydrocarbon via hydrodeoxygenation over Mo promoter nickel-based catalyst. In: *Journal of Molecular Catalysis A: Chemical* 2015. Vol. 398. p. 72-78.

[58] TSUJI, J and OHNO, K. Organic syntheses by means of noble metal compounds. XXXIV. Carbonylation and decarbonylation reactions catalyzed by palladium. In: *Journal of the American Chemical Society* 1968. Vol. 90. p. 94-98.

[59] BOCK, H and BREUER, O. Decarbonylation on Carbon-Supported Nickel Catalysts. In: *Angewandte Chemie International Edition* 1987. Vol. 26. p. 461-462.

[60] DAVIS, JL and BARTEAU, MA. Decarbonylation and decomposition pathways of alcohols on Pd (111). In: *Surface Science* 1987. Vol. 187. p. 387-406.

[61] SHEKHAR, R and BARTEAU, MA. Decarbonylation and hydrogenation reactions of allyl alcohol and acrolein on Pd(110). In: *Surface Science* 1994. Vol. 319. p. 298-314.

[62] DAVIS, JL and BARTEAU, MA. Polymerization and decarbonylation reactions of aldehydes on the Pd(111) surface. In: *Journal of the American Chemical Society* 1989. Vol. 111. p. 1782-1792.

[63] SHEKHAR, R, et al. Adsorption and Reaction of Aldehydes on Pd Surfaces. In: *Journal of Physical Chemistry B* 1997. Vol. 101. p. 7939-7951.

[64] MAVRIKAKIS, M and BARTEAU, MA. Oxygenate reaction pathways on transition metal surfaces. In: *Journal of Molecular Catalysis A: Chemical* 1998. Vol. 131. p. 135-147.

[65] ZHOU, Y-H, et al. DFT studies of methanol decomposition on Ni(1 0 0) surface: Compared with Ni(1 1 1) surface. In: *Journal of Molecular Catalysis A: Chemical* 2006. Vol. 258. p. 203-215.

[66] KELLY, TG, et al. Comparison of O−H, C−H, and C−O Bond Scission Sequence of Methanol on Tungsten Carbide Surfaces Modified by Ni, Rh, and Au. In: *Journal of Physical Chemistry C* 2011. Vol. 115. p. 6644-6650.

[67] JENNESS, GR and VLACHOS, DG. DFT Study of the Conversion of Furfuryl Alcohol to 2-Methylfuran on RuO2 (110). In: *Journal of Physical Chemistry C* 2015. Vol. 119. p. 5938-5945.

[68] YANG, Y, et al. Conversion of furfural into cyclopentanone over Ni-Cu bimetallic catalysts. In: *Green Chemistry* 2013. Vol. 15. p. 1932-1940.

[69] OHYAMA, J, et al. Conversion of 5-hydroxymethylfurfural to a cyclopentanone derivative by ring rearrangement over supported Au nanoparticles. In: *Chemical Communications* 2014. Vol. 50. p. 5633-5636.

[70] MODAK, A, et al. A general and efficient aldehyde decarbonylation reaction by using a palladium catalyst. In: *Chemical Communications* 2012. Vol. 48. p. 4253-4255.

[71] MERAT, N, et al. High selective production of tetrahydrofurfuryl alcohol: Catalytic hydrogenation of furfural and furfuryl alcohol. In: *Journal of Chemical Technology and Biotechnology* 1990. Vol. 48. p. 145-159.

[72] VOROTNIKOV, V, et al. DFT Study of Furfural Conversion to Furan, Furfuryl Alcohol, and 2-Methylfuran on Pd(111). In: *ACS Catalysis* 2012. Vol. 2. p. 2496-2504.

[73] PANAGIOTOPOULOU, P, et al. Liquid-Phase Catalytic Transfer Hydrogenation of Furfural over Homogeneous Lewis Acid–Ru/C Catalysts. In: *ChemSusChem* 2015. Vol. 8. p. 2046-2054.

[74] ATIA, H, et al. Dehydration of glycerol in gas phase using heteropolyacid catalysts as active compounds. In: *Journal of Catalysis* 2008. Vol. 258. p. 71-82.

[75] MELO, L, et al. Effect of the metallic/acid site (nPt/nA) ratio on the transformation of acetone towards methyl isobutyl ketone. In: *Catalysis Letters* 1997. Vol. 44. p. 201-204.

[76] SOMASUNDARAN, P. *Encyclopedia of Surface and Colloid Science*. Second ed. New York: Taylor & Francis; 2006.

[77] DIJKSTRA, TW, et al. Silsesquioxane Models for Geminal Silica Surface Silanol Sites. A Spectroscopic Investigation of Different Types of Silanols. In: *Journal of the American Chemical Society* 2002. Vol. 124. p. 9856-9864.

[78] WANG, Z, et al. Surface structure and catalytic behavior of silica-supported copper catalysts prepared by impregnation and sol–gel methods. In: *Applied Catalysis A: General* 2003. Vol. 239. p. 87-94.

[79] MA, J, et al. Synthesis and properties of furan-based imine-linked porous organic frameworks. In: *Polymer Chemistry* 2012. Vol. 3. p. 2346-2349.

[80] RYCZKOWSKI, J. IR spectroscopy in catalysis. In: *Catalysis Today* 2001. Vol. 68. p. 263-381.

[81] ROGERS, LH and WILLIAMS, D. The Infrared Absorption Spectra of Some Sugars and Furans. In: *Journal of the American Chemical Society* 1938. Vol. 60. p. 2619-2621.

[82] JAE, J, et al. Cascade of Liquid-Phase Catalytic Transfer Hydrogenation and Etherification of 5-Hydroxymethylfurfural to Potential Biodiesel Components over Lewis Acid Zeolites. In: *ChemCatChem* 2014. Vol. 6. p. 508-513.

[83] GOMEZ, H, et al. NbP catalyst for furfural production: FT IR studies of surface properties. In: *Applied Catalysis A: General* 2015. Vol. 502. p. 388-398.

[84] ROBINSON, E and ROSS, RA. The sorption of furans on silica gels. In: *Journal of the Chemical Society A: Inorganic, Physical, Theoretical* 1970. Vol. p. 84-87.

[85] FERREIRA-APARICIO, P, et al. Mechanistic aspects of the dry reforming of methane over ruthenium catalysts. In: *Applied Catalysis A: General* 2000. Vol. 202. p. 183-196.

[86] MAETZ, P, et al. Hydrogenation of But-1-yne on Platinum/Silica Catalysts: An in Situ Dynamic Infrared Study. In: *Journal of Catalysis* 1994. Vol. 147. p. 48-56.

[87] BOSSI, A, et al. Preparation aspects of Ru-supported catalysts and their influence on the final products. In: *Preparation of Catalysts II*. DELMON, B; GRANGE, P; JACOBS, P; PONCELET, G. Eds. First ed. Amsterdam: Elsevier; 1979. p. 405-416.

[88] KIM, P, et al. Synthesis and characterization of mesoporous alumina with nickel incorporated for use in the partial oxidation of methane into synthesis gas. In: *Applied Catalysis A: General* 2004. Vol. 272. p. 157-166.

[89] FENG, JT, et al. Enhanced metal dispersion and hydrodechlorination properties of a Ni/Al_2O_3 catalyst derived from layered double hydroxides. In: *Journal of Catalysis* 2009. Vol. 266. p. 351-358.

[90] ZANGOUEI, M, et al. The influence of nickel loading on reducibility of NiO/Al_2O_3 catalysts synthesized by sol-gel method. In: *Chemical Engineering Research Bulletin* 2010. Vol. 14. p. 97-102.

[91] BARRIO, VL, et al. Evaluation of silica-alumina-supported nickel catalysts in dibenzothiophene hydrodesulphurisation. In: *Applied Catalysis A: General* 2003. Vol. 248. p. 211-225.

[92] SMEDS, S, et al. Chemisorption and TPD studies of hydrogen on Ni/Al_2O_3. In: *Applied Catalysis A: General* 1996. Vol. 144. p. 177-194.

[93] BABU, NS, et al. Characterization and reactivity of alumina-supported Pd catalysts for the room-temperature hydrodechlorination of chlorobenzene. In: *Journal of Physical Chemistry C* 2007. Vol. 111. p. 6447-6453.

[94] MENDEZ, CM, et al. On the role of Pd β-hydride in the reduction of nitrate over Pd based catalyst. In: *Applied Catalysis B: Environmental* 2008. Vol. 84. p. 156-161.

[95] MAHATA, N and VISHWANATHAN, V. Influence of palladium precursors on structural properties and phenol hydrogenation characteristics of supported palladium catalysts. In: *Journal of Catalysis* 2000. Vol. 196. p. 262-270.

[96] LÓPEZ-SUÁREZ, FE, et al. Cu/Al_2O_3 catalysts for soot oxidation: Copper loading effect. In: *Applied Catalysis B: Environmental* 2008. Vol. 84. p. 651-658.

[97] PERNICONE, N, et al. On the measurement of copper surface area by oxygen chemisorption. In: *Applied Catalysis A: General* 2003. Vol. 240. p. 199-206.

[98] SING, KSW, et al. Reporting Physisorption Data for Gas/Solid Systems. In: *Pure and Applied Chemistry* 1985. Vol. 57. p. 603-619.

[99] LUO, MF, et al. In situ XRD, Raman, and TPR studies of CuO/Al_2O_3 catalysts for CO oxidation. In: *Journal of Molecular Catalysis A: Chemical* 2005. Vol. 239. p. 243-248.

[100] DOW, WP, et al. Yttria-stabilized zirconia supported copper oxide catalyst: I. Effect of oxygen vacancy of support on copper oxide reduction. In: *Journal of Catalysis* 1996. Vol. 160. p. 155-170.

[101] CHANDRA SHEKAR, S, et al. Characterization of palladium supported on γ-Al_2O_3 catalysts in hydrodechlorination of CCl_2F_2. In: *Applied Catalysis A: General* 2005. Vol. 294. p. 235-243.

[102] LI, C and CHEN, YW. Temperature-programmed-reduction studies of nickel oxide/alumina catalysts: effects of the preparation method. In: *Thermochim. Acta* 1995. Vol. 256. p. 457-465.

[103] RYNKOWSKI, JM, et al. On the nature of oxidic nickel phases in NiO/γ-Al_2O_3 catalysts. In: *Applied Catalysis A: General* 1993. Vol. 106. p. 73-82.

[104] CHARY, KVR, et al. Catalytic functionalities of nickel supported on different polymorphs of alumina. In: *Catalysis Communications* 2008. Vol. 9. p. 886-893.

[105] BOUKHA, Z, et al. Synthesis, characterisation and performance evaluation of spinel-derived Ni/Al_2O_3 catalysts for various methane reforming reactions. In: *Applied Catalysis B: Environmental* 2014. Vol. 158–159. p. 190-201.

[106] YANG, R, et al. Hydrotreating of crude 2-ethylhexanol over Ni/Al_2O_3 catalysts: Surface Ni species-catalytic activity correlation. In: *Applied Catalysis A: General* 2009. Vol. 368. p. 105-112.

[107] WU, M and HERCULES, DM. Studies of supported nickel catalysts by X-ray photoelectron and ion scattering spectroscopies. In: *Journal of Physical Chemistry* 1979. Vol. 83. p. 2003-2008.

[108] CHANG, FW, et al. Effect of calcination temperature on catalyst reducibility and hydrogenation reactivity in rice husk ash–alumina supported nickel systems. In: *Journal of Chemical Technology and Biotechnology* 2004. Vol. 79. p. 691-699.

[109] BETANCOURT, P, et al. A study of the ruthenium–alumina system. In: *Applied Catalysis A: General* 1998. Vol. 170. p. 307-314.

[110] MAZZIERI, V, et al. XPS, FTIR and TPR characterization of Ru/Al2O3 catalysts. In: *Applied Surface Science* 2003. Vol. 210. p. 222-230.

[111] KOOPMAN, PGJ, et al. Activation of ruthenium on silica hydrogenation catalysts. In: *Reaction Kinetics and Catalysis Letters* 1978. Vol. 8. p. 389-393.

[112] ALEGRE, VV, et al. Catalytic combustion of methane over palladium alumina modified by niobia. In: *Catalysis Communications* 2006. Vol. 7. p. 314-322.

[113] GUTIERREZ, V, et al. Liquid phase selective hydrogenation of cinnamaldehyde over copper supported catalysts. In: *Applied Catalysis A: General* 2012. Vol. 413–414. p. 358-365.

[114] WU, G, et al. Hydrogen Production via Glycerol Steam Reforming over Ni/Al2O3: Influence of Nickel Precursors. In: *ACS Sustainable Chemistry and Engineering* 2013. Vol. 1. p. 1052-1062.

[115] KADKHODAYAN, A and BRENNER, A. Temperature-programmed reduction and oxidation of metals supported on γ-alumina. In: *Journal of Catalysis* 1989. Vol. 117. p. 311-321.

[116] MEDINA, F, et al. Characterization of several [gamma]-alumina-supported nickel catalysts and activity for selective hydrogenation of hexanedinitrile. In: *Journal of the Chemical Society, Faraday Transactions* 1994. Vol. 90. p. 1455-1459.

[117] VAN STEEN, E and PRINSLOO, FF. Comparison of preparation methods for carbon nanotubes supported iron Fischer–Tropsch catalysts. In: *Catalysis Today* 2002. Vol. 71. p. 327-334.

[118] JASIK, A, et al. Study of nickel catalysts supported on Al2O3, SiO2 or Nb2O5 oxides. In: *Journal of Molecular Catalysis A: Chemical* 2005. Vol. 242. p. 81-90.

[119] GONÇALVES, G, et al. Preparation and characterization of nickel based catalysts on silica, alumina and titania obtained by sol–gel method. In: *Journal of Non-Crystalline Solids* 2006. Vol. 352. p. 3697-3704.

[120] VAN RYNEVELD, E, et al. A catalytic route to lower alcohols from glycerol using Ni-supported catalysts. In: *Green Chemistry* 2011. Vol. 13. p. 1819-1827.

[121] SHEN, W-J, et al. The influence of the support on the activity and selectivity of Pd in CO hydrogenation. In: *Applied Catalysis A: General* 2001. Vol. 213. p. 225-232.

[122] REYES, P, et al. o-xylene hydrogenation on supported ruthenium catalysts. In: *Catalysis Letters* 1997. Vol. 46. p. 71-75.

[123] LAFAYE, G, et al. Citral hydrogenation over alumina supported Rh-Ge catalysts: Effects of the reduction temperature. In: *Applied Catalysis A: General* 2004. Vol. 257. p. 107-117.

[124] WANG, JA, et al. Effects of structural defects and acid–basic properties on the activity and selectivity of isopropanol decomposition on nanocrystallite sol–gel alumina catalyst. In: *Journal of Molecular Catalysis A: Chemical* 1999. Vol. 137. p. 239-252.

[125] NAKAGAWA, Y and TOMISHIGE, K. Total hydrogenation of furan derivatives over silica-supported Ni–Pd alloy catalyst. In: *Catalysis Communications* 2010. Vol. 12. p. 154-156.

[126] KUMALAPUTRI, AJ, et al. Tunable and Selective Conversion of 5-HMF to 2,5-Furandimethanol and 2,5-Dimethylfuran over Copper-Doped Porous Metal Oxides. In: *ChemSusChem* 2014. Vol. 7. p. 2266-2275.

[127] SHIN, E-J and KEANE, MA. Gas-Phase Hydrogenation/Hydrogenolysis of Phenol over Supported Nickel Catalysts. In: *Industrial & Engineering Chemistry Research* 2000. Vol. 39. p. 883-892.

[128] ZHANG, B, et al. Selective conversion of furfuryl alcohol to 1,2-pentanediol over a Ru/MnOx catalyst in aqueous phase. In: *Green Chemistry* 2012. Vol. 14. p. 3402-3409.

[129] LESIAK, M, et al. Hydrogenation of furfural over Pd–Cu/Al_2O_3 catalysts. The role of interaction between palladium and copper on determining catalytic properties. In: *Journal of Molecular Catalysis A: Chemical* 2014. Vol. 395. p. 337-348.

[130] WILSON, CL. 18. Reactions of furan compounds. Part V. Formation of furan from furfuraldehyde by the action of nickel or cobalt catalysts: importance of added hydrogen. In: *J. Chem. Soc.* 1945. Vol. p. 61-63.

[131] SINGH, H, et al. Metal support interactions in the palladium-catalysed decomposition of furfural to furan. In: *Journal of Chemical Technology and Biotechnology* 1980. Vol. 30. p. 293-296.

[132] LEJEMBLE, P, et al. From biomass to furan through decarbonylation of furfural under mild conditions. In: *Biomass* 1984. Vol. 4. p. 263-274.

[133] ZHANG, W, et al. A study of furfural decarbonylation on K-doped Pd/Al_2O_3 catalysts. In: *Journal of Molecular Catalysis A: Chemical* 2011. Vol. 335. p. 71-81.

[134] LASHDAF, M, et al. Behaviour of palladium and ruthenium catalysts on alumina and silica prepared by gas and liquid phase deposition in cinnamaldehyde hydrogenation. In: *Applied Catalysis A: General* 2003. Vol. 241. p. 65-75.

[135] BRADLEY, MK, et al. The structure and bonding of furan on Pd (111). In: *Surface Science* 2010. Vol. 604. p. 920-925.

[136] BURNETT, LW, et al. Production of 2-Methylfuran by Vapor-Phase Hydrogenation of Furfural. In: *Industrial and Engineering Chemistry* 1948. Vol. 40. p. 502-505.

[137] SEO, G and CHON, H. Hydrogenation of furfural over copper-containing catalysts. In: *Journal of Catalysis* 1981. Vol. 67. p. 424-429.

[138] STONKUS, VV, et al. Characteristics of the catalytic hydrogenation of 5-methylfurfural. In: *Chemistry of Heterocyclic Compounds* 1990. Vol. 26. p. 1214-1218.

[139] SCHOLZ, D, et al. Catalytic Transfer Hydrogenation/Hydrogenolysis for Reductive Upgrading of Furfural and 5-(Hydroxymethyl)furfural. In: *ChemSusChem* 2014. Vol. 7. p. 268-275.

[140] DEUTSCH, KL and SHANKS, BH. Copper mixed metal oxide catalysts in the hydrogenolysis of 5-methylfurfuryl alcohol. In: *Applied Catalysis A: General* 2014. Vol. 470. p. 390-397.

[141] BIENHOLZ, A, et al. Selective hydrogenolysis of glycerol over copper catalysts both in liquid and vapour phase: Correlation between the copper surface area and the catalyst's activity. In: *Applied Catalysis A: General* 2011. Vol. 391. p. 153-157.

[142] VASILIADOU, ES and LEMONIDOU, AA. Kinetic study of liquid-phase glycerol hydrogenolysis over Cu/SiO_2 catalyst. In: *Chemical Engineering Journal* 2013. Vol. 231. p. 103-112.

[143] BARTEAU, MA. Linear free energy relationships for C1-oxygenate decomposition on transition metal surfaces. In: *Catalysis Letters* 1991. Vol. 8. p. 175-183.

[144] GREELEY, J and MAVRIKAKIS, M. Methanol Decomposition on Cu(111): A DFT Study. In: *Journal of Catalysis* 2002. Vol. 208. p. 291-300.

[145] CHEN, Z-X, et al. CH3O Decomposition on PdZn(111), Pd(111), and Cu(111). A Theoretical Study. In: *Langmuir* 2004. Vol. 20. p. 8068-8077.

[146] MEI, D, et al. Potential Energy Surface of Methanol Decomposition on Cu(110). In: *Journal of Physical Chemistry C* 2009. Vol. 113. p. 4522-4537.

[147] NAKAGAWA, Y, et al. Catalytic Reduction of Biomass-Derived Furanic Compounds with Hydrogen. In: *ACS Catalysis* 2013. Vol. 3. p. 2655-2668.

[148] HRONEC, M, et al. Effect of catalyst and solvent on the furan ring rearrangement to cyclopentanone. In: *Applied Catalysis A: General* 2012. Vol. 437–438. p. 104-111.

[149] HRONEC, M, et al. Highly selective rearrangement of furfuryl alcohol to cyclopentanone. In: *Applied Catalysis B: Environmental* 2014. Vol. 154–155. p. 294-300.

[150] PANAGIOTOPOULOU, P and VLACHOS, DG. Liquid phase catalytic transfer hydrogenation of furfural over a Ru/C catalyst. In: *Applied Catalysis A: General* 2014. Vol. 480. p. 17-24.

[151] JACQUIN, M, et al. Novel supported Rh, Pt, Ir and Ru mesoporous aluminosilicates as catalysts for the hydrogenation of naphthalene. In: *Applied Catalysis A: General* 2003. Vol. 251. p. 131-141.

[152] GUISNET, M and MAGNOUX, P. Organic chemistry of coke formation. In: *Applied Catalysis A: General* 2001. Vol. 212. p. 83-96.

[153] NIMMANWUDIPONG, T, et al. Cyclohexanone Conversion Catalyzed by Pt/γ-Al2O3: Evidence of Oxygen Removal and Coupling Reactions. In: *Catalysis Letters* 2011. Vol. 141. p. 1072-1078.

[154] BARTHOLOMEW, CH. Mechanisms of catalyst deactivation. In: *Applied Catalysis A: General* 2001. Vol. 212. p. 17-60.

[155] LIU, D, et al. Deactivation mechanistic studies of copper chromite catalyst for selective hydrogenation of 2-furfuraldehyde. In: *Journal of Catalysis* 2013. Vol. 299. p. 336-345.

[156] VILLAVERDE, MM, et al. Selective liquid-phase hydrogenation of furfural to furfuryl alcohol over Cu-based catalysts. In: *Catalysis Today* 2013. Vol. 213. p. 87-92.

[157] VARGAS-HERNÁNDEZ, D, et al. Furfuryl alcohol from furfural hydrogenation over copper supported on SBA-15 silica catalysts. In: *Journal of Molecular Catalysis A: Chemical* 2014. Vol. 383–384. p. 106-113.

[158] MCMANUS, JR and VOHS, JM. Deoxygenation of glycolaldehyde and furfural on Mo_2C/Mo(100). In: *Surface Science* 2014. Vol. 630. p. 16-21.

[159] ALRIOLS, MG, et al. Combined organosolv and ultrafiltration lignocellulosic biorefinery process. In: *Chemical Engineering Journal* 2010. Vol. 157. p. 113-120.

[160] IBARRA, JV, et al. Fourier transform infrared spectroscopic study of coke deposits on a Cr_2O_3-Al_2O_3 catalyst. In: *Vibrational Spectroscopy* 1995. Vol. 9. p. 191-196.

[161] AOSHIMA, A, et al. New synthetic route of polyoxytetramethyleneglycol by use of heteropolyacids as catalyst. In: *Polymers for Advanced Technologies* 1990. Vol. 1. p. 127-132.

[162] BARSBERG, S and THYGESEN, LG. Poly(furfuryl alcohol) formation in neat furfuryl alcohol and in cymene studied by ATR-IR spectroscopy and density functional theory (B3LYP) prediction of vibrational bands. In: *Vibrational Spectroscopy* 2009. Vol. 49. p. 52-63.

[163] EBERLY, PE. High-temperature infrared spectroscopy of olefins adsorbed on faujasites. In: *Journal of Physical Chemistry* 1967. Vol. 71. p. 1717-1722.

[164] VAN DOORN, J and MOULIJN, JA. Extraction of spent hydrotreating catalysts studied by fourier transform infra-red spectroscopy. In: *Fuel Processing Technology* 1990. Vol. 26. p. 39-51.

[165] GONZÁLEZ, D, et al. Effect of La_2O_3 in Carbon Deposition on Pt/Al_2O_3 during Methylcyclopentane Reaction. In: *Industrial and Engineering Chemistry Research* 2007. Vol. 46. p. 4335-4340.

[166] RAO, R, et al. Properties of Copper Chromite Catalysts in Hydrogenation Reactions. In: *Journal of Catalysis* 1997. Vol. 171. p. 406-419.

[167] RAO, R, et al. Furfural hydrogenation over carbon-supported copper. In: *Catalysis Letters* 1999. Vol. 60. p. 51-57.

[168] SIMÓN, E, et al. Study of the deactivation of copper-based catalysts for dehydrogenation of cyclohexanol to cyclohexanone. In: *Catalysis Today* 2012. Vol. 187. p. 150-158.

[169] FOUILLOUX, P. Selective Hydrogenation of Cinnamaldehyde to Cinnamyl Alcohol on Pt-Co and Pt-Ru/C Catalysts. In: *Heterogeneous Catalysis and Fine Chemicals*. GUISNET, M; BARRAULT, J; BOUCHOULE, C; DUPREZ, D; MONTASSIER, C; PÉROT, G. Eds. First ed. Amsterdam: Elsevier; 1988. p. 123-129.

[170] COQ, B and FIGUERAS, F. Bimetallic palladium catalysts: influence of the co-metal on the catalyst performance. In: *Journal of Molecular Catalysis A: Chemical* 2001. Vol. 173. p. 117-134.

[171] CARRERO, A, et al. Hydrogen production by ethanol steam reforming over Cu-Ni/SBA-15 supported catalysts prepared by direct synthesis and impregnation. In: *Applied Catalysis A: General* 2007. Vol. 327. p. 82-94.

[172] DE ROGATIS, L, et al. Methane partial oxidation on NiCu-based catalysts. In: *Catalysis Today* 2009. Vol. 145. p. 176-185.

[173] SACHTLER, WMH and VAN DER PLANK, P. The role of individual surface atoms in chemisorption and catalysis by nickel-copper alloys. In: *Surface Science* 1969. Vol. 18. p. 62-79.

[174] GANDARIAS, I, et al. Liquid-phase glycerol hydrogenolysis to 1,2-propanediol under nitrogen pressure using 2-propanol as hydrogen source. In: *Journal of Catalysis* 2011. Vol. 282. p. 237-247.

[175] KANG, M, et al. γ-Alumina supported Cu-Ni bimetallic catalysts: Characterization and selective hydrogenation of 1,3-butadiene. In: *Canadian Journal of Chemical Engineering* 2002. Vol. 80. p. 63-70.

[176] LEE, JH, et al. Stabilization of Ni/Al2O3 catalyst by Cu addition for CO2 reforming of methane. In: *Applied Catalysis A: General* 2004. Vol. 269. p. 1-6.

[177] MIRANDA, BC, et al. Influence of copper on nickel-based catalysts in the conversion of glycerol. In: *Applied Catalysis B: Environmental* 2015. Vol. 166–167. p. 166-180.

[178] JUSZCZYK, W, et al. The effect of copper and gold on the catalytic behavior of nickel/alumina catalysts in hydrogen-assisted dechlorination of 1,2-dichloroethane. In: *Catalysis Today* 2011. Vol. 169. p. 186-191.

[179] VELON, A and OLEFJORD, I. Oxidation Behavior of Ni_3Al and Fe_3Al: I. XPS Calibrations of Pure Compounds and Quantification of the Results. In: *Oxidation of Metals* 2001. Vol. 56. p. 415-424.

[180] WAGNER, CD, et al. *Handbook of X-ray Photoelectron Spectroscopy*. First ed. Eden-Prairie: Perkin-Elmer Corp.; 1979.

[181] ASEDEGBEGA-NIETO, E, et al. Modification of catalytic properties over carbon supported Ru–Cu and Ni–Cu bimetallics: I. Functional selectivities in citral and cinnamaldehyde hydrogenation. In: *Applied Catalysis A: General* 2006. Vol. 300. p. 120-129.

[182] BIESINGER, MC, et al. Resolving surface chemical states in XPS analysis of first row transition metals, oxides and hydroxides: Sc, Ti, V, Cu and Zn. In: *Applied Surface Science* 2010. Vol. 257. p. 887-898.

[183] STROHMEIER, BR, et al. Surface spectroscopic characterization of Cu/Al2O3 catalysts. In: *Journal of Catalysis* 1985. Vol. 94. p. 514-530.

[184] PUDI, SM, et al. Selective Hydrogenolysis of Glycerol to 1,2-Propanediol Over Bimetallic Cu-Ni Catalysts Supported on ³-Al2O3. In: *Journal of the Brazilian Chemical Society* 2015. Vol. 26. p. 1551-1564.

[185] RESHETENKO, TV, et al. Carbon capacious Ni-Cu-Al2O3 catalysts for high-temperature methane decomposition. In: *Applied Catalysis A: General* 2003. Vol. 247. p. 51-63.

[186] GANDARIAS, I, et al. Liquid-phase glycerol hydrogenolysis by formic acid over Ni–Cu/Al2O3 catalysts. In: *Journal of Catalysis* 2012. Vol. 290. p. 79-89.

[187] SACIA, ER, et al. Synthesis of biomass-derived methylcyclopentane as a gasoline additive via aldol condensation/hydrodeoxygenation of 2,5-hexanedione. In: *Green Chemistry* 2015. Vol. 17. p. 2393-2397.

[188] CENTENO, A, et al. Influence of the Support of CoMo Sulfide Catalysts and of the Addition of Potassium and Platinum on the Catalytic Performances for the

Hydrodeoxygenation of Carbonyl, Carboxyl, and Guaiacol-Type Molecules. In: *Journal of Catalysis* 1995. Vol. 154. p. 288-298.

[189] GHAMPSON, IT, et al. Comparison of alumina- and SBA-15-supported molybdenum nitride catalysts for hydrodeoxygenation of guaiacol. In: *Applied Catalysis A: General* 2012. Vol. 435–436. p. 51-60.

[190] YANG, Y, et al. Effect of metal–support interaction on the selective hydrodeoxygenation of anisole to aromatics over Ni-based catalysts. In: *Applied Catalysis B: Environmental* 2014. Vol. 145. p. 91-100.

[191] HU, S, et al. The effect of surface acidic and basic properties on the hydrogenation of aromatic rings over the supported nickel catalysts. In: *Chemical Engineering Journal* 2010. Vol. 162. p. 371-379.

[192] KARPIŃSKI, Z. Catalysis by Supported, Unsupported and Electron-Deficient Palladium. In: *Advances in Catalysis*. ELEY, DD; PINES, H; WEISZ, PB. Eds. First ed. San Diego: Academic Press, Inc.; 1990. p. 45-94.

[193] TESSIER, D, et al. Spectroscopic study of the interaction of carbon monoxide with cationic and metallic palladium in palladium-alumina catalysts. In: *Journal of the Chemical Society, Faraday Transactions* 1992. Vol. 88. p. 741-749.

[194] STAKHEEV, AY and KUSTOV, LM. Effects of the support on the morphology and electronic properties of supported metal clusters: modern concepts and progress in 1990s. In: *Applied Catalysis A: General* 1999. Vol. 188. p. 3-35.

[195] BARBIER, J and MARECOT, P. Effect of presulfurization on the formation of coke on supported metal catalysts. In: *Journal of Catalysis* 1986. Vol. 102. p. 21-28.

[196] PARERA, JM, et al. Influence of sulfurization on coke formation over catalysts for naphtha reforming. In: *Applied Catalysis* 1986. Vol. 23. p. 15-22.

[197] PARERA, JM, et al. The role of Re and S in the Pt-Re-S/Al2O3 catalyst. In: *Journal of Catalysis* 1986. Vol. 99. p. 39-52.

BIBLIOGRAPHY

ALAMILLO, R, et al. The selective hydrogenation of biomass-derived 5-hydroxymethylfurfural using heterogeneous catalysts. In: *Green Chemistry* 2012. Vol. 14. p. 1413-1419.

ALEGRE, VV, et al. Catalytic combustion of methane over palladium alumina modified by niobia. In: *Catalysis Communications* 2006. Vol. 7. p. 314-322.

ALOTHMAN, Z. A Review: Fundamental Aspects of Silicate Mesoporous Materials. In: *Materials* 2012. Vol. 5. p. 2874-2902.

ALRIOLS, MG, et al. Combined organosolv and ultrafiltration lignocellulosic biorefinery process. In: *Chemical Engineering Journal* 2010. Vol. 157. p. 113-120.

ANET, EFLJ. 3-Deoxyglycosuloses (3-Deoxyglycosones) and the Degradation of Carbohydrates. In: *Advances in Carbohydrate Chemistry*. MELVILLE, LW. Ed. First ed. London: Academic Press; 1964. p. 181-218.

ANTAL JR, MJ, et al. Mechanism of formation of 5-(hydroxymethyl)-2-furaldehyde from d-fructose and sucrose. In: *Carbohydrate research* 1990. Vol. 199. p. 91-109.

AOSHIMA, A, et al. New synthetic route of polyoxytetramethyleneglycol by use of heteropolyacids as catalyst. In: *Polymers for Advanced Technologies* 1990. Vol. 1. p. 127-132.

ASEDEGBEGA-NIETO, E, et al. Modification of catalytic properties over carbon supported Ru–Cu and Ni–Cu bimetallics: I. Functional selectivities in citral and cinnamaldehyde hydrogenation. In: *Applied Catalysis A: General* 2006. Vol. 300. p. 120-129.

ATIA, H, et al. Dehydration of glycerol in gas phase using heteropolyacid catalysts as active compounds. In: *Journal of Catalysis* 2008. Vol. 258. p. 71-82.

BABU, NS, et al. Characterization and reactivity of alumina-supported Pd catalysts for the room-temperature hydrodechlorination of chlorobenzene. In: *Journal of Physical Chemistry C* 2007. Vol. 111. p. 6447-6453.

BARBIER, J and MARECOT, P. Effect of presulfurization on the formation of coke on supported metal catalysts. In: *Journal of Catalysis* 1986. Vol. 102. p. 21-28.

BARRIO, VL, et al. Evaluation of silica-alumina-supported nickel catalysts in dibenzothiophene hydrodesulphurisation. In: *Applied Catalysis A: General* 2003. Vol. 248. p. 211-225.

BARSBERG, S and THYGESEN, LG. Poly(furfuryl alcohol) formation in neat furfuryl alcohol and in cymene studied by ATR-IR spectroscopy and density functional theory (B3LYP) prediction of vibrational bands. In: *Vibrational Spectroscopy* 2009. Vol. 49. p. 52-63.

BARTEAU, MA. Linear free energy relationships for C1-oxygenate decomposition on transition metal surfaces. In: *Catalysis Letters* 1991. Vol. 8. p. 175-183.

BARTHOLOMEW, CH. Mechanisms of catalyst deactivation. In: *Applied Catalysis A: General* 2001. Vol. 212. p. 17-60.

BECK, A, et al. Pd nanoparticles prepared by “controlled colloidal synthesis” in solid/liquid interfacial layer on silica. I. Particle size regulation by reduction time. In: *Catalysis Letters* 2000. Vol. 65. p. 33-42.

BETANCOURT, P, et al. A study of the ruthenium–alumina system. In: *Applied Catalysis A: General* 1998. Vol. 170. p. 307-314.

BIENHOLZ, A, et al. Selective hydrogenolysis of glycerol over copper catalysts both in liquid and vapour phase: Correlation between the copper surface area and the catalyst's activity. In: *Applied Catalysis A: General* 2011. Vol. 391. p. 153-157.

BIESINGER, MC, et al. Resolving surface chemical states in XPS analysis of first row transition metals, oxides and hydroxides: Sc, Ti, V, Cu and Zn. In: *Applied Surface Science* 2010. Vol. 257. p. 887-898.

BOCK, H and BREUER, O. Decarbonylation on Carbon-Supported Nickel Catalysts. In: *Angewandte Chemie International Edition* 1987. Vol. 26. p. 461-462.

BOSS, CB and FREDEEN, KJ. *Concepts, Instrumentation and Techniques in Inductively Coupled Plasma Optical Emission Spectrometry*. Third edition ed. USA: Perkin Elmer; 2004.

BOSSI, A, et al. Preparation aspects of Ru-supported catalysts and their influence on the final products. In: *Preparation of Catalysts II*. DELMON, B; GRANGE, P; JACOBS, P; PONCELET, G. Eds. First ed. Amsterdam: Elsevier; 1979. p. 405-416.

BOUKHA, Z, et al. Synthesis, characterisation and performance evaluation of spinel-derived Ni/Al_2O_3 catalysts for various methane reforming reactions. In: *Applied Catalysis B: Environmental* 2014. Vol. 158–159. p. 190-201.

BOZELL, JJ and PETERSEN, GR. Technology development for the production of biobased products from biorefinery carbohydrates-the US Department of Energy's "Top 10" revisited. In: *Green Chemistry* 2010. Vol. 12. p. 539-554.

BRADLEY, MK, et al. The structure and bonding of furan on Pd (111). In: *Surface Science* 2010. Vol. 604. p. 920-925.

BRUNAUER, S, et al. Adsorption of Gases in Multimolecular Layers. In: *Journal of the American Chemical Society* 1938. Vol. 60. p. 309-319.

BUNTARA, T, et al. Caprolactam from Renewable Resources: Catalytic Conversion of 5-Hydroxymethylfurfural into Caprolactone. In: *Angewandte Chemie International Edition* 2011. Vol. 50. p. 7083-7087.

BURNETT, LW, et al. Production of 2-Methylfuran by Vapor-Phase Hydrogenation of Furfural. In: *Industrial and Engineering Chemistry* 1948. Vol. 40. p. 502-505.

CAÑIZARES, P, et al. Characterization of Ni and Pd supported on H-mordenite catalysts: Influence of the metal loading method. In: *Applied Catalysis A: General* 1998. Vol. 169. p. 137-150.

CARRERO, A, et al. Hydrogen production by ethanol steam reforming over Cu-Ni/SBA-15 supported catalysts prepared by direct synthesis and impregnation. In: *Applied Catalysis A: General* 2007. Vol. 327. p. 82-94.

CENTENO, A, et al. Influence of the Support of CoMo Sulfide Catalysts and of the Addition of Potassium and Platinum on the Catalytic Performances for the Hydrodeoxygenation of Carbonyl, Carboxyl, and Guaiacol-Type Molecules. In: *Journal of Catalysis* 1995. Vol. 154. p. 288-298.

COQ, B and FIGUERAS, F. Bimetallic palladium catalysts: influence of the co-metal on the catalyst performance. In: *Journal of Molecular Catalysis A: Chemical* 2001. Vol. 173. p. 117-134.

CHANDRA SHEKAR, S, et al. Characterization of palladium supported on γ-Al_2O_3 catalysts in hydrodechlorination of CCl_2F_2. In: *Applied Catalysis A: General* 2005. Vol. 294. p. 235-243.

CHANG, FW, et al. Effect of calcination temperature on catalyst reducibility and hydrogenation reactivity in rice husk ash–alumina supported nickel systems. In: *Journal of Chemical Technology and Biotechnology* 2004. Vol. 79. p. 691-699.

CHARY, KVR, et al. Catalytic functionalities of nickel supported on different polymorphs of alumina. In: *Catalysis Communications* 2008. Vol. 9. p. 886-893.

CHEN, C-S, et al. Synthesis of Cu nanoparticles in mesoporous silica SBA-15 functionalized with carboxylic acid groups. In: *Chemical Communications* 2011. Vol. 47. p. 2288-2290.

CHEN, Z-X, et al. CH3O Decomposition on PdZn(111), Pd(111), and Cu(111). A Theoretical Study. In: *Langmuir* 2004. Vol. 20. p. 8068-8077.

CHIDAMBARAM, M and BELL, AT. A two-step approach for the catalytic conversion of glucose to 2,5-dimethylfuran in ionic liquids. In: *Green Chemistry* 2010. Vol. 12. p. 1253-1262.

DANDEKAR, A and VANNICE, MA. Determination of the dispersion and surface oxidation states of supported Cu catalysts. In: *Journal of Catalysis* 1998. Vol. 178. p. 621-639.

DAVIS, JL and BARTEAU, MA. Decarbonylation and decomposition pathways of alcohols on Pd (111). In: *Surface Science* 1987. Vol. 187. p. 387-406.

DAVIS, JL and BARTEAU, MA. Polymerization and decarbonylation reactions of aldehydes on the Pd(111) surface. In: *Journal of the American Chemical Society* 1989. Vol. 111. p. 1782-1792.

DE ROGATIS, L, et al. Methane partial oxidation on NiCu-based catalysts. In: *Catalysis Today* 2009. Vol. 145. p. 176-185.

DE, S, et al. Hydrodeoxygenation processes: Advances on catalytic transformations of biomass-derived platform chemicals into hydrocarbon fuels. In: *Bioresource Technology* 2015. Vol. 178. p. 108-118.

DEUTSCH, KL and SHANKS, BH. Copper mixed metal oxide catalysts in the hydrogenolysis of 5-methylfurfuryl alcohol. In: *Applied Catalysis A: General* 2014. Vol. 470. p. 390-397.

DÍAZ, A, et al. Characterization of Alkali-Doped Ni/SiO2 Catalysts. In: *Journal of Physical Chemistry B* 1997. Vol. 101. p. 1782-1790.

DIJKSTRA, TW, et al. Silsesquioxane Models for Geminal Silica Surface Silanol Sites. A Spectroscopic Investigation of Different Types of Silanols. In: *Journal of the American Chemical Society* 2002. Vol. 124. p. 9856-9864.

DOW, WP, et al. Yttria-stabilized zirconia supported copper oxide catalyst: I. Effect of oxygen vacancy of support on copper oxide reduction. In: *Journal of Catalysis* 1996. Vol. 160. p. 155-170.

DUAN, Y, et al. Towards conversion of octanoic acid to liquid hydrocarbon via hydrodeoxygenation over Mo promoter nickel-based catalyst. In: *Journal of Molecular Catalysis A: Chemical* 2015. Vol. 398. p. 72-78.

EBERLY, PE. High-temperature infrared spectroscopy of olefins adsorbed on faujasites. In: *Journal of Physical Chemistry* 1967. Vol. 71. p. 1717-1722.

ERMAKOVA, MA and ERMAKOV, DY. High-loaded nickel–silica catalysts for hydrogenation, prepared by sol–gel: Route: structure and catalytic behavior. In: *Applied Catalysis A: General* 2003. Vol. 245. p. 277-288.

FAGHERAZZI, G, et al. Structural investigation on the stoichiometry of β-PdHx in Pd/SiO2 catalysts as a function of metal dispersion. In: *Catalysis Letters* 1995. Vol. 32. p. 293-303.

FENG, JT, et al. Enhanced metal dispersion and hydrodechlorination properties of a Ni/Al_2O_3 catalyst derived from layered double hydroxides. In: *Journal of Catalysis* 2009. Vol. 266. p. 351-358.

FERREIRA-APARICIO, P, et al. Mechanistic aspects of the dry reforming of methane over ruthenium catalysts. In: *Applied Catalysis A: General* 2000. Vol. 202. p. 183-196.

FOUILLOUX, P. Selective Hydrogenation of Cinnamaldehyde to Cinnamyl Alcohol on Pt-Co and Pt-Ru/C Catalysts. In: *Heterogeneous Catalysis and Fine Chemicals*. GUISNET, M; BARRAULT, J; BOUCHOULE, C; DUPREZ, D; MONTASSIER, C; PÉROT, G. Eds. First ed. Amsterdam: Elsevier; 1988. p. 123-129.

GALLO, A, et al. Size controlled copper nanoparticles hosted in mesoporous silica matrix: Preparation and characterization. In: *Applied Catalysis B: Environmental* 2012. Vol. 126. p. 161-171.

GANDARIAS, I, et al. Liquid-phase glycerol hydrogenolysis to 1,2-propanediol under nitrogen pressure using 2-propanol as hydrogen source. In: *Journal of Catalysis* 2011. Vol. 282. p. 237-247.

GANDARIAS, I, et al. Liquid-phase glycerol hydrogenolysis by formic acid over Ni–Cu/Al2O3 catalysts. In: *Journal of Catalysis* 2012. Vol. 290. p. 79-89.

GANDINI, A and BELGACEM, MN. Furans in polymer chemistry. In: *Progress in Polymer Science* 1997. Vol. 22. p. 1203-1379.

GHAMPSON, IT, et al. Comparison of alumina- and SBA-15-supported molybdenum nitride catalysts for hydrodeoxygenation of guaiacol. In: *Applied Catalysis A: General* 2012. Vol. 435–436. p. 51-60.

GOMEZ, H, et al. NbP catalyst for furfural production: FT IR studies of surface properties. In: *Applied Catalysis A: General* 2015. Vol. 502. p. 388-398.

GONÇALVES, G, et al. Preparation and characterization of nickel based catalysts on silica, alumina and titania obtained by sol–gel method. In: *Journal of Non-Crystalline Solids* 2006. Vol. 352. p. 3697-3704.

GONZÁLEZ, D, et al. Effect of La_2O_3 in Carbon Deposition on Pt/Al_2O_3 during Methylcyclopentane Reaction. In: *Industrial and Engineering Chemistry Research* 2007. Vol. 46. p. 4335-4340.

GREELEY, J and MAVRIKAKIS, M. Methanol Decomposition on Cu(111): A DFT Study. In: *Journal of Catalysis* 2002. Vol. 208. p. 291-300.

GUISNET, M and MAGNOUX, P. Organic chemistry of coke formation. In: *Applied Catalysis A: General* 2001. Vol. 212. p. 83-96.

GUTIERREZ, V, et al. Liquid phase selective hydrogenation of cinnamaldehyde over copper supported catalysts. In: *Applied Catalysis A: General* 2012. Vol. 413–414. p. 358-365.

Process for producing 5-methylfurfural. HAMADA, K, et al. US Patent No. 4,335,049. 30-June-1982. USA. Utility patent.

HE, S, et al. Characterization and catalytic properties of Ni/SiO2 catalysts prepared with nickel citrate as precursor. In: *Materials Research Bulletin* 2014. Vol. 49. p. 108-113.

HRONEC, M, et al. Effect of catalyst and solvent on the furan ring rearrangement to cyclopentanone. In: *Applied Catalysis A: General* 2012. Vol. 437–438. p. 104-111.

HRONEC, M, et al. Highly selective rearrangement of furfuryl alcohol to cyclopentanone. In: *Applied Catalysis B: Environmental* 2014. Vol. 154–155. p. 294-300.

HU, L, et al. Selective Transformation of 5-Hydroxymethylfurfural into the Liquid Fuel 2,5-Dimethylfuran over Carbon-Supported Ruthenium. In: *Industrial and Engineering Chemistry Research* 2014. Vol. 53. p. 3056-3064.

HU, S, et al. The effect of surface acidic and basic properties on the hydrogenation of aromatic rings over the supported nickel catalysts. In: *Chemical Engineering Journal* 2010. Vol. 162. p. 371-379.

HUANG, YB, et al. Nickel–Tungsten Carbide Catalysts for the Production of 2,5-Dimethylfuran from Biomass-Derived Molecules. In: *ChemSusChem* 2014. Vol. 7. p. 1068-1072.

IBARRA, JV, et al. Fourier transform infrared spectroscopic study of coke deposits on a Cr_2O_3-Al_2O_3 catalyst. In: *Vibrational Spectroscopy* 1995. Vol. 9. p. 191-196.

JACQUIN, M, et al. Novel supported Rh, Pt, Ir and Ru mesoporous aluminosilicates as catalysts for the hydrogenation of naphthalene. In: *Applied Catalysis A: General* 2003. Vol. 251. p. 131-141.

JAE, J, et al. Cascade of Liquid-Phase Catalytic Transfer Hydrogenation and Etherification of 5-Hydroxymethylfurfural to Potential Biodiesel Components over Lewis Acid Zeolites. In: *ChemCatChem* 2014. Vol. 6. p. 508-513.

JAE, J, et al. Production of Dimethylfuran from Hydroxymethylfurfural through Catalytic Transfer Hydrogenation with Ruthenium Supported on Carbon. In: *ChemSusChem* 2013. Vol. 6. p. 1158-1162.

JAMES, OO, et al. Towards the conversion of carbohydrate biomass feedstocks to biofuels via hydroxylmethylfurfural. In: *Energy and Environmental Science* 2010. Vol. 3. p. 1833-1850.

JASIK, A, et al. Study of nickel catalysts supported on Al2O3, SiO2 or Nb2O5 oxides. In: *Journal of Molecular Catalysis A: Chemical* 2005. Vol. 242. p. 81-90.

JENNESS, GR and VLACHOS, DG. DFT Study of the Conversion of Furfuryl Alcohol to 2-Methylfuran on RuO2 (110). In: *Journal of Physical Chemistry C* 2015. Vol. 119. p. 5938-5945.

JORGENSEN, AD, et al. Prediction of gas chromatography flame ionization detector response factors from molecular structures. In: *Analytical Chemistry* 1990. Vol. 62. p. 683-689.

JUSZCZYK, W, et al. The effect of copper and gold on the catalytic behavior of nickel/alumina catalysts in hydrogen-assisted dechlorination of 1,2-dichloroethane. In: *Catalysis Today* 2011. Vol. 169. p. 186-191.

KADKHODAYAN, A and BRENNER, A. Temperature-programmed reduction and oxidation of metals supported on γ-alumina. In: *Journal of Catalysis* 1989. Vol. 117. p. 311-321.

KANG, M, et al. γ-Alumina supported Cu-Ni bimetallic catalysts: Characterization and selective hydrogenation of 1,3-butadiene. In: *Canadian Journal of Chemical Engineering* 2002. Vol. 80. p. 63-70.

KARPIŃSKI, Z. Catalysis by Supported, Unsupported and Electron-Deficient Palladium. In: *Advances in Catalysis*. ELEY, DD; PINES, H; WEISZ, PB. Eds. First ed. San Diego: Academic Press, Inc.; 1990. p. 45-94.

KELLY, TG, et al. Comparison of O−H, C−H, and C−O Bond Scission Sequence of Methanol on Tungsten Carbide Surfaces Modified by Ni, Rh, and Au. In: *Journal of Physical Chemistry C* 2011. Vol. 115. p. 6644-6650.

KIM, P, et al. Synthesis and characterization of mesoporous alumina with nickel incorporated for use in the partial oxidation of methane into synthesis gas. In: *Applied Catalysis A: General* 2004. Vol. 272. p. 157-166.

KLASS, DL. Chapter 3 - Photosynthesis of Biomass and Its Conversion-Related Properties. In: *Biomass for Renewable Energy, Fuels, and Chemicals*. KLASS, DL. Ed. First ed. San Diego: Academic Press; 1998. p. 51-90.

KOBAYASHI, M and SHIRASAKI, T. The chemisorption of CO on ruthenium metals and ruthenium-silica catalysts. In: *Journal of Catalysis* 1973. Vol. 28. p. 289-295.

KONG, X, et al. Switchable synthesis of 2,5-dimethylfuran and 2,5-dihydroxymethyltetrahydrofuran from 5-hydroxymethylfurfural over Raney Ni catalyst. In: *RSC Advances* 2014. Vol. 4. p. 60467-60472.

KOOPMAN, PGJ, et al. Activation of ruthenium on silica hydrogenation catalysts. In: *Reaction Kinetics and Catalysis Letters* 1978. Vol. 8. p. 389-393.

KOOPMAN, PGJ, et al. Characterization of ruthenium catalysts as studied by temperature programmed reduction. In: *Journal of Catalysis* 1981. Vol. 69. p. 172-179.

KUMALAPUTRI, AJ, et al. Tunable and Selective Conversion of 5-HMF to 2,5-Furandimethanol and 2,5-Dimethylfuran over Copper-Doped Porous Metal Oxides. In: *ChemSusChem* 2014. Vol. 7. p. 2266-2275.

LAFAYE, G, et al. Citral hydrogenation over alumina supported Rh-Ge catalysts: Effects of the reduction temperature. In: *Applied Catalysis A: General* 2004. Vol. 257. p. 107-117.

LASHDAF, M, et al. Behaviour of palladium and ruthenium catalysts on alumina and silica prepared by gas and liquid phase deposition in cinnamaldehyde hydrogenation. In: *Applied Catalysis A: General* 2003. Vol. 241. p. 65-75.

LEE, JH, et al. Stabilization of Ni/Al2O3 catalyst by Cu addition for CO2 reforming of methane. In: *Applied Catalysis A: General* 2004. Vol. 269. p. 1-6.

LEJEMBLE, P, et al. From biomass to furan through decarbonylation of furfural under mild conditions. In: *Biomass* 1984. Vol. 4. p. 263-274.

LESIAK, M, et al. Hydrogenation of furfural over Pd–Cu/Al_2O_3 catalysts. The role of interaction between palladium and copper on determining catalytic properties. In: *Journal of Molecular Catalysis A: Chemical* 2014. Vol. 395. p. 337-348.

LEWKOWSKI, J. Synthesis, chemistry and applications of 5-hydroxymethylfurfural and its derivatives. In: *Arkivoc* 2001. Vol. 1. p. 17-54.

LI, C and CHEN, YW. Temperature-programmed-reduction studies of nickel oxide/alumina catalysts: effects of the preparation method. In: *Thermochim. Acta* 1995. Vol. 256. p. 457-465.

LI, G, et al. Comparison of reducibility and stability of alumina-supported Ni catalysts prepared by impregnation and co-precipitation. In: *Applied Catalysis A: General* 2006. Vol. 301. p. 16-24.

LIU, D, et al. Deactivation mechanistic studies of copper chromite catalyst for selective hydrogenation of 2-furfuraldehyde. In: *Journal of Catalysis* 2013. Vol. 299. p. 336-345.

LÓPEZ-SUÁREZ, FE, et al. Cu/Al_2O_3 catalysts for soot oxidation: Copper loading effect. In: *Applied Catalysis B: Environmental* 2008. Vol. 84. p. 651-658.

LUIJKX, GC, et al. Ether formation in the hydrogenolysis of hydroxymethylfurfural over palladium catalysts in alcoholic solution. In: *Heterocycles* 2009. Vol. 77. p. 1037-1044.

LUO, MF, et al. In situ XRD, Raman, and TPR studies of CuO/Al_2O_3 catalysts for CO oxidation. In: *Journal of Molecular Catalysis A: Chemical* 2005. Vol. 239. p. 243-248.

MA, J, et al. Synthesis and properties of furan-based imine-linked porous organic frameworks. In: *Polymer Chemistry* 2012. Vol. 3. p. 2346-2349.

MAETZ, P, et al. Hydrogenation of But-1-yne on Platinum/Silica Catalysts: An in Situ Dynamic Infrared Study. In: *Journal of Catalysis* 1994. Vol. 147. p. 48-56.

MAHATA, N and VISHWANATHAN, V. Influence of palladium precursors on structural properties and phenol hydrogenation characteristics of supported palladium catalysts. In: *Journal of Catalysis* 2000. Vol. 196. p. 262-270.

MARTIN, GA, et al. Chemistry of silica-supported catalysts: preparation activation and reduction. In: *Applied Catalysis* 1981. Vol. 1. p. 367-382.

MATSUMURA, Y, et al. Selective dehydrogenation of ethanol over highly dehydrated silica. In: *Journal of Catalysis* 1989. Vol. 117. p. 135-143.

MAVRIKAKIS, M and BARTEAU, MA. Oxygenate reaction pathways on transition metal surfaces. In: *Journal of Molecular Catalysis A: Chemical* 1998. Vol. 131. p. 135-147.

MAZZIERI, V, et al. XPS, FTIR and TPR characterization of Ru/Al2O3 catalysts. In: *Applied Surface Science* 2003. Vol. 210. p. 222-230.

MCMANUS, JR and VOHS, JM. Deoxygenation of glycolaldehyde and furfural on Mo_2C/Mo(100). In: *Surface Science* 2014. Vol. 630. p. 16-21.

MEDINA, F, et al. Characterization of several [gamma]-alumina-supported nickel catalysts and activity for selective hydrogenation of hexanedinitrile. In: *Journal of the Chemical Society, Faraday Transactions* 1994. Vol. 90. p. 1455-1459.

MEI, D, et al. Potential Energy Surface of Methanol Decomposition on Cu(110). In: *Journal of Physical Chemistry C* 2009. Vol. 113. p. 4522-4537.

MELO, L, et al. Effect of the metallic/acid site (nPt/nA) ratio on the transformation of acetone towards methyl isobutyl ketone. In: *Catalysis Letters* 1997. Vol. 44. p. 201-204.

MENDEZ, CM, et al. On the role of Pd β-hydride in the reduction of nitrate over Pd based catalyst. In: *Applied Catalysis B: Environmental* 2008. Vol. 84. p. 156-161.

MERAT, N, et al. High selective production of tetrahydrofurfuryl alcohol: Catalytic hydrogenation of furfural and furfuryl alcohol. In: *Journal of Chemical Technology and Biotechnology* 1990. Vol. 48. p. 145-159.

MIRANDA, BC, et al. Influence of copper on nickel-based catalysts in the conversion of glycerol. In: *Applied Catalysis B: Environmental* 2015. Vol. 166–167. p. 166-180.

MODAK, A, et al. A general and efficient aldehyde decarbonylation reaction by using a palladium catalyst. In: *Chemical Communications* 2012. Vol. 48. p. 4253-4255.

MUSOLINO, MG, et al. Supported palladium catalysts for the selective conversion of cis-2-butene-1,4-diol to 2-hydroxytetrahydrofuran: effect of metal particle size and support. In: *Applied Catalysis A: General* 2007. Vol. 325. p. 112-120.

NAKAGAWA, Y, et al. Catalytic Reduction of Biomass-Derived Furanic Compounds with Hydrogen. In: *ACS Catalysis* 2013. Vol. 3. p. 2655-2668.

NAKAGAWA, Y and TOMISHIGE, K. Total hydrogenation of furan derivatives over silica-supported Ni–Pd alloy catalyst. In: *Catalysis Communications* 2010. Vol. 12. p. 154-156.

NEYERTZ, C, et al. Palladium–vanadium interaction in binary supported catalysts. In: *Catalysis Today* 2000. Vol. 57. p. 255-260.

NIMMANWUDIPONG, T, et al. Cyclohexanone Conversion Catalyzed by Pt/γ-Al2O3: Evidence of Oxygen Removal and Coupling Reactions. In: *Catalysis Letters* 2011. Vol. 141. p. 1072-1078.

NISHIMURA, S, et al. Selective hydrogenation of biomass-derived 5-hydroxymethylfurfural (HMF) to 2,5-dimethylfuran (DMF) under atmospheric hydrogen pressure over carbon supported PdAu bimetallic catalyst. In: *Catalysis Today* 2014. Vol. 232. p. 89-98.

NURUNNABI, M, et al. Effect of Mn addition on activity and resistance to catalyst deactivation for Fischer–Tropsch synthesis over Ru/Al2O3 and Ru/SiO2 catalysts. In: *Catalysis Communications* 2007. Vol. 8. p. 1531-1537.

OHYAMA, J, et al. Conversion of 5-hydroxymethylfurfural to a cyclopentanone derivative by ring rearrangement over supported Au nanoparticles. In: *Chemical Communications* 2014. Vol. 50. p. 5633-5636.

PAN, Y-X, et al. Preparation and characterization of coke resistant Ni/SiO2 catalyst for carbon dioxide reforming of methane. In: *Journal of Power Sources* 2008. Vol. 176. p. 46-53.

PANAGIOTOPOULOU, P, et al. Liquid-Phase Catalytic Transfer Hydrogenation of Furfural over Homogeneous Lewis Acid–Ru/C Catalysts. In: *ChemSusChem* 2015. Vol. 8. p. 2046-2054.

PANAGIOTOPOULOU, P and VLACHOS, DG. Liquid phase catalytic transfer hydrogenation of furfural over a Ru/C catalyst. In: *Applied Catalysis A: General* 2014. Vol. 480. p. 17-24.

PANPRANOT, J, et al. Effects of Pd precursors on the catalytic activity and deactivation of silica-supported Pd catalysts in liquid phase hydrogenation. In: *Applied Catalysis A: General* 2005. Vol. 292. p. 322-327.

PARERA, JM, et al. The role of Re and S in the Pt-Re-S/Al2O3 catalyst. In: *Journal of Catalysis* 1986. Vol. 99. p. 39-52.

PARERA, JM, et al. Influence of sulfurization on coke formation over catalysts for naphtha reforming. In: *Applied Catalysis* 1986. Vol. 23. p. 15-22.

PERNICONE, N, et al. On the measurement of copper surface area by oxygen chemisorption. In: *Applied Catalysis A: General* 2003. Vol. 240. p. 199-206.

PUDI, SM, et al. Selective Hydrogenolysis of Glycerol to 1,2-Propanediol Over Bimetallic Cu-Ni Catalysts Supported on ^{3}-Al2O3. In: *Journal of the Brazilian Chemical Society* 2015. Vol. 26. p. 1551-1564.

RAO, R, et al. Furfural hydrogenation over carbon-supported copper. In: *Catalysis Letters* 1999. Vol. 60. p. 51-57.

RAO, R, et al. Properties of Copper Chromite Catalysts in Hydrogenation Reactions. In: *Journal of Catalysis* 1997. Vol. 171. p. 406-419.

RESHETENKO, TV, et al. Carbon capacious Ni-Cu-Al2O3 catalysts for high-temperature methane decomposition. In: *Applied Catalysis A: General* 2003. Vol. 247. p. 51-63.

REYES, P, et al. o-xylene hydrogenation on supported ruthenium catalysts. In: *Catalysis Letters* 1997. Vol. 46. p. 71-75.

ROBINSON, E and ROSS, RA. The sorption of furans on silica gels. In: *Journal of the Chemical Society A: Inorganic, Physical, Theoretical* 1970. Vol. p. 84-87.

ROGERS, LH and WILLIAMS, D. The Infrared Absorption Spectra of Some Sugars and Furans. In: *Journal of the American Chemical Society* 1938. Vol. 60. p. 2619-2621.

ROMÁN-LESHKOV, Y, et al. Production of dimethylfuran for liquid fuels from biomass-derived carbohydrates. In: *Nature* 2007. Vol. 447. p. 982-985.

RYCZKOWSKI, J. IR spectroscopy in catalysis. In: *Catalysis Today* 2001. Vol. 68. p. 263-381.

RYNKOWSKI, JM, et al. On the nature of oxidic nickel phases in NiO/γ-Al_2O_3 catalysts. In: *Applied Catalysis A: General* 1993. Vol. 106. p. 73-82.

SACIA, ER, et al. Synthesis of biomass-derived methylcyclopentane as a gasoline additive via aldol condensation/hydrodeoxygenation of 2,5-hexanedione. In: *Green Chemistry* 2015. Vol. 17. p. 2393-2397.

SACHTLER, WMH and VAN DER PLANK, P. The role of individual surface atoms in chemisorption and catalysis by nickel-copper alloys. In: *Surface Science* 1969. Vol. 18. p. 62-79.

SAHA, B, et al. Zinc-Assisted Hydrodeoxygenation of Biomass-Derived 5-Hydroxymethylfurfural to 2,5-Dimethylfuran. In: *ChemSusChem* 2014. Vol. 7. p. 3095-3101.

SCANLON, JT and WILLIS, DE. Calculation of Flame Ionization Detector Relative Response Factors Using the Effective Carbon Number Concept. In: *Journal of Chromatographic Science* 1985. Vol. 23. p. 333-340.

SCHIAVO, V, et al. Hydrogénation catalytique du 5-hydroxyméthylfurfural en milieu aqueux. In: *Bulletin de la Société chimique de France* 1991. Vol. 128. p. 704-711.

SCHOLZ, D, et al. Catalytic Transfer Hydrogenation/Hydrogenolysis for Reductive Upgrading of Furfural and 5-(Hydroxymethyl)furfural. In: *ChemSusChem* 2014. Vol. 7. p. 268-275.

SEO, G and CHON, H. Hydrogenation of furfural over copper-containing catalysts. In: *Journal of Catalysis* 1981. Vol. 67. p. 424-429.

SEPÚLVEDA, J and FÍGOLI, NS. Ni/SiO2 catalysts, effect of Ni reduction on activity and thiotolerance during ethylbenzene hydrogenation. In: *Reaction Kinetics and Catalysis Letters* 1995. Vol. 55. p. 383-389.

SHEKHAR, R and BARTEAU, MA. Decarbonylation and hydrogenation reactions of allyl alcohol and acrolein on Pd(110). In: *Surface Science* 1994. Vol. 319. p. 298-314.

SHEKHAR, R, et al. Adsorption and Reaction of Aldehydes on Pd Surfaces. In: *Journal of Physical Chemistry B* 1997. Vol. 101. p. 7939-7951.

SHEN, W-J, et al. The influence of the support on the activity and selectivity of Pd in CO hydrogenation. In: *Applied Catalysis A: General* 2001. Vol. 213. p. 225-232.

SHIN, E-J and KEANE, MA. Gas-Phase Hydrogenation/Hydrogenolysis of Phenol over Supported Nickel Catalysts. In: *Industrial & Engineering Chemistry Research* 2000. Vol. 39. p. 883-892.

SIETSMA, JRA, et al. Ordered Mesoporous Silica to Study the Preparation of Ni/SiO2 ex Nitrate Catalysts: Impregnation, Drying, and Thermal Treatments. In: *Chemistry of Materials* 2008. Vol. 20. p. 2921-2931.

SIMÓN, E, et al. Study of the deactivation of copper-based catalysts for dehydrogenation of cyclohexanol to cyclohexanone. In: *Catalysis Today* 2012. Vol. 187. p. 150-158.

SING, KSW, et al. Reporting Physisorption Data for Gas/Solid Systems. In: *Pure and Applied Chemistry* 1985. Vol. 57. p. 603-619.

SINGH, H, et al. Metal support interactions in the palladium-catalysed decomposition of furfural to furan. In: *Journal of Chemical Technology and Biotechnology* 1980. Vol. 30. p. 293-296.

SITTHISA, S and RESASCO, DE. Hydrodeoxygenation of furfural over supported metal catalysts: A comparative study of Cu, Pd and Ni. In: *Catalysis Letters* 2011. Vol. 141. p. 784-791.

SMEDS, S, et al. Chemisorption and TPD studies of hydrogen on Ni/Al_2O_3. In: *Applied Catalysis A: General* 1996. Vol. 144. p. 177-194.

SOMASUNDARAN, P. *Encyclopedia of Surface and Colloid Science*. Second ed. New York: Taylor & Francis; 2006.

STAKHEEV, AY and KUSTOV, LM. Effects of the support on the morphology and electronic properties of supported metal clusters: modern concepts and progress in 1990s. In: *Applied Catalysis A: General* 1999. Vol. 188. p. 3-35.

STONKUS, VV, et al. Characteristics of the catalytic hydrogenation of 5-methylfurfural. In: *Chemistry of Heterocyclic Compounds* 1990. Vol. 26. p. 1214-1218.

STROHMEIER, BR, et al. Surface spectroscopic characterization of Cu/Al2O3 catalysts. In: *Journal of Catalysis* 1985. Vol. 94. p. 514-530.

TESSIER, D, et al. Spectroscopic study of the interaction of carbon monoxide with cationic and metallic palladium in palladium-alumina catalysts. In: *Journal of the Chemical Society, Faraday Transactions* 1992. Vol. 88. p. 741-749.

TOUPANCE, T, et al. Conditions of Formation of Copper Phyllosilicates in Silica-Supported Copper Catalysts Prepared by Selective Adsorption. In: *The Journal of Physical Chemistry B* 2002. Vol. 106. p. 2277-2286.

TSUJI, J and OHNO, K. Organic syntheses by means of noble metal compounds. XXXIV. Carbonylation and decarbonylation reactions catalyzed by palladium. In: *Journal of the American Chemical Society* 1968. Vol. 90. p. 94-98.

VAN DOORN, J and MOULIJN, JA. Extraction of spent hydrotreating catalysts studied by fourier transform infra-red spectroscopy. In: *Fuel Processing Technology* 1990. Vol. 26. p. 39-51.

VAN RYNEVELD, E, et al. A catalytic route to lower alcohols from glycerol using Ni-supported catalysts. In: *Green Chemistry* 2011. Vol. 13. p. 1819-1827.

VAN STEEN, E and PRINSLOO, FF. Comparison of preparation methods for carbon nanotubes supported iron Fischer–Tropsch catalysts. In: *Catalysis Today* 2002. Vol. 71. p. 327-334.

VARGAS-HERNÁNDEZ, D, et al. Furfuryl alcohol from furfural hydrogenation over copper supported on SBA-15 silica catalysts. In: *Journal of Molecular Catalysis A: Chemical* 2014. Vol. 383–384. p. 106-113.

VASILAKOS, NP and BARREIROS, MT. Homogeneous catalytic hydrogenolysis of biomass. In: *Ind. Eng. Chem. Process Des. Dev.* 1984. Vol. 23. p. 755-763.

VASILIADOU, ES, et al. Ru-based catalysts for glycerol hydrogenolysis—Effect of support and metal precursor. In: *Applied Catalysis B: Environmental* 2009. Vol. 92. p. 90-99.

VASILIADOU, ES and LEMONIDOU, AA. Kinetic study of liquid-phase glycerol hydrogenolysis over Cu/SiO_2 catalyst. In: *Chemical Engineering Journal* 2013. Vol. 231. p. 103-112.

VELON, A and OLEFJORD, I. Oxidation Behavior of Ni_3Al and Fe_3Al: I. XPS Calibrations of Pure Compounds and Quantification of the Results. In: *Oxidation of Metals* 2001. Vol. 56. p. 415-424.

VILLAVERDE, MM, et al. Selective liquid-phase hydrogenation of furfural to furfuryl alcohol over Cu-based catalysts. In: *Catalysis Today* 2013. Vol. 213. p. 87-92.

VOROTNIKOV, V, et al. DFT Study of Furfural Conversion to Furan, Furfuryl Alcohol, and 2-Methylfuran on Pd(111). In: *ACS Catalysis* 2012. Vol. 2. p. 2496-2504.

WAGNER, CD, et al. *Handbook of X-ray Photoelectron Spectroscopy*. First ed. Eden-Prairie: Perkin-Elmer Corp.; 1979.

WANG, G-H, et al. Platinum–cobalt bimetallic nanoparticles in hollow carbon nanospheres for hydrogenolysis of 5-hydroxymethylfurfural. In: *Nature Materials* 2014. Vol. 13. p. 293-300.

WANG, JA, et al. Effects of structural defects and acid–basic properties on the activity and selectivity of isopropanol decomposition on nanocrystallite sol–gel alumina catalyst. In: *Journal of Molecular Catalysis A: Chemical* 1999. Vol. 137. p. 239-252.

WANG, Z, et al. Surface structure and catalytic behavior of silica-supported copper catalysts prepared by impregnation and sol–gel methods. In: *Applied Catalysis A: General* 2003. Vol. 239. p. 87-94.

WILSENS, CHRM, et al. Thermotropic Polyesters from 2,5-Furandicarboxylic Acid and Vanillic Acid: Synthesis, Thermal Properties, Melt Behavior, and Mechanical Performance. In: *Macromolecules* 2014. Vol. 47. p. 3306-3316.

WILSON, CL. 18. Reactions of furan compounds. Part V. Formation of furan from furfuraldehyde by the action of nickel or cobalt catalysts: importance of added hydrogen. In: *J. Chem. Soc.* 1945. Vol. p. 61-63.

WU, G, et al. Hydrogen Production via Glycerol Steam Reforming over Ni/Al2O3: Influence of Nickel Precursors. In: *ACS Sustainable Chemistry and Engineering* 2013. Vol. 1. p. 1052-1062.

WU, M and HERCULES, DM. Studies of supported nickel catalysts by X-ray photoelectron and ion scattering spectroscopies. In: *Journal of Physical Chemistry* 1979. Vol. 83. p. 2003-2008.

WYMAN, CE. BIOMASS ETHANOL: Technical Progress, Opportunities, and Commercial Challenges. In: *Annual Review of Energy and the Environment* 1999. Vol. 24. p. 189-226.

YANG, R, et al. Hydrotreating of crude 2-ethylhexanol over Ni/Al_2O_3 catalysts: Surface Ni species-catalytic activity correlation. In: *Applied Catalysis A: General* 2009. Vol. 368. p. 105-112.

YANG, Y, et al. Conversion of furfural into cyclopentanone over Ni-Cu bimetallic catalysts. In: *Green Chemistry* 2013. Vol. 15. p. 1932-1940.

YANG, Y, et al. Effect of metal–support interaction on the selective hydrodeoxygenation of anisole to aromatics over Ni-based catalysts. In: *Applied Catalysis B: Environmental* 2014. Vol. 145. p. 91-100.

ZANGOUEI, M, et al. The influence of nickel loading on reducibility of NiO/Al_2O_3 catalysts synthesized by sol-gel method. In: *Chemical Engineering Research Bulletin* 2010. Vol. 14. p. 97-102.

ZHANG, B, et al. Selective conversion of furfuryl alcohol to 1,2-pentanediol over a Ru/MnOx catalyst in aqueous phase. In: *Green Chemistry* 2012. Vol. 14. p. 3402-3409.

ZHANG, W, et al. A study of furfural decarbonylation on K-doped Pd/Al_2O_3 catalysts. In: *Journal of Molecular Catalysis A: Chemical* 2011. Vol. 335. p. 71-81.

ZHOU, Y-H, et al. DFT studies of methanol decomposition on Ni(1 0 0) surface: Compared with Ni(1 1 1) surface. In: *Journal of Molecular Catalysis A: Chemical* 2006. Vol. 258. p. 203-215.

ZHU, Y-Y, et al. The Influence of Copper Particle Dispersion in Cu/SiO2 Catalysts on the Hydrogenation Synthesis of Ethylene Glycol. In: *Catalysis Letters* 2010. Vol. 135. p. 275-281.

ZU, Y, et al. Efficient production of the liquid fuel 2,5-dimethylfuran from 5-hydroxymethylfurfural over Ru/Co3O4 catalyst. In: *Applied Catalysis B: Environmental* 2014. Vol. 146. p. 244-248.

ANNEXES

ANNEX A.
MASS SPECTRA OF FURANIC COMPOUNDS

5-hydroxymethylfurfural (HMF)

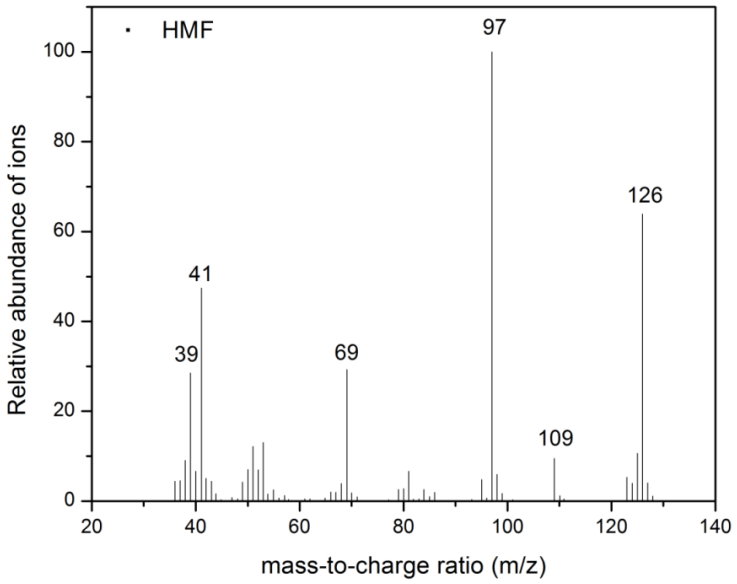

2,5-bis(hydroxymethyl)furan (BHF)

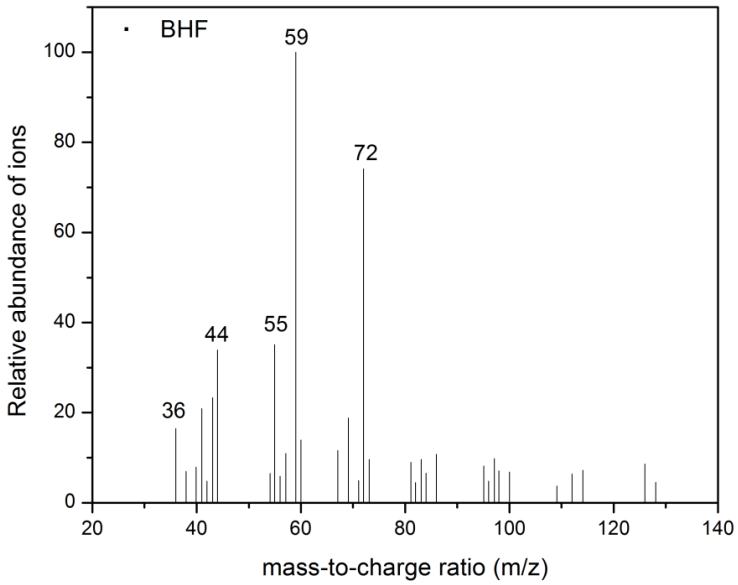

5-methylfurfural (MFAL)

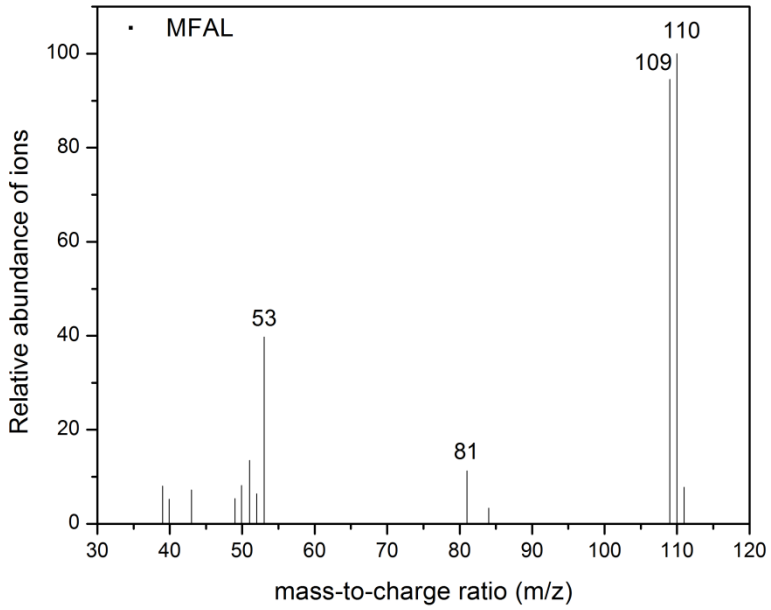

5-methyl-2-furfuryl alcohol (MFOL)

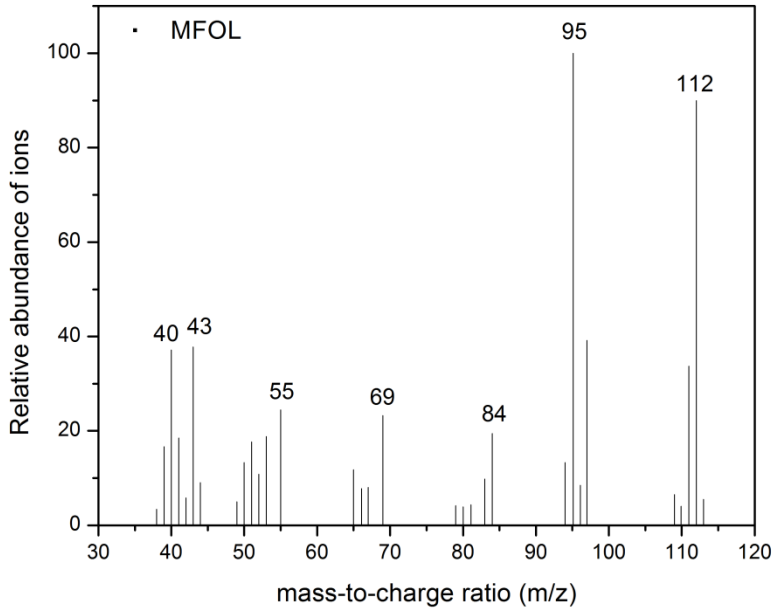

2,5-dimethylfuran (DMF)

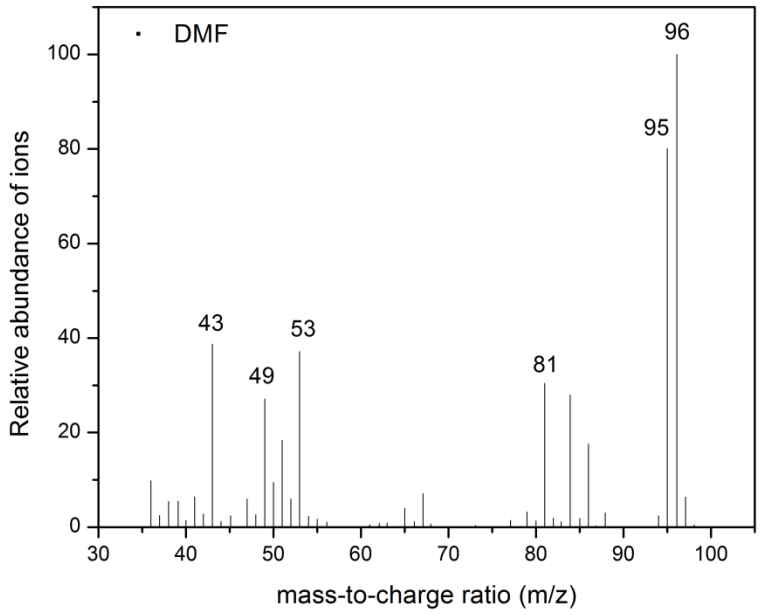

2,5-dimethyl-tetrahydrofuran, cis & trans (DMTHF)

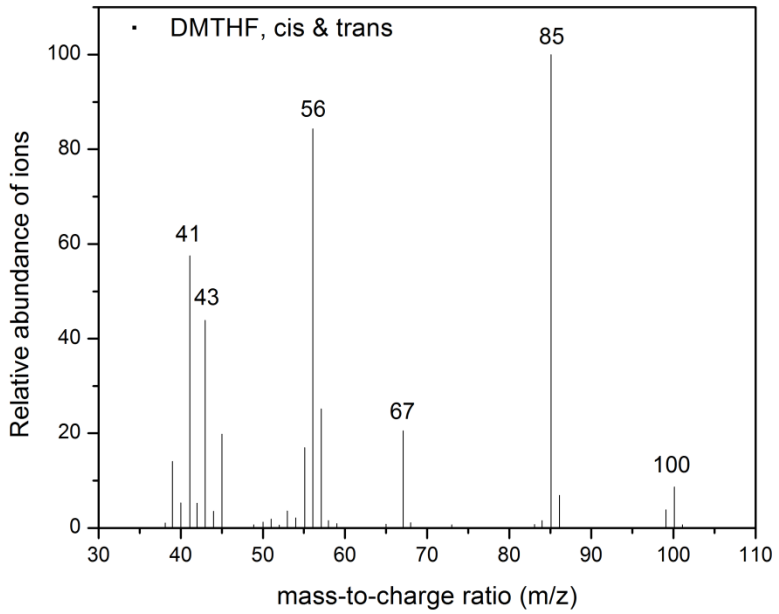

2-furfuryl alcohol (FOL)

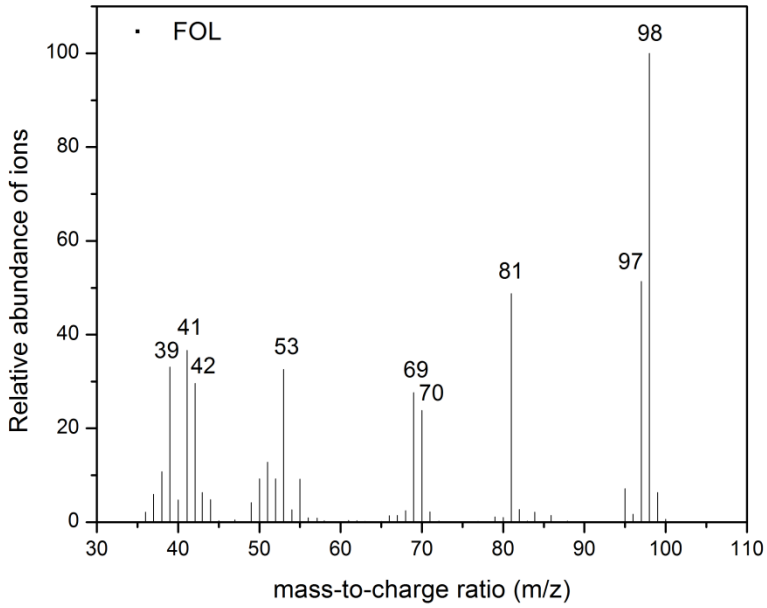

2-tetrahydrofurfuryl alcohol (THFOL)

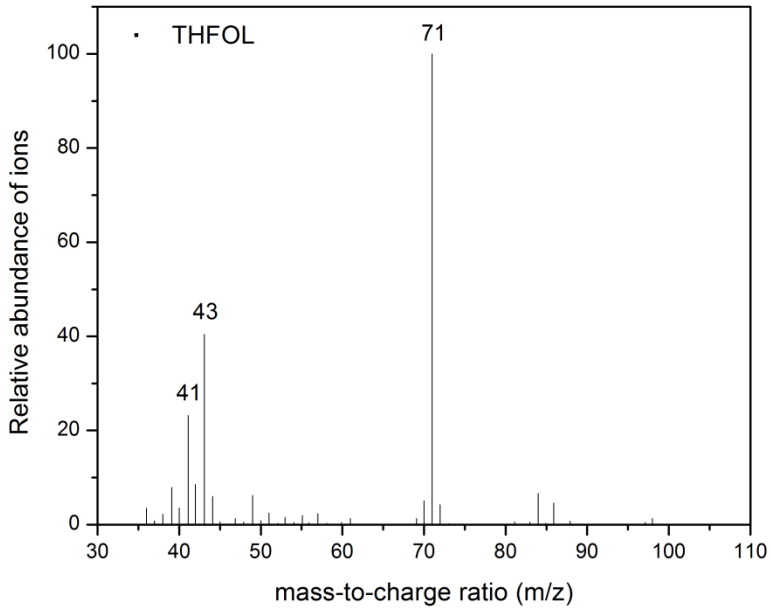

2,5-hexanedione (HD)

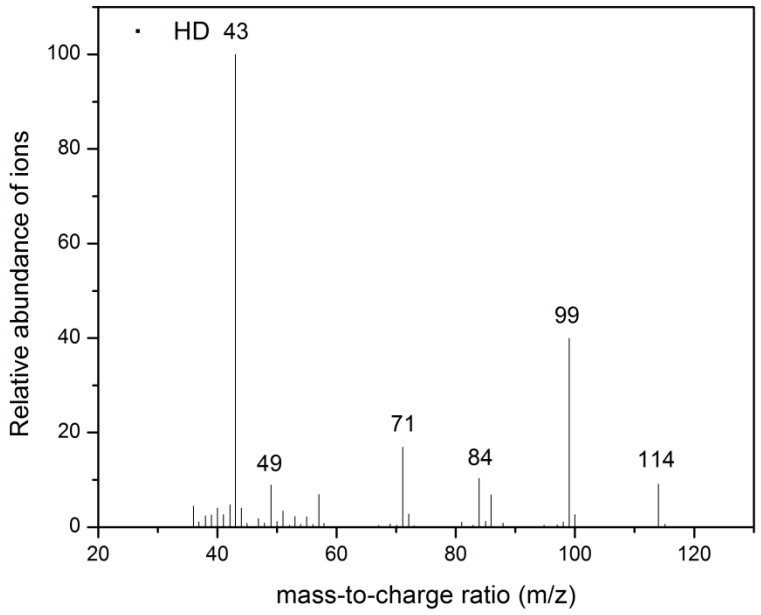

1-hydroxy-2,5-hexanedione

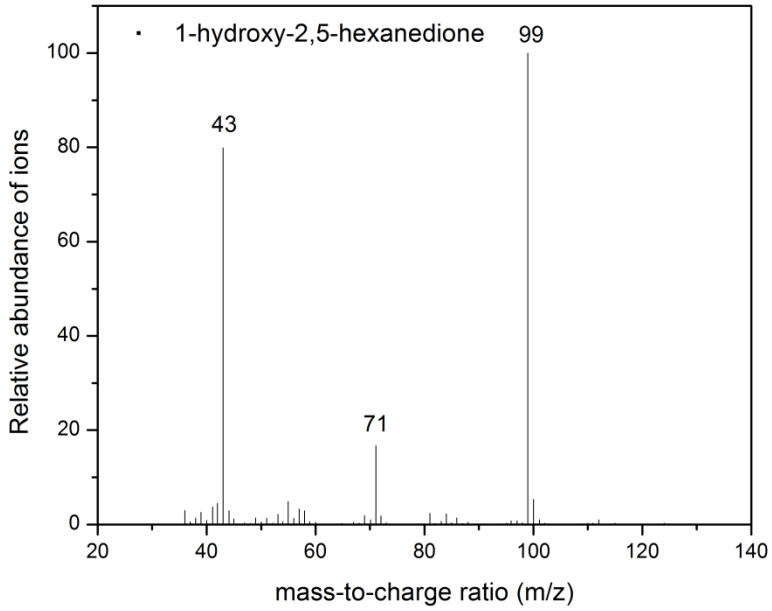

Cyclopentanone, 3-methyl

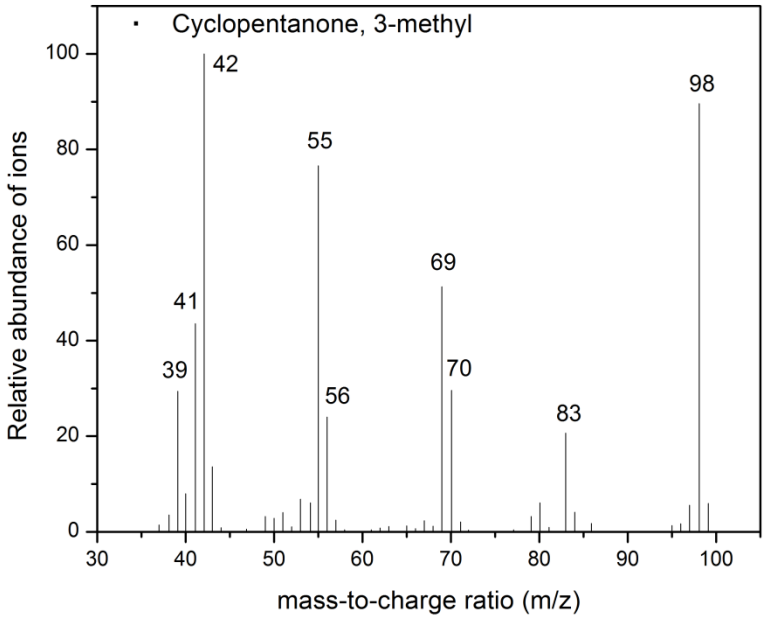

Cyclopenten-1-one, 3-methyl

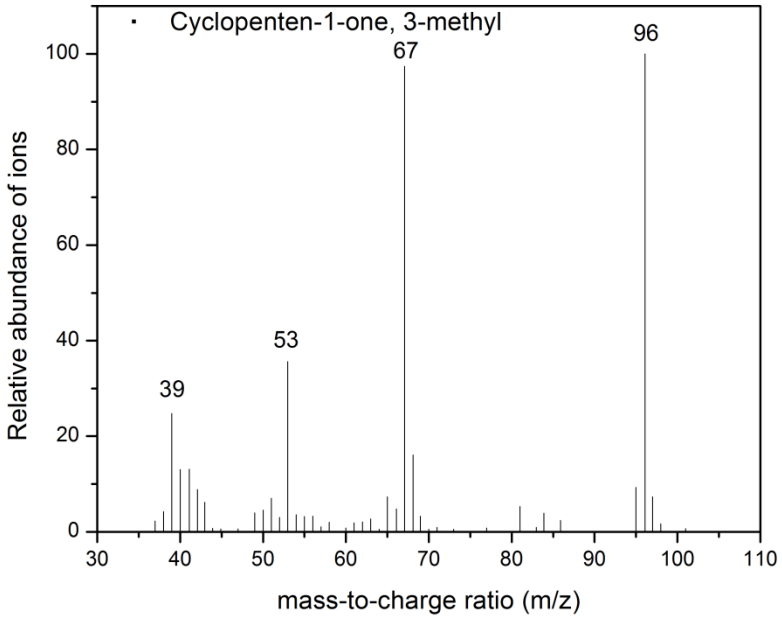

ANNEX B.
RELATIVE RESPONSE FACTOR AND RETENTION TIME OF FURANIC COMPOUNDS

Compound	Molecular Structure	Molecular Formula	Retention time (min)	Experimental RRF	Theoretical RRF
HMF	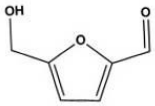	$C_6H_6O_3$	30.5	2.35	2.35
DFF	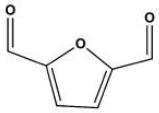	$C_6H_40_3$	22.6	2.76	2.42
MFAL	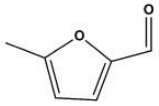	$C_6H_6O_2$	15.5	1.69	1.76
MFOL	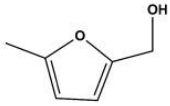	$C_6H_8O_2$	15.0	2.00	1.72
HD	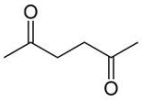	$C_6H_{10}O_2$	13.6	1.83	1.83
THFOL	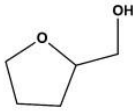	$C_5H_{10}O_2$	11.1	2.83	2.01
FOL	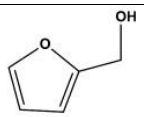	$C_5H_6O_2$	9.7	1.94	1.93
FAL	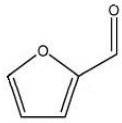	$C_5H_4O_2$	8.8	2.16	1.98
DMTHF (cis&trans)	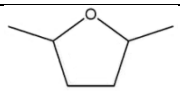	$C_6H_{12}O$	3.3	1.38	1.35
DMF	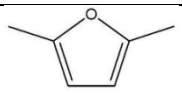	C_6H_8O	2.9	1.49	1.30
MTHFOL (cis&trans)	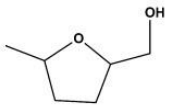	$C_6H_{12}O_2$	12.8	-	1.79

BHF	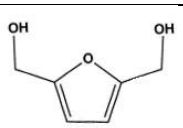	$C_6H_8O_3$	75.6	-	2.29
5-methyl-2-hexanone	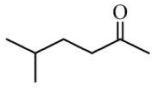	$C_7H_{14}O$	12.6	-	1.30
2-hexanone	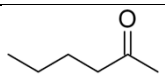	$C_6H_{12}O$	5.7	-	1.36
2-hexanol	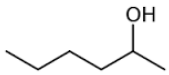	$C_6H_{14}O$	6.5	-	1.34
1-hydroxy-2,5-hexanedione	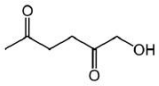	$C_6H_{10}O_3$	22.5	-	2.43
1,2-pentanediol	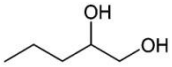	$C_5H_{12}O_2$	14.7	-	1.97
2-pentenal	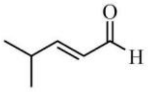	C_5H_8O	25.6	-	1.41
1-pentanol	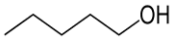	$C_5H_{11}O$	3.6	-	1.42
cyclopentanone	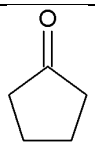	C_5H_8O	5.5	-	1.41
2-cyclopenten-1-one, 3-methyl	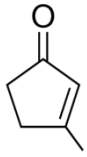	C_6H_8O	12.2	-	1.63
3-methyl-1,2-cyclopentane-dione	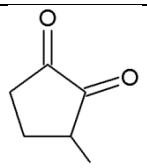	$C_6H_8O_2$	19.0	-	2.32
2-cyclopenten-1-one,2-hydroxy-3-methyl	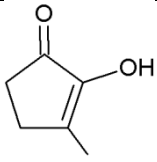	$C_6H_8O_2$	22.0	-	1.75